NATIONAL TECHNICAL UNIVERSITY OF ATHENS
SCHOOL OF NAVAL ARCHITECTURE AND MARINE ENGINEERING
DIVISION OF SHIP AND MARINE HYDRODYNAMICS

Weather ship routing focusing on propulsion energy efficiency

---

Diploma Thesis

June 2017

Author : N.G. Lamprinidis

Supervisor : K.A. Belibassakis, Associate Professor, NTUA

Commitee : G.K. Politis, Professor, NTUA

Gr. Grigoropoulos, Professor, NTUA

Acknowledgements

The present Diploma Thesis is part of my graduate studies at the School of Naval Architecture and Marine Engineering of National Technical University of Athens. Thus, I grab the chance to express my sincere gratitude to a number of people whose contribution where invaluable for the success and completion of this work.

First of all, I would like to thank my supervisor and mentor Associate Professor K. Belibassakis for his guidance and support and immeasurable patience during the preparation of this thesis. He was the best mentor someone could possible ever have. Invaluable was also the help of professor Th. Gerostathis and assistant researcher Aris Kapelonis for their help and guidance in the GUI constructing and Matlab tricks respectively.

Last but not least, I would like to thank Demi and my friends as without their help and support it would be nigh impossible to finish my studies.

Contents

Abstract ……5

1 INTRODUCTION ……6

2 SHIP HYDRODYNAMICS ……13

2.1 Calm water resistance ……13
2.1.1 Frictional resistance ……13
2.1.2 Form Drag ……14
2.1.3 Wave resistance ……14
2.1.4 Other Components ……17
2.2 Propulsion ……17
2.2.1 Propeller ……17
2.2.2 Propulsion Plant ……19
2.3 Ship Dynamics in waves ……19
2.3.1. Plane waves ……19
2.3.2 Linear wave-body interaction ……23
2.3.3 Ship seakeeping ……26
2.4 Added resistance in waves ……29
2.5 Added resistance in wind ……31

3 STATISTICS AND MODELING OF OCEAN WAVES……33
3.1 Statistical representation of ocean waves ……33
3.2 System theory and output spectrum ……36

4 SHIP ROUTING OPTIMIZATION ……38
4.1 Coordinate system and map projection……38
4.2 Calculation of fuel consumption in waves ……39
4.3 description of method ……41

.

5 MATLAB-GUI IMPLEMENTATION AND NUMERICAL RESULTS ……44
5.1 AFRAMAX tanker ……44
5.2 Added resistance calculation ……48
5.3 Travel path with control points and land avoidance features ……51
5.4 Geographical and weather data ……52
5.5 Numerical results ……53

CONCLUSIONS AND PROPOSAL FOR FUTURE WORK ……59

REFERENCES ……60

APPENDICES ……64

A: Solution of certain problems of calculus of variations reformulated as multidimensional optimization problems ……64
B: Validation of algorithm through the Sturm Liouville problem ……84
C: Matlab® and GUI implementation ……89

Abstract

In this thesis a direct method for modeling weather ship routing with regards to energy efficiency is presented, in the case of ships traveling with constant speed. Except of weather data and ship added resistance, also bathymetry and coastline are considered. The ship route is represented by Fourier (sine) series in the geographical coordinate system (Mercator's projection) on the surface of the earth, permitting the reformulation of the optimization problem with respect to the series coefficients. The optimization algorithm is validated in specific test problems from physics. Subsequently, the present method is implemented as a Matlab GUI, and, as a first application, the software tool is demonstrated for specific ships, in conjunction with hindcast weather (wave and wind) data in the Mediterranean Sea region. Numerical results illustrate the performance of the present method concerning robustness, accuracy of results and speed of computations.

Περίληψη

Στα πλαίσια αυτής της διπλωματικής εργασίας αναπτύσσεται μια μέθοδος για το πρόβλημα της βέλτιστης ως προς την κατανάλωση καυσίμων, διαδρομής του πλοίου σε πραγματικές συνθήκες υπηρεσίας. Στοιχεία που λαμβάνονται υπ' οψιν είναι μετεωρολογικά δεδομένα (άνεμος και κύμα), η βαθυμετρία, η ακτογραμμή, η αντίσταση του πλοίου σε ήρεμο νερό και η πρόσθετη αντίσταση σε κυματισμούς. Η διαδρομή του πλοίου αναπαρίσταται σαν ημιτονική σειρά Fourier στο γεωγραφικό σύστημα συντεταγμένων πάνω στην επιφάνεια της γης. Η επιλογή αυτή επιτρέπει την αναγωγή του προβλήματος σε ένα πρόβλημα βελτιστοποίησης ως προς τους συντελεστές της προηγούμενης αναπαράστασης. Η εγκυρότητα του αλγόριθμου βελτιστοποίησης καταδεικνύεται και ελέγχεται με χρήση επιλεγμένων παραδειγμάτων που προέρχονται από τη κυματική και μαθηματική φυσική. Ακολούθως, παρουσιάζεται ένα εργαλείο λογισμικού (GUI) που αναπτύχθηκε σε περιβάλλον σε Matlab® και παρουσιάζονται παραδείγματα εφαρμογής για συγκεκριμένα πλοία σε συνδυασμό με πραγματικά δεδομένα καιρού στη περιοχή της Μεσογείου θαλάσσης. Τα αριθμητικά αποτελέσματα κατάδυκνείουν την απόδοση της μεθόδου όσον αφορά την στιβαρότητα του αλγορίθμου, την ακρίβεια των αποτελεσμάτων και την ταχύτητα των υπολογισμών.

Chapter 1

INTRODUCTION

No one can dispute the necessity and size of the shipping industry. Around 90% of the world trade is carried away by ships, while consuming 4 million barrels of oil per day. In addition, we are entering an era of greening of transportation, where energy efficiency is of outmost importance. With the use of ship routing optimization algorithms, energy and time can be significantly saved, as well as increase in safety at sea and travel comfort. Thus, environmentally friendly technical solutions with reduction of exhaust gases are requested, including methods for ship weather routing, taking into account hydrodynamic responses of specific ship, and its propulsion system characteristics for a particular voyage. To this aim, except of ship responses, also added resistance in waves and other factors are examined.

The optimal route can be considered in regards to safety and comfort (Maki, Akimoto et al 2011, Kosmas et al 2012), maximum energy efficiency (Calvert et al 1991, Dewit et al 1990), minimum voyage time (Zhong et all 1992, Lunnon et al 1992) or the combinations of these factors (Padhy et al 2008, Hinnenthal et al 2010) under the encountered weather circumstances. Various mehods have been developed, as e.g., calculus of variations and the modified isochrone method (Hagiwara et al 1987 & 1989), the isopone method (Spaans 1995, Klompstra et al 1992). In addition to above algorithms, many other approaches have also been employed, such as the iterative dynamic programming (Avgouleas 2008), augmented Lagrange multiplier (Tsujimoto et al 2006) and genetic algorithms (Bekker et al

2006, Vettor et al 2016). In the present work a ship weather routing method is developed and tested through numerical simulations based on hindcast weather data in the Mediterranean Sea. The method is based on minimization of fuel consumption taking into account the influence of wave added resistance, in conjunction with the effects of vertical stern motion of the ship in waves on the overall propulsion system efficiency; see Belibassakis et al (2013). Also, seakeeping criteria are implemented as additional operability constraints.Finding the optimal route however, is not an easy task. An analytical solution under the framework of the rigorous mathematical approach (Calculus of Variations) is not possible in practice, due to the complexity of the problem and the sparseness of the data. Below we give a small analysis of the aforementioned methods.

Calculus of Variations

Calculus of variations (see, e.g., Gelfand & Fomin 2000) aims to minimize or maximize functionals often expressed as integrals, in order to find extremals, thus to find the arc connecting start and destination in a manner leading to minimum voyage time. This approach is equivalent to solving the Euler-Lagrange equations numerically. A time-independent approach (Hamilton, 1961) is based on the variation of the ship's course by assuming that the environmental field is static and the ship's speed is time-independent. The calculation of a ship's least-time track is approached by Bijlsma (1975) using calculus of variations, or the special case of optimal control. An absolute minimum, thus an extremal, though, requires the consideration of time fronts consisting of a set of points reachable within a certain time step given by wave data being available every 12 hours or interpolated every 6 hours. The points reachable within one time step, hence, defines a grid. Besides wave and current data at the grid points, further data that is assigned initially includes departure time and location, arrival location and the ship's data including speed reduction in waves. For each time step, the points reachable along the extremals but also along the great circle route and rhumb line are computed. Due to boundaries, such as land, the destination might not be reachable along any extremal from the start. A suitable new point may be introduced as intermediate starting point for a new extremal. The method can be applied to minimize fuel consumption by considering speed and heading as control variables. The speed is constrained by a minimum and a maximum. However, the fuel function is often derived from empirical data. Thus, due to inhomogeneity of equations to be solved, Bijlsma (1975) considers the application of ap-

proximations to be more accurate in practical cases than application of the same numerical method as for the least-time track.

3D Dynamic Programming

In the context of weather routing, Dynamic Programming in a two-dimensional approach has been originally applied by de Wit (1990) and Calvert et al. (1991). The discrete optimization problem aims to minimize fuel consumption, while engine power and propeller revolutions are assumed constant throughout the voyage. As only the route is optimized, the focus will be on the three-dimensional approach in the following. 3D Dynamic Programming describes a Forward Dynamic Programming method where both, the ship's power settings and its heading, are considered to minimize fuel consumption (Shao, Zhou, & Thong, 2012). The resulting discrete optimization problem with one objective function and several constraints is solved deterministically. In general, Forward Dynamic Programming is based on Bellman's principle of optimality (Bellman, 1952) and therefore on the idea that a path is optimal if and only if the choice of the previous path is optimal for any intermediate stage. A stage describes a small part of the original problem defined by the common value of a stage variable. The settings of the control variables (in this case engine power and ship's heading) are assumed constant between two consecutive stages. Therefore, the final solution consists of the optimal choice of settings for the control variables at every stage in total resulting in the optimal path. Every stage is composed of many states, while a state is defined by a location (grid point) and a discretized time. The optimization procedure starts with the calculation of the ship's heading from the initial state to each grid point on the second stage, while any headings violating constraints are neglected. For each heading, the fuel consumption upon arrival at the next stage as well as the time travelled between the two stages is calculated for each possible discretized calm water ship speed; calculations for speeds violating constraints are abandoned. In order to enable the comparison of fuel consumed on various routes leading to the same grid point within a certain time interval, all times at a state are defined by the closest smaller discretized arrival time. The fuel consumptions of all routes leading to a certain state (same location and arrival within a predefined time interval) are compared and only the route corresponding to the minimal fuel consumption of each state is saved for future reference. Then the ship's headings from each of the grid points on the second stage to each of the grid points on the third stage are determined and the whole procedure is repeated. Since the optimal route to reach any state is saved for all states of any stage, the final optimal

route may be reconstructed easily once the optimal route from the second-last stage to the final state has been determined.

Iterative Dynamic Programming

Avgouleas (2008) defines weather routing as an optimal control problem with the objective to solve a deterministic nonlinear fuel minimization problem under consideration of safety constraints. A solution is obtained through the development of a MATLAB program employing an Iterative Dynamic Programming (IDP) algorithm (Luus, 2000) based on Bellman's principle of optimality (Bellman, 1952). Using conventional dynamic programming a fine grid is required to ensure convergence to a global optimum increasing computation time. IDP, therefore, does not take into account a complete grid of feasible states but a single grid point. An initial guess for optimal control of the whole sequence provides the basis for an iterative procedure of piecewise constant control. Both, number of controls and increment can be defined. The number of control settings, thus the number of allowed speeds and headings, allows influencing computation time. Avgouleas considers accurate modeling of the ship's hydrodynamic behavior as important as mathematical modeling and the development of an efficient optimization algorithm. Thus, great attention is paid towards the ship hydrodynamics and wave modeling when aiming “to find the optimal combination of speed and heading to minimize fuel consumption.

Isopone Method

The isopone method defines planes of equal fuel consumption (energy fronts) instead of time fronts. As a result, the isopones are not two- but three-dimensional, because they are not only defined by location but also by time . Non-uniform weather conditions will not result in barrel-shaped energy fronts but the procedure is similar. The first isopone is determined by calculating the outer boundary of points reachable from the initial point with a fixed amount of fuel when heading roughly along the great circle. Then, all points on the first isopone are regarded as initial points and for each of them, an outer boundary of points reachable with an amount of fuel equivalent to the one considered in the first iteration is calculated. The second isopone is described by the envelope of the resulting energy fronts. Before the third isopone is calculated, several subsectors are defined by parabolic planes. In each subsector, the point of the boundary, which is closest to the destination, is chosen as an initial point for

the next iteration. This procedure is repeated until an isopone reaches the destination, after which the minimum fuel path may be reconstructed by tracing back the headings and speeds used to reach the point on the isopone tangent to the destination. If the final isopone surpasses the destination, it should be recalculated considering a smaller amount of fuel. In the case where the last isopone is plane, that is when the estimated time of arrival coincides with the time needed to travel along the minimum fuel path, the resulting path is not only fuel optimal but time optimal as well.

Original Isochrone Method

The isochrone method proposed by James (1957) is a practical deterministic method for finding the minimum time route obtained through varying ship headings while assuming constant engine power. The first isochrone or time front is formed by a line connecting points on the map that a ship departing from the starting port may reach at a specified time by traveling straight ahead in various directions and at constant engine power. Similarly, the next isochrone is calculated as a line connecting points, which may be reached at a specified time by a ship starting from the first isochrone and traveling straight ahead at constant engine power and in a direction perpendicular to the first isochrone. This process may be repeated until an isochrone coincides with the destination and the optimal route can be reconstructed. Implementation of this method for computer applications is problematic since so-called isochrone loops may occur.

Modified Isochrone Method

Hagiwara (1989) presents a modified isochrone method suitable for computerized calculation since it deterministically solves a discretized optimization problem containing a single-objective function and various constraints regarding time, position (latitude and longitude), control (heading and propeller revolutions) and ship motion (probabilities of slamming, shipping green water, propeller racing, etc). For this method, the great circle route between departure and destination as well as several great circle routes departing from the initial port at slightly different angles are used as reference. After the points forming the first isochrone have been calculated as in the basic isochrone method, these points are treated as initial points for the second iteration. Therefore, the points forming the second isochrone are not simply calculated by considering only paths departing perpendicularly with respect to the

first isochrone. Instead, all pathways along the great circle route leading to the point under consideration of the first isochrone as well as pathways departing at slightly varying angles are considered. In order to maintain a reasonable number of points forming each isochrone, the area around the great circle route coinciding with the destination is divided into subsectors defined by the previously described reference routes. The number of subsections may vary depending on the chosen number of reference routes and the subsector width, which in turn determine the accuracy of the result. Within each subsector, the point furthest along the great circle route connecting the departure point and the point under consideration is chosen to be part of the next isochrone. The selected points are then treated as initial points for the next iteration and the same procedure is repeated until the first point on an isochrone coincides with the destination. The optimal path may be found by tracing it back. In addition, an iterative procedure for finding not only a minimum time route but also a minimum fuel or minimum total cost route for a given estimated time of arrival is introduced. As the procedure, though, is based on the assumption of constant engine power, the resulting route does not actually minimize the fuel consumption. The reduced consumption results from the optimal path being the least fuel-consuming path for constant engine power providing on-time arrival. Similarly, a suboptimal minimum total cost route may be found by a cost comparison of the fastest routes found for various values of constant engine power.

3D Modified Isochrone Method

According to Lin et al. (2013) this method utilizes a so-called recursive forward technique with a floating grid system, which achieves a route meeting the estimated time of arrival "with minimum fuel consumption and minimum passage time based on the constraints of safety and land avoidance. Variables are the ship's speed and heading angle. It is "formulated as a multi-stage discrete process subjected to stochastic and dynamic condition". Thus, the floating grid system accounts for the dynamically changing environmental conditions. The stages are defined as the segments between two isochrones and are determined through the ship's speed in calm water. This also leads to an estimation of the arrival time considering speed and engine power constraints. Each stage consists of several states as also indicated by Hagiwara (1989). The states are defined by their location taking into account weather conditions, corresponding ship responses and speed as well as passage time and the diversion of the course angle from the great circle route, which is chosen as reference route, thus classifying the method as local search one. The speed in this case is influenced by the weather con-

ditions and is subject to voluntary and involuntary speed reduction. Considering the reduced speed, the actual position can be determined recursively. Moreover, the speed is discretized leading to a discrete optimization problem. A set of states at a certain time forms an isochrone. At each isochrone, computation time is reduced by choosing the state with the shortest distance along the great cirlce as new departure point. Consequently, optimal voyage progress and a weight are derived at each stage. The method allows determining routes of minimum time, minimum fuel consumption or minimum ship motions. Fang and Lin (2015) have developed two routing strategies to further improve the optimization of minimum time routes and minimum fuel routes, ETA (Estimated Time of Arrival) and FUEL.

Dijkstra's Algorithm

Dijkstra's algorithm for finding the shortest path between two given nodes in a graph with positive edge weights and with more edges than nodes provides a deterministic method for solving a discrete optimization problem consisting of one objective, e.g. minimum distance or time, and only implicitly defined constraints. In weather routing, Sen and Padhy (2015) apply Dijkstra's algorithm for finding the minimum time route in the North-Indian Ocean and Takashima et al. (2009) for determining the minimum fuel route considering variable heading in coastal shipping. Sen and Padhy (2015) assume a grid covering the region under consideration and define the present environmental conditions at each point, and thus in each square, of the grid based on a wave model. The grid provides a reference for a directed graph, which is composed of edges connecting the nodes defined by the midpoints of each square of the grid. For the weather routing problem, Sen and Padhy (2015) define the weights assigned to the edges as the time needed to travel along each edge. The required time is the distance between two nodes divided by the reduced speed. The reduced speed results from the ship's calm water speed for constant engine power as well as involuntary and/or voluntary speed reductions due to the present weather conditions or intentionally decreased speed to avoid potentially dangerous excessive motions. Natural geographical constraints are implicitly defined through the assignment of very large weights. Similarly, high wind velocities or wave heights imply large weights. Engine limits are not considered, because engine power is assumed constant (unless voluntary speed reduction occurs). As to Sen and Padhy (2015), the main disadvantage of the application of Dijkstra's algorithm is that the resulting path is not smooth. Takashima et al. (2009) address the minimum fuel consumption route problem for coastal merchant ships operating in confined waters by assuming

a constant number of propeller revolutions for each optimization run, while varying the heading. The speed is calculated depending on the heading and the weather conditions by applying speed reduction curves. Computing the ship's resistance and the required propeller thrust the fuel consumption can be derived. The number of propeller revolutions is gradually adjusted in each optimization run in order to meet the required time of arrival. The grid is defined by nodes with a spacing of two miles located on lines perpendicular to a defined standard route. Although this method leads to fuel savings particularly due to avoidance of strong opposite currents in the region of Japan as well as in the case of updated weather forecasts and subsequent rerouting, the obtained route is only a sub-optimal route and not a global optimum. Moreover, Takashima et al. (2009) as well as Sen and Padhy (2015) only deal with single-objective optimization problems .

Evolutionary Algorithms

Evolutionary algorithms may provide good approximate solutions of problems that cannot be solved easily by other methods. As stochastic local search methods, evolutionary algorithms are based on a randomly created initial population and further generations created by mutation, selection or reproduction mechanisms. Each population consists of individuals representing candidate solutions to the problem. A fitness parameter is assigned to every individual describing the quality of the specific solution. Individuals with the highest quality are selected as parents for a new generation. The process of producing generations is terminated when a satisfactory solution has been found. The level of satisfaction that the found solution achieves is highly dependent on the starting population and mutation function. Applied in weather routing methods the algorithm aims to solve multi-objective optimization problems, thus optimizing speed and course of the ship throughout its voyage.

In this thesis the problem of weather ship routing, formulated with regards to energy saving criteria, with the aid of a specific representation of the route based on Fourier sine series, is reduced to a finite variable optimization problem. The innovation of the present work is the efficient representation of every possible path (which is highly accurate, robust and quickly calculated), in conjunction with a Matlab-GUI implementation supporting the consideration of combined hindcast weather and geographical data, as well as ship responses to calculate the optimal route.

Chapter 2 is mainly concerned with hydrodynamics. The various components of ship resistance and their connection with propulsion system and propeller characteristics are discussed. Ideal flow hydrodynamics is briefly described as it serves as the standard method to derive numerical results concerning added resistance in waves.

Chapter 3 deals with the statistics and modeling of ocean waves. The energy spectrum definition is provided and the relation between the spectrum of the ship responses (included added wave resistance) and the input (sea condition) is presented, based on linear system analysis.

Chapter 4 provides some basic definitions about terminology and explanations on the ship routing problem, as treated in the present work. After that, the algorithm developed in this thesis is described in more detail.

Chapter 5 presents a numerical example/demonstration of the GUI tool developed for the ship routing problem in the case of a particular AFRAMAX ship and routes in Mediterranean Sea region.

The present thesis contains three Appendices. In Appendix A, the properties of the minimization method, in conjunction with the specific representation, are presented and discussed for specific problems from waves and mathematical physics, illustrating the performance of the present method in comparison with other numerical methods of solution. In particular the initial and boundary value problems of ray theory are considered, which present similarities with the studied problem. Also, variational formulation of Sturm-Liouville problems in the form of quotient minimization are considered and their solution by the present method is demonstrated and discussed in Appendix B. Finally, Appendix C is a small tutorial and explanation for the GUI software tool, containing also a description of the form of the input data.

Chapter 2

SHIP HYDRODYNAMICS

2.1 Calm Water Resistance

This term contains the steady components of the resistance of a ship and its main parts are: viscous resistance including frictional resistance and form drag and wave resistance (Lewis 1989). As it will be presented in more detail below, the first components are estimated by means of experimental methods and can be calculated by means of modern CFD methods, while the latter is still today treated by ideal flow methods, usually BEM. Also resistance in calm water is calculated from standard statistical methods (e.g., Holtrop 1984, FORMDATA series 60,..), which however provide only a rough estimation appropriate for preliminary ship design studies.

2.1.1 Frictional Resistance

Frictional resistance is the net forces upon the ship due to tangential shear stresses due to the viscosity of the fluid. Frictional resistance together with form drag (described below) accounts for large part of total resistance in slow-speed ships as in the case of oil tankers and as much as 50% in high-speed ships as in the case of container vessels and fast ferries. It is usually estimated as a function of Reynolds number

$$\mathrm{Re} = \frac{UL}{\nu} \tag{2.1}$$

where, U is the ship speed and L is the ship length, and ν is the kinematic viscosity of the fluid.

There exist many formulations for the calculation of the frictional drag. One commonly used is the ITTC 1957 model ship correction line,

$$C_F = \frac{0.075}{\left(\log_{10}\mathrm{Re} - 2\right)^2} \quad , \tag{2.2}$$

from which we obtain

$$R_F = \frac{1}{2}\rho S U^2 \quad , \tag{2.3}$$

where ρ is the fluid density and S is the wetted surface of the ship's hull.

2.1.2 Form Drag

In an ideal flow around a solid body the total kinetic energy of the fluid is converted to potential energy (in the form of high pressure) at the forward stagnation point. As the fluid moves around the body it gradually acquires kinetic energy at the expense of its potential energy. As it overcomes the maximum lateral dimension of the solid, the fluid is now moving around the back of it. In this part of the flow the motion is decelerated as a result of an adverse pressure gradient and potential energy (and pressure) starts building up again. In the absence of any loss mechanism the potential energy is fully recovered at the rear stagnation point where the fluid is at rest. Unlike an inviscid fluid, a real fluid would experience energy losses due to viscous dissipation. As a result, the fluid cannot fully regain its potential energy upon reaching the rear stagnation point. Instead, the flow separates earlier leaving turbulent wake, in which the average pressure is on the same order as the far field pressure.

This imbalance of pressure, namely high stagnation pressure at the front end and lower pressure on the back, manifests itself through an additional drag component called pressure drag or eddy resistance. Due to its strong dependence on the body geometry it is often called form drag. The calculation of pressure drag is an extremely difficult process. In most cases its dependence on Reynolds number is neglected and is lumped together with the wave resistance (Gillmer and Johnson, 1982). The calculation of both components (in the form of residuary resistance) can be achieved via model testing. An estimate is possible through statistical analysis of the model data (Holtrop and Mennen, 1982).

2.1.3 Wave Resistance

The ship as it travels, due to existence of the free surface, creates a flow disturbance. The resistance of the wave born this way is the wave resistance. This component, same as with 2.1.1 and 2.1.2, is also referring to the steady problem of ship traveling at constant speed U, so no ambient wave is implied.

The common way to calculate wave resistance is through model experiments. The respective combined drag coefficient C_R is assumed to depend only on the Froude number

$$Fn = \frac{U}{\sqrt{gL}} \tag{2.4}$$

The Froude hypothesis claims that the total resistance coefficient can be calculated as the sum of the frictional and residuary drag coefficients, as seen below

$$C_T\left(\mathrm{Re}, Fn\right) = C_F(\mathrm{Re}) + C_R(\mathrm{Fn}) \tag{2.5}$$

This approximation neglects correlation effects between viscosity and wave making resistance, yet it is invaluable in the estimation of total resistance in a towing tank.

Another possibility in common practice today is the calculation of wave resistance through the application of BEM and the calculation of the ship wave pattern. In this context the calm water resistance is mainly composed of wave-making and frictional resistance. For a given ship speed, frictional resistance is in proportion to the wetted surface area. However, wetted surface does not vary greatly for a given ship displacement, thus the decrease of frictional resistance is limited. However, for a given Froude number, wave-making resistance is extremely sensitive to the shape of the ship hull. Modification of the hull shape can obviously decrease wavemaking resistance, thus the calculation of wave-making resistance by numerical simulation is meaningful. The main difficulty is the nonlinearity of the boundary conditions. First, the shape of ship hull surface is nonlinear; second, the free surface boundary condition contains nonlinear terms; third, the free surface boundary is satisfied on exact free surface, which is not necessarily linear. The free surface can only be gotten after solving Laplace's equation, which makes the whole solution iterative. There is not a close form analytic solution to this highly nonlinear problem. The first stage of research is linear theory, which solves the problem on linearized ship hull and free surface boundary conditions, for example, Michell's thin ship theory. In linear theory, the Kelvin source is only distributed on flat plane. However, Linear ship theory is only effective under assumption that the ship form is linear and the free surface boundary condition is also linear. For realistic hull forms, these assumptions are violated, thus the linear theory can not give satisfactory result. After the linear theory, the Neumann-Kelvin method appeared. The Neumann-Kelvin method satisfies the hull surface boundary on the accurate hull surface but only satisfies the linearized free surface boundary condition on the calm water surface. In the Neumann-Kelvin method, the

point sources are distributed on the accurate ship hull surface, Havelock and Peters gave the analytic expressions for these point source. Noblesse analyzed these expressions and fitted them into a uniform form, which was the sum of three parts. The first part is the Rankine source component, it denotes the influence of point source in an infinite fluid domain, Hess and Smith gave the potential generated by such source distributed on flat panel. The second part is a double integral part, which represents the near-field influence of the point source in fluid domain with the free surface. Newman (1987) derived the result of near-field disturbance by a sum of Chebyshev series and a term for the singularity; Ponizy and Noblesse (1994) gave the result of the double integral by numerical interpolation. The third part is the single integral part, which represents the far-field influence. The highly oscillatory behavior of the integral brings difficulties in cultivations (JJM Baar et al. 1986/1988) One way to calculate this single integral is by the Chebyshev series. The other way is by numerical integral. One numerical method is adaptive integration (Milton Abramowitz and Irene A Stegun 1964). Oleg (2014) developed two efficient methods for this highly oscillatory integral. As the research of wave-making resistance develops, the totally nonlinear method came to being, which is called the Rankine source method. The Rankine source method satisfies the ship hull surface boundary condition on an accurate ship hull surface; and satisfies the nonlinear free surface boundary condition on the exact free surface. Since the free surface boundary condition is satisfied on the exact free surface, the process of calculation is iterative. The Rankine source methods requires the distribution of Rankine source both on ship hull surface and on exact free surface. Dawson (1977) calculated wave-making resistance by the Rankine source, however, he used linear free surface boundary condition. Raven (1996) and Janson (1997) developed the method of totally nonlinear approach by the Rankine source method. Hess used higher order panels in his research. The prevailing numerical methods of wave-making resistance are the Neumann-Kelvin method and the Rankine source method. Since the Rankine source method considers the nonlinear free surface boundary condition, theoretically it is more accurate than the Neumann-Kelvin method. However, the Neumann-Kelvin method only requires meshing on the ship hull surface. The Rankine source method needs meshing both on the ship hull and free surface. Both the hull surface and free surface need to be remeshed in every iteration. This brings difficulties in modeling and calculation. On the other side, Neumann-Kelvin method can work with other Kelvin source method to solve wave-current coupling problems. So there are pros and cons for these two methods, thus it is meaningful to test the limitations of these two methods. The published results about these two methods are limited.

2.1.4 Other Components

Besides the ones described above, other components of resistance are

1. Added Resistance in waves

2. Wind Resistance

3. Appendage Resistance

4. Resistance due to trim effects

5. Shallow water effects

Of the above components (1) and (2) are very connected with the ship in a seaway and also are found to be crucial in connection to the ship routing problem. For this purpose added wave resistance and wind resistance and are going to be described separately in sections 2.4,2.5 respectively. An additional effect which can be considered is the propeller performance in waves due to the vertical stern motion of the ship. An analysis concerning the effect of waves on the propeller performance is provided in Belibassakis et al (2013) where this issue is discussed in more detail .

2.2 Propulsion

The propulsion system is fundamentally related to the ship routing formulation since it affects the total resistance and the fuel consumption. Therefore in this section the mathematical description of the propeller action will be provided and its relation with the propulsion plant.

2.2.1 Propeller

Out of all the mechanisms that exist nowadays for ship propulsion, the propeller is by far the most commonly used. In order to study and characterize the geometry and performance of a propeller, we categorize them in methodical series (ex Wageningen B-Series), that contain charts of dimensionless quantities that define a propeller. Some of the most important are described below.

- Torque coefficient:

$$K_Q = \frac{Q}{\rho n^2 D^5} \tag{2.6}$$

where Q is the propeller torque , ρ the density of the water , D the diameter of the propeller disk, n the rotational speed.

- Thrust coefficient:

$$K_T = \frac{T}{\rho n^2 D^4} \tag{2.7}$$

where T is the propeller thrust.

- Advance ratio coefficient:

$$J = \frac{U_A}{nD} \tag{2.8}$$

where U_A is the speed of advance, which denotes the forward speed of the propeller relative to the water. The speed of advance is not equal to the speed of the ship. That is because as the ship moves, it drags the water around it. Therefore, the speed of advance is lower.

- Wake fraction:

$$w = \frac{U - U_A}{U} \tag{2.9}$$

- Open water efficiency coefficient:

$$\eta_o = \frac{P_T}{P_o} = \frac{\mathrm{T}U_A}{2\pi n Q_o} \tag{2.10}$$

where Q_o is the propeller toque as measured in the open water test and P_T, P_o are described in the section below.

- Thrust deduction factor:

$$t_d = \frac{k_p T - R}{k_p T} \tag{2.11}$$

where k_p is the number of propellers, T the thrust of each propeller and R the towing resistance of the ship. The reason that t is not equal to one, is because the operation of the propeller causes a drop of the pressure at the stern and modifies the tangent strain, increasing the resistance.

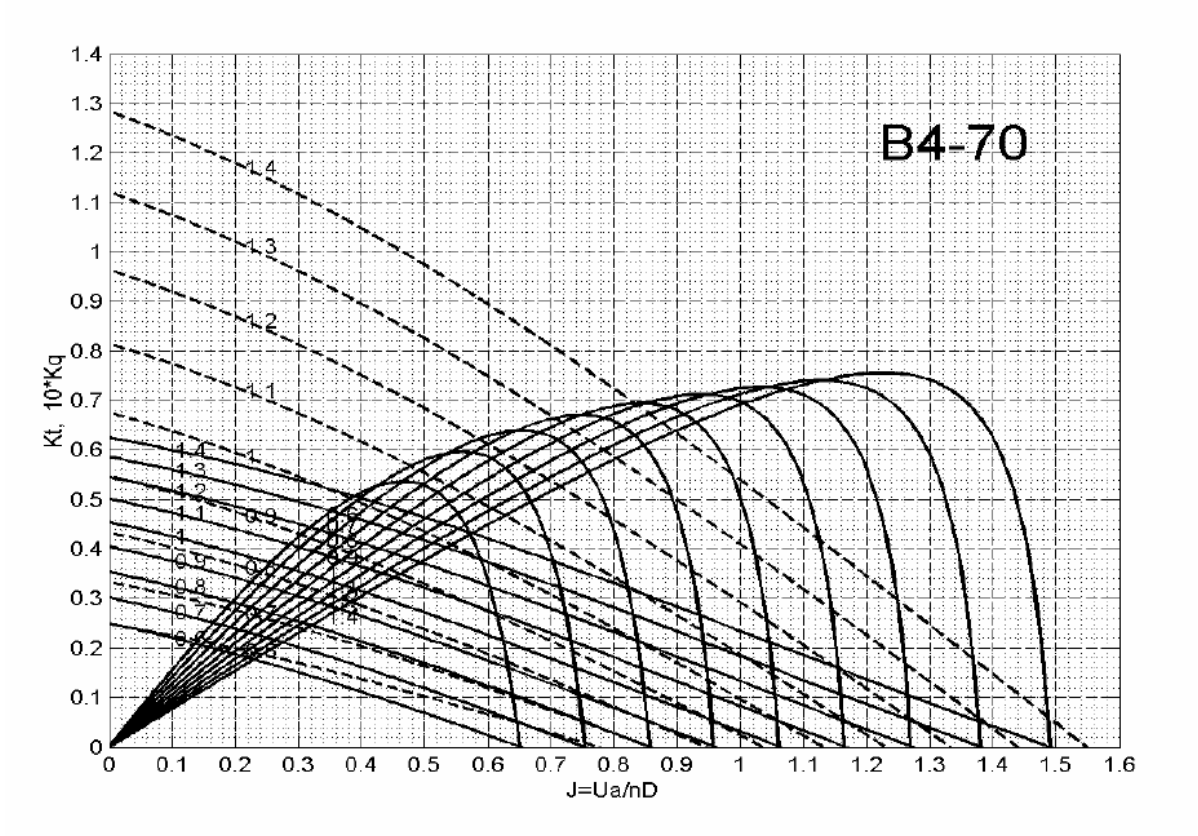

Figure 2.1 Example of a propeller chart (Wageningen B-series, 4-bladed EAR=70%).

- Expanded Area ratio:

$$EAR = \frac{A_E}{A_o} \tag{2.12}$$

where A_E is the expanded area of the blades and $A_o = \pi D^2 / 4$ the area of the propeller disk.

- Pitch Ratio:

$$PR = \frac{P}{D} \tag{2.13}$$

where P is the propeller pitch.

2.2.2 Propulsion Plant

In this section the typical propulsion system of a ship with one main engine as a prime mover will be described.

The *effective power* of an engine is the power required to tow the ship at speed V.

$$P_E = EHP = R \cdot U \tag{2.14}$$

where R is the towing resistance of the ship.

For a shelf-propelled ship the *thrust power* delivered by the propeller is equal to

$$P_T = T \cdot U_A \tag{2.15}$$

For reasons mentioned before, the powers P_E and P_T are not equal due to the present of the wake and the increase of resistance (thrust deduction). Thus, the *hull efficiency coefficient* is defined by

$$\eta_H = \frac{P_E}{P_T} = \frac{R \cdot U}{T \cdot U_A} = \frac{1 - t_d}{1 - w} \tag{2.16}$$

In (2.10) the definition of open water coefficient was given. Its meaning is that in order to get power P_T out of a propeller in open water operating at a nominal efficiency η_o, one has to rotate it in the water at speed n ,while applying a torque Q_o, satisfying the η_o ratio

$$\eta_o = \frac{P_T}{P_o} = \frac{\mathrm{T}U_A}{2\pi n Q_o} \tag{2.10}$$

However, due to the existence of the hull the required torque for propulsion is higher than Q_o and is denoted as M_P . The input power to the propeller is not the open water P_o, but the *propeller power* defined as:

$$P_P = 2\pi n M_P \tag{2.17}$$

The efficiency that results from this is called *relative rotative efficiency*

$$n_R = \frac{P_o}{P_P} = \frac{Q_o}{M_P} \tag{2.18}$$

The energy losses due to frictions in struts, bearings and stern tubes can be expressed with the use of the *shaft efficiency*

$$\eta_s = \frac{P_P}{P_S} \tag{2.19}$$

where P_S or *shaft power* is P_P plus the aforementioned losses and is the energy required from the shaft in order for the propeller to provide power P_P. Also for the P_S we have

$$P_S = SHP = 2\pi n M_S \tag{2.20}$$

Another coefficient that will appear in our formulation is the *specific fuel consumption* (*sfc) a*nd is associated with the conversion of the fuel's chemical energy into mechanical work. It is provided by the engine manufacturer usually in g/kWh and corresponds to how much fuel is consumed in one hour for every unit of engine power in kW. For a diesel engine this parameter is roughly constant for different service conditions and in this work it is considered constant.

2.3 Ship Dynamics in Waves

2.3.1 Harmonic waves

Potential flow theory provides the framework for the mathematical formulation of water waves. Assume an earth fixed coordinate system $Oxyz$, where $z = 0$ corresponds to the free surface at rest.

In the ideal flow the water is incompressible and has zero viscocity. If we also assume irrotanionality

$$\nabla \times \mathbf{v} = 0 \tag{2.12}$$

Then, by Helmholtz decomposition, there exists a potential function $\Phi = \Phi(x, y, z)$, such as

$$\mathbf{v} = \nabla \Phi \tag{2.13}$$

Using irrotationality assumption, the condition of conservation of mass

$$\nabla \mathbf{v} = \mathbf{0} \tag{2.14}$$

becomes the Laplace equation

$$\nabla^2 \Phi = 0 \tag{2.15}$$

The conservation of momentum is as follows:

$$\frac{\partial \mathbf{v}}{\partial t} = -(\mathbf{v} \cdot \nabla) \cdot \mathbf{v} - \frac{1}{\rho} \nabla p + \mathbf{g} \tag{2.16}$$

where ρ is the water density, $\mathbf{g}$ the gravitational (vector) acceleration and p is the fluid pressure field.

Inserting (2.13) to (2.16) and using vector calculus yields the *Bernoulli* equation:

$$\frac{\partial \Phi}{\partial t} + \frac{1}{2}\nabla \Phi^2 + \frac{p}{\rho} + gz = const. \tag{2.17}$$

Let $\eta(\mathrm{x}, \mathrm{y})$ be the wave elevation of the free surface. Every particle of the free surface must stay there at all times. In mathematical formulation this means that the total derivative of $\eta - z$ must be equal to 0. This is known as the free surface kinematic boundary condition.

$$\frac{D}{Dt}(\eta - z) = 0 \quad \text{on } z = \eta \tag{2.18}$$

The dynamic boundary condition on the free surface equalizes the fluid pressure on the free surface and the atmospheric pressure.

$$p\big|_{z=\eta} = p_{atm} \;\Rightarrow\; -\rho\left(\frac{\partial \Phi}{\partial t} + \frac{1}{2}\nabla \Phi^2 + gz\right)\Bigg|_{z=\eta} = p_{atm} \tag{2.19}$$

The equation (2.15) with the boundary conditions (2.18) and (2.19) formulate the nonlinear wave boundary value problem for deep water.

Assuming small wave slopes and linearizing the free surface conditions around $z = 0$, the BVP system becomes:

$$\begin{aligned}
&\nabla^2 \Phi = 0, && z \le 0 \\
&\frac{\partial \Phi}{\partial t} + g\eta = 0, && z = 0 \\
&\frac{\partial \eta}{\partial t} = \frac{\partial \Phi}{\partial z}, && z = 0 \\
&\left|\nabla \Phi\right| \to 0, && z \to -\infty
\end{aligned} \tag{2.20}$$

The solution to the aforementioned (2.20) deep water BVP (Newman 1977) is:

$$\Phi(x, y, z, t) = \mathrm{A}\,.\,\mathscr{Re}\left\{\frac{ig}{\omega} e^{kz - i\left[k(x\cos b + y\sin b) - \omega t\right]}\right\} \tag{2.21}$$

and

$$\eta = \mathrm{A}\cos\left(kx - \omega t\right) \tag{2.22}$$

Where ω is an arbitrary wave angular frequency, b is the wave propagation angle with respect to x' axis and k is the wavenumber.

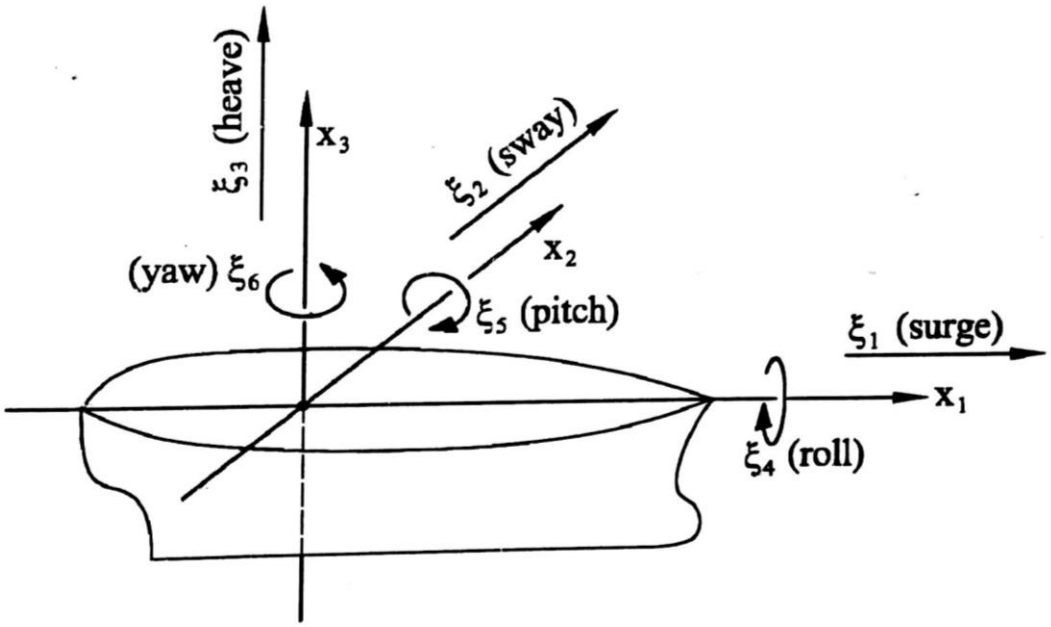

Figure 2.2 Ship's degrees of freedom (from Athanassoulis & Belibassakis 2012)

The dynamic and kinematic conditions can be combined into a single free surface condition

$$\frac{\partial^2 \Phi}{\partial t^2} + g\frac{\partial \Phi}{\partial z} = 0, \quad z = 0 \tag{2.23}$$

From which the dispersion relation is derived

$$\omega^2 = gk \tag{2.24}$$

The dispersion relation is used in order to find the corresponding wave numbers for different ω . Also, we denote by $\lambda = \frac{2\pi}{k}$ as the wavelength .

2.3.2 Linear Wave-Body Interaction

Within linear theory the ship can be modeled as a linear time-invariant hydromechanical oscillator with six degrees of freedom as shown in figure below. We start by considering the more simple case of the dynamics of a floating object with zero mean speed and the effect of forward speed in the case of a ship traveling in waves will be examined below in Sec.2.3.3.

In analogy to the simple mass-string-dashpot dynamical system the ship is subjected to:

- Inertial forces acting on the solid mass and hydrodynamic added mass
- Damping forces arising from the energy dissipation during wave making.
- Hydrostatic restoring forces
- Extrernal excitation forces

The general time domain equations of motion can be written as

$$\left[\sum_{j=1}^{6}\left(M_{ij}+A_{ij}\right)\frac{d^2\xi_j(t)}{dt^2}+B_{ij}\frac{d\xi_j(t)}{dt}+C_{ij}\xi_j(t)\right]=F_i(t) \qquad i=1,2,...,6\,, \tag{2.25}$$

where ξ_j are the generalized modes of freedom, M_{ij} and A_{ij} are the mass and added mass matrixes respectively, B_{ij} is the damping matrix, C_{ij} is the hydrostatic stiffness matrix and F_i the generalized excitation forces (Athanassoulis & Belibassakis 2012). The term generalized modes of freedom means that ξ_j can be both displacements and rotations and F_i are the corresponding generalized forces (forces and moments).

Although (2.25) holds for harmonic ξ_i , it is possible within linear theory to superimpose harmonic responses in order to obtain a general function of time. Also, a harmonic input in a linear time invariant system will result in a harmonic output with a phase shift.

The exciting forces consist of three components: one due to the incident wave impacting the ship called *Froude-Krylov* force, another one due to the wave diffraction forces and the one due to radiation forces.

The *Froude–Krylov* force , denoted as F_j^{FK} can be calculated by direct integration of the pressure around the mean wetted surface of the body (∂D_B):

$$F_j^{FK}=\iint_{\partial D_B} p_I n_j dS \tag{2.24}$$

where n_j is the j^{th} component of the generalized unit vector normal with regards the ship's wetted surface.

$$n_j=n_j,\quad j=1,2,3 \tag{2.25a}$$

$$n_j=\left|\mathbf{x}\times\mathbf{n}\right|_{j-3},\quad j=4,5,6 \tag{2.25b}$$

and

$$p_I=-\rho\frac{\partial\Phi_{\mathrm{I}}}{\partial t} \tag{2.26}$$

where Φ_{I} is the incidence wave potential given by (2.21).

The force is considered harmonic and can be expressed as follows

$$F_j^{FK} = \mathscr{Re}\left\{ X_j^{FK}(\omega)\, \mathrm{e}^{i\omega t} \right\} \tag{2.27}$$

Similar relations also hold for the diffraction force, denoted as F_j^D :

$$F_j^D = \iint_{\partial D_B} p_D n_j dS \tag{2.28}$$

And the linearized Bernoulli is used for expressing the dynamic pressure

$$p_D = -\rho \frac{\partial \Phi_D}{\partial t} \tag{2.29}$$

Φ_D can be acquired by solving the following BVP problem:

$$\nabla^2 \Phi_D = 0, \qquad z \le 0 \tag{2.30a}$$

$$\mathbf{n} \nabla \Phi_D = -\mathbf{n} \nabla \Phi_I, \quad \text{on } \partial D_B \tag{2.30b}$$

$$\left(\frac{\partial^2}{\partial t^2} + g \frac{\partial}{\partial z} \right) \Phi_D = 0, \text{ on } z = 0 \tag{2.30a}$$

As in (2.27) the diffraction forces can be written as:

$$F_j^D = \mathscr{Re}\left\{ X_j^D(\omega)\, \mathrm{e}^{i\omega t} \right\} \tag{2.31}$$

The radiational potential formulation is a little more complicated than the previous ones. Let the ship oscillate at a given angular frequency ω and amplitude over of the an not excited by other means water. After some time, when only steady phenomena are left, the water, due to linearity, will also oscillate at the same frequency ω. The total radiation potential is denoted Φ_R. We assume the following linear decomposition of Φ_R:

$$\Phi_R = \sum_{k=1}^{6} \dot{\xi}_\kappa \Phi_k(\mathbf{x}) \tag{2.32}$$

where Φ_k unknown functions.

The radiation potential must satisfy the “no slip” condition :

$$\mathbf{n} \nabla \Phi_R = \sum_{k=1}^{6} \dot{\xi}_k n_k \tag{2.33}$$

By inserting (2.32) into (2.33) we get

$$\mathbf{n} \nabla \Phi_R = n_k \qquad k = 1, 2, ..., 6 \tag{2.34}$$

Therefore, the radiation potential can be found by solving the following BVP for $k = 1, 2, ..., 6$:

$$\nabla^2 \Phi_k = 0 \qquad z \le 0 \tag{2.45a}$$

$$\mathbf{n} \nabla \Phi_k = n_k \quad \text{on } \partial D_B \tag{2.45b}$$

$$\left(\frac{\partial^2}{\partial t^2} + g \frac{\partial}{\partial z} \right) \Phi_k = 0, \quad \text{on } z = 0 \tag{2.45c}$$

In addition to the above eq (2.45) the diffraction potential must also satisfy the Sommefeld radiation condition at infinity (see, e.g., Athanassoulis & Belibassakis 2012).

The total exciting force, denoted as F_j will be the sum:

$$F_j = \mathscr{R}e\left\{ X_j(\omega) \mathrm{e}^{i\omega t} \right\} = \mathscr{R}e\left\{ \left[X_j^{FK}(\omega) + X_j^{D}(\omega) \right] \mathrm{e}^{i\omega t} \right\} \tag{2.46}$$

By considering harmonic representation for the responses:

$$\xi_j = \mathscr{R}e\left\{ \Xi_j(\omega) \mathrm{e}^{i\omega t} \right\} \tag{2.47}$$

where $\Xi_j(\omega)$ are the corresponding complex amplitudes of the responses, and usingthe complex forms of (2.48) and (2.50), the equation of motion (2.25) becomes:

$$\sum_{j=1}^{6} \left[-\omega^2 \left(\mathrm{M}_{kj} + A_{kj}(\omega) \right) + i\omega B_{kj}(\omega) + C_{kj} \right] \Xi_j(\omega) = X_k(\omega) \qquad k = 1, ..., 6 \tag{2.49}$$

where the hydrodynamic coefficients A_{kj}, B_{kj} are computed by solving the radiation BVP.

2.3.3 Ship Seakeeping

Assume a ship-fixed coordinate system Oxyz. The plane z = 0 coincides with the water surface and, together with the ship, the coordinate system is translating with forward speed U in the x-direction. Harmonic wave of absolute frequency ω_o propagates in a direction b relative to the x-axis. The moving reference frame is related to the earth-fixed OXYZ via the Galilean transformation (Sclavounos, 2007)

$$\mathrm{X} = x + Ut \ , \ Y = y \ , \ Z = z \tag{2.50}$$

Substituting (2.52) in (2.21) the wave potential is expressed in the moving frame

$$\Phi\left(x,\ y,\ z,t\right) = \frac{Ag}{\omega_0}\mathscr{R}e\left\{ie^{kz-ik\left(x\cos b+y\sin b\right)-i\left(kU\cos b-\omega_o\right)t}\right\} \tag{2.51}$$

Equation (2.48) assumes the exact same form as (2.35). The difference lies in the frequency of the time harmonic term. It is no longer the absolute wave frequency ω_0, but the encounter frequency defined as

$$\omega = \omega_0 - kU\cos b \tag{2.52}$$

It follows that the wave elevation can now be expressed relative to the moving frame as

$$\eta(\mathrm{x,y,t}) = A\mathscr{R}e\left\{\frac{ig}{\omega_0}e^{-ik\left(x\cos b+y\sin b\right)+i\omega t}\right\} \tag{2.53}$$

The total velocity potential can be decomposed as:

$$\Phi(\mathbf{x},t) = \bar{\Phi}(\mathbf{x}) + \varphi(\mathbf{x},t) \tag{2.54}$$

The first term on the right-hand side represents the steady flow potential. It can be further decomposed into a basis flow $\bar{\varphi}$ and a disturbance flow ψ :

$$\bar{\Phi}(\mathbf{x}) = \bar{\varphi}(\mathbf{x}) + \psi(\mathbf{x},t) \tag{2.55}$$

The decomposition facilitates the linearization of the nonlinear steady flow around the basis flow, assuming that ψ is small compared to $\bar{\varphi}$ (Nakos and Sclavounos, 1990). It is noted here that if the parallel flow is used as basis flow $\bar{\varphi}(\mathbf{x}) = -Ux$ and $\psi = 0$, the problem reduced to Neumann-Kelvin formulation. Together with the free surface condition, the field equation and the radiation condition the formulated BVP can be numerically solved. The solution $\bar{\Phi}$ represents the potential of a steady, outgoing wave pattern known as the Kelvin wake.

The second term on the right-hand side of (2.54) is a time-dependent potential associated with the wave excitation, and is expressed as:

$$\varphi(\mathbf{x},t) = \mathscr{R}e\left\{\tilde{\varphi}(\mathbf{x})e^{i\omega t}\right\}$$

where ω is the frequency of encounter. This expression is the cornerstone of the frequency domain formulation of the linear seakeeping problem. It is assumed that under the incidence of monochromatic plane waves of frequency ω_o , the ship undergoes small oscillations at

frequency ω . The complex potential $\tilde{\varphi}$ is a superposition of the incident wave potential $\tilde{\varphi}_I$, the diffraction potential $\tilde{\varphi}_D$ and the radiation potentials $\tilde{\varphi}_j$, $j=1,2,...,6$ for all modes of motion

$$\tilde{\varphi}=\tilde{\varphi}_I+\tilde{\varphi}_D+\sum_{j=1}^{6}\tilde{\varphi}_j \tag{2.56}$$

Upon solving the relevant BVP's for all the (complex) potentials in (2.56), pressure can be calculated from Bernoulli equation. Then, by integration over the hull mean wetted surface ∂D_B , the forces can be obtained. An outline of the procedure is as presented below. Using the appropriate version of the Bernoulli equation in the ship-fixed frame of reference travelling at constant speed U , we obtain the pressure associated with the incident and the diffraction potenrial

$$\tilde{p}=-\rho\left(i\omega-U\frac{\partial}{dx}\right)\left(\varphi_I+\tilde{\varphi}_D\right) \tag{2.57}$$

and the calculation of the exciting forces (Froude-Krylov and diffraction components) is obtained by pressure integration of the wetted surface of the hull,

$$X_j=\iint_{\partial D_B}\tilde{p}n_j dS \tag{2.58}$$

These forces are balanced by inertial, damping and hydrostatic restoring forces by virtue of Newton's law. The equations of motion are

$$\sum_{j=1}^{6}\left[-\omega^2\left(M_{kj}+A_{kj}(\omega)\right)+i\omega\left(B_{kj}+UN_{ij}\right)(\omega)+C_{kj}\right]\Xi_j(\omega)=\mathrm{X}_k(\omega)\quad k=1,...,6 \tag{2.59a}$$

from which the corresponding Response Amplitude Operators are calculated as follows

$$RAO_j(\omega)=\frac{|\Xi_j|}{A},\ j=1,2,3,\ RAO_j(\omega)=\frac{|\Xi_j|}{kA},\ j=4,5,6 \tag{2.59b}$$

In this case, however, ω stands for the encounter frequency, not the absolute frequency of the ambient wave. In the examined case, the added mass and damping coefficients A_{kj}, and B_{kj} are computed by solving the corresponding radiation BVPs. Once the radiation potentials are known, the complex amplitudes of the respective forces are calculated:

$$\tilde{F}_k = \iint_{\partial D_B} \tilde{p} n_j dS = \iint_{\partial D_B} \hat{p}_j \Xi_j n_k dS = \Xi_j \left(\iint_{\partial D_B} \hat{p}_j n_k dS \right) \tag{2.60}$$

where

$$\hat{p}_j = -\rho \left(i\omega - U \frac{\partial}{dx} \right) \hat{\varphi}_j \tag{2.61}$$

and

$$\tilde{\varphi}_j = \Xi_j \hat{\varphi}_j \tag{2.62}$$

where, in the case of ship hulls of relatively slim form $\hat{\varphi}_j$ are approximately obtained as the solution of the Laplace equation(s) $\nabla^2 \hat{\varphi}_k = 0$, with boundary condition $\left[\left(j\omega - U \frac{\partial}{\partial x_1} \right)^2 + g \frac{\partial}{\partial x_3} \right] \hat{\varphi}_k = 0$, on the free surface, and $\frac{\partial \hat{\varphi}_k}{\partial n} = n_k$, $k = 1,2,3,4$, $\frac{\partial \hat{\varphi}_5}{\partial n} = n_5 + \frac{U}{j\omega} n_3$ and $\frac{\partial \hat{\varphi}_6}{\partial n} = n_6 - \frac{U}{j\omega} n_2$, on the wetted surface of the ship hull, in conjunction with appropriate radiation conditions. Finally, added mass and damping components are obtained by pressure integration on the ship's hull

$$\iint_{\partial D_B} \hat{p}_k n_j dS = \omega^2 A_{kj}(\omega) - i\omega B_{kj}(\omega) \tag{2.63}$$

2.4 Added Wave Resistance

We will now deal with the calculation of the ship's added resistance due to waves and the resulting oscillation. During travel in wavy seas the propulsion system has to overcome the calm water resistance and the added wave resistance. The added resistance plays a major role in the ship routing with minimum fuel consumption. We shall consider the case of incident waves with $b = 180^o$.

Many different formulations and methods been proposed to calculate the added wave resistance (see Arribas 2007). From previous experience it has been shown that the following energy method, due to Gerritsma & Beukelman (1972), despite being simple it gives very satisfactory results with good accuracy.

According to the aforementioned formulation, in the case of front incident waves, the energy

$$E_{AW} = R_{AW}(U + c)T_m = R_{AW}\lambda \tag{2.64}$$

associated with the added resistance R_{AW} in monochromatic harmonic waves , during one time period T_m, corresponds to the wave energy radiated far away from the ship due to the vertical speed oscillations with regards to the free surface elevation oscillation of the incident wave.

The vertical speed of every transverse section along the length of the ship is given:

$$V_R = \frac{d\xi_R}{dt}(x,t),$$

where $\xi_R(x,t) = (\xi_3 - \mathrm{x}\,\xi_5 - \eta(x,\mathrm{t})\mathrm{e}^{i\omega t})$

$\xi_{3,}\xi_5$ is the heave and pitch respectively, and $\eta(x,t) = \mathrm{A}e^{i(\mathrm{k}_0\mathrm{x}+\omega\,\mathrm{t})}$ the free surface elevation due to the incident wave. We remind that $\omega = \omega_0 + k_0 U$ is the encounter frequency and $k_0 = \frac{\omega_0^2}{g}$ the wavenumber. The radiated energy during one time period due to the vertical oscillations of the ship is:

$$E = \frac{\pi}{\omega}\int_L b_{33}(x_1)\bar{V}_R^2 dx_1, \tag{2.65}$$

where $b_{33}(x_1)$ the damping coefficient of every transverse section in vertical oscillation and $\bar{V}_R^2$ the mean square value of the relative speed. From (2.66) and (2.67) we get the following expression for the calculation of the added resistance:

$$R_{AW} = \frac{\pi}{\lambda\omega}\int_L b_{33}(x_1)\bar{V}_R^2 dx_1, \tag{2.66}$$

where $\lambda = 2\pi/k_0$.

It is noted that in high magnitude waves the added resistance is comparable to the calm water resistance. This shows the importance of well posing and calculating of the added resistance, especially when it comes to the ship routing problem where the fitting function itself depends on R_{AW} . An example of calculation is presented in Figs. 2.3 and 2.4.

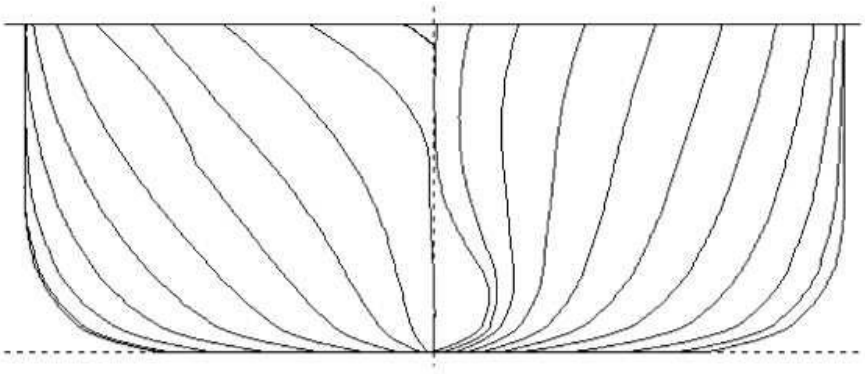

Figure 2.3 Tranverse section of a ship (from Arribas 2007)

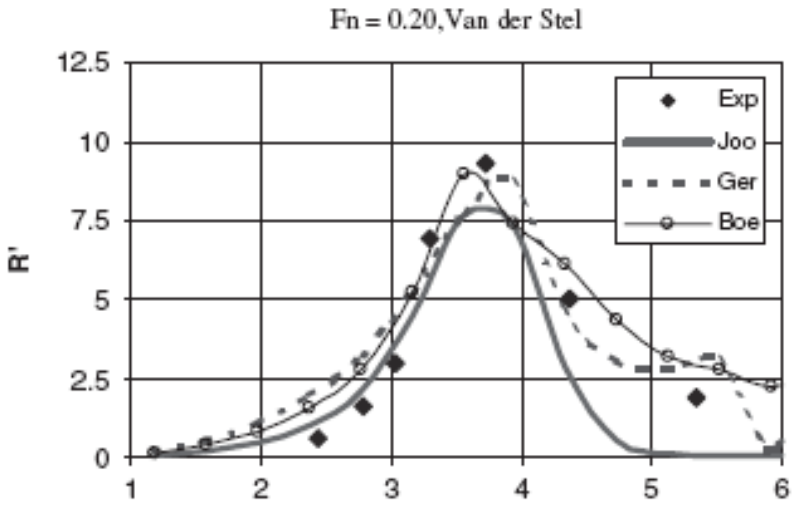

Figure 2.4 Comparison of added wave resistance calculations for the ship of Fig 2.3 with experimental data for different values of the dimensional frequency and for two values of Froude number $Fn = 0.20$, (from Arribas 2007).

2.5 Wind Resistance

A ship sailing on a smooth sea and still air experiences a resistance due to the movement of the above –water hull through air. This resistance depends on the ship's speed and on the area and shape of the upper works. In the case of blowing wind the resistance also depends on the wind speed and its relative direction according to the ship.

In this work we are going to use a heuristic approximation of the wind resistance (PNA Vol.II, p.31) due to Hughes, (Lewis 1989) and it is as follows (see also Figs.2.5 and 2.6):

$$F = \frac{K\rho_a (U_R{}^2)\left(A_L \sin^2(\theta) + \mathrm{A_T}\cos^2(\theta)\right)}{\cos(a-\theta)} \tag{2.67}$$

where F is the wind resistance, ρ_a is the air density, U_R, θ is the value and angle (with respect to the ship) relative wind speed, a is the true wind angle, A_T is the transverse projected area and A_L is the longitudinal projected area of the ship. The constant K takes values between for 0.5-0.65 for normal designs and in this work we take $K = 0.6$.

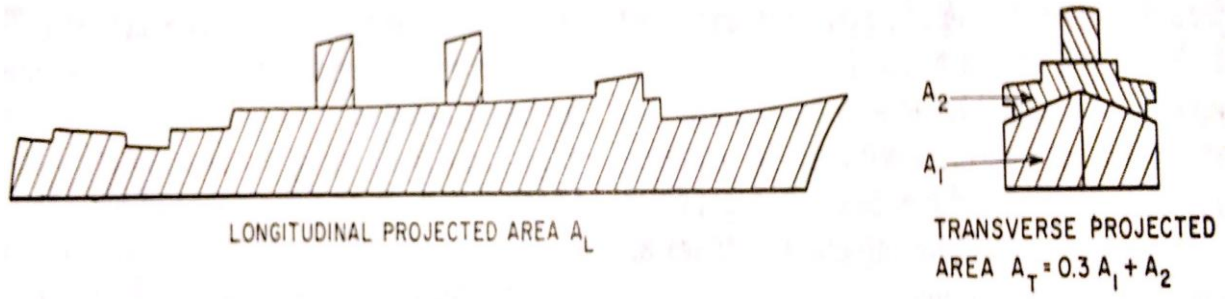

Figure 2.5 Definitions of A_T, A_L (from PNA vol. II, Lewis 1989)

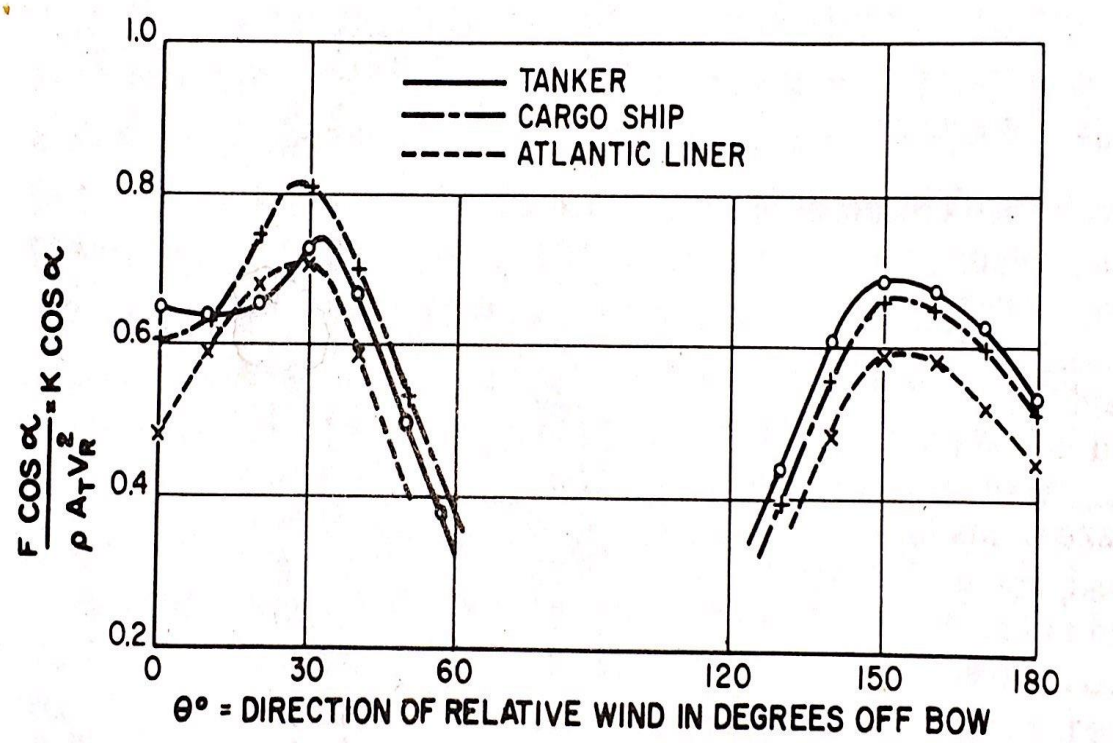

Figure 2.6 Resistance coefficients for relative wind ahead or astern (from PNA vol.II, Lewis 1989).

Chapter 3

OCEAN WAVES MODELING

In this section we will define the sea wave spectrum, its statistical properties and characteristics. We will also define the parameters required to model the sea state (important wave height and time period) and describe how it is applied to the ship optimal routing.

3.1 Statistical Representation of Ocean Waves

Assuming a fix point on the surface of the sea (deep water) denoted as $\mathbf{x}$, stochastic representation of the elevation of that point can be achieved by the following random-phase model:

$$\zeta_{\mathbf{x}}(t;\beta) = \sum_{n} A_n \cos\left(\omega_n t + \Theta_n(\beta)\right) \tag{3.1}$$

where $\omega_n = \sqrt{k_n g}$ are deterministic quantities that are paying the role of the frequencies of each wave, A_n are also deterministic and quantify the magnitudes of each harmonic wave and $\Theta_n(\beta)$ are random variables that affect the various phases of each term and are considered to be:

- Independent.
- All $\Theta_n(\beta)$ have the same distribution.
- Each $\Theta_n(\beta)$ is uniformly distributed on $[0, 2\pi]$.

For the sake of completeness in the presentation we give below the following definitions:

1. *Mean value* of a stochastic process $\zeta_x(t,\beta)$ as in (3.1) and is denoted as $m_{\zeta_x}(t)$ or $E^{\beta}\left[\zeta_x(t,\beta)\right]$

$$m_{\zeta_x}(t) = E^{\beta}\left[\zeta_x(t,\beta)\right] = \int_{-\infty}^{\infty} x f_t(x) dx \tag{3.2}$$

where $f_t(x)$ is the probability density function of the random variable $\zeta_x(t,\beta)$, $t = const.$

2. *Variance* of a stochastic process $\zeta_x(t,\beta)$

$$\sigma^2_{\zeta_x} = \mathrm{E}^{\beta}\left[\left(\zeta_x(t,\beta) - m_{\zeta_x}(t)\right)^2\right] = \int_{-\infty}^{\infty}\left(x - m_{\zeta_x}(t)\right)^2 f_t(x)dx \tag{3.3}$$

3. *Correlation* of a stochastic process $\zeta_x(t,\beta)$

$$R_{\zeta_x\zeta_x}(t_1,t_2) = E^{\beta}\left[\zeta_x(t_1,\beta)\zeta_x(t_2,\beta)\right] = \iint_{R^2} x_1 x_2 f_{t_1t_2}(x_1,\mathrm{x}_2)d\mathbf{x} \tag{3.4}$$

where $f_{t_1t_2}(x_1,\mathrm{x}_2)$ is the joint probability density function of $\zeta_x(t_1,\beta),\zeta_x(t_2,\beta)$.

4. *Covariance* of a stochastic process $\zeta_x(t,\beta)$

$$C_{\zeta_x\zeta_x}(t_1,t_2) = E^{\beta}\left[\left(\zeta_x(t_1,\beta) - \mathrm{m}_{\zeta_x}(t_1)\right)\left(\zeta_x(t_2,\beta) - \mathrm{m}_{\zeta_x}(t_2)\right)\right] =$$

$$= \iint_{R^2}\left(x_1 - \mathrm{m}_{\zeta_x}(t_1)\right)\left(x_2 - \mathrm{m}_{\zeta_x}(t_2)\right) f_{t_1t_2}(x_1,\mathrm{x}_2)d\mathbf{x} \tag{3.5}$$

Random sea waves are assumed an ergodic process, which allows the extraction of statistics not from the ensemble (as should be formally done) but from a single realization by time averages (Ochi, 1998). If all the statistics of a process are time invariant then the process is stationary. Ocean waves are only weakly stationary as the first two moments (namely the mean and the covariance) are time invariant. Also the Central Limit Theorem guarantees that the sum of many identically distributed, independent random variables (or processes) is itself a Gaussian random variable (or process) with mean and variance which are the sums of the means and variances of the individual constituent variables. In this sense, the process defined in (3.1) can be treated as normally distributed with zero mean. Therefore, for the random phase model we have:

$$m_{\zeta_x}(t) = 0 \tag{3.6}$$

$$R_{\zeta_x\zeta_x}(t_1,\tau+t_1) = R_{\zeta_x\zeta_x}(\tau) \tag{3.7}$$

$$C_{\zeta_x\zeta_x}(t_1,\tau+t_1) = R_{\zeta_x\zeta_x}(t_1,\tau+t_1) = R_{\zeta_x\zeta_x}(\tau) \tag{3.8}$$

We can now define the spectrum of the water wave free surface elevation by means of the cosine Fourier transform of the correlation function $C_{\zeta_x\zeta_x}(\tau)$ of the stationary stochastic process $\zeta_{\mathbf{x}}(t;\beta)$. The *spectral density function* of $C_{\zeta_x\zeta_x}(\tau)$ is denoted simply as $S_{\zeta_x\zeta_x}(\omega)$.

By the Wiener-Khinchin theorem (Ochi, 1998) we have that for the random phase waves the autocorrelation and spectral density are Fourier transform pairs, namely:

$$S_{\zeta_x\zeta_x}(\omega) = \frac{2}{\pi}\int_0^\infty C_{\zeta_x\zeta_x}(\tau)\cos(\omega\tau)\,d\tau \tag{3.9}$$

$$C_{\zeta_x\zeta_x}(\tau) = \frac{2}{\pi}\int_0^\infty S_{\zeta_x\zeta_x}(\omega)\cos(\omega\tau)\,d\omega \tag{3.10}$$

The n^{th} spectral moment is defined as:

$$m_n = \int_0^\infty \omega^n S_{\zeta_x\zeta_x}(\omega)\,\mathrm{d}\omega \tag{3.11}$$

From this definition two useful spectral characteristics are extracted, which are later used extensively in the routing problem. Their definitions are provided below (Massel, 1996).

Significant Wave Height:

$$H_s = 4\sqrt{m_0} \tag{3.12}$$

where $m_0 = \int_0^\infty S_{\zeta_x\zeta_x}(\omega)\,\mathrm{d}\omega$ as seen in (3.11).

Mean Frequency:

$$\bar{\omega} = \frac{m_1}{m_o} \tag{3.14}$$

Modal frequency/Period (ω_p, T_p) :

It is defined as the frequency for which $S_{\zeta_x\zeta_x}(\omega)$ becomes maximum. If $S_{\zeta_x\zeta_x}(\omega)$ is differentiable then it can be found as the solution of

$$\frac{dS_{\zeta_x\zeta_x}}{d\omega} = 0$$

and keeping only the solutions that correspond to local minimum. Also, the modal time period is defined as $T_p = \frac{2\pi}{\omega_p}$.

3.2 System theory and output spectrum

In this subsection we shall provide the response of a linear oscillator, denoted $Y(t;\beta)$, excited by a random force $X(t;\beta)$. This is written in the form:

$$m\ddot{Y}(t;\beta)+b\dot{Y}(t;\beta)+cY(t;\beta)=X(t;\beta) \tag{3.15}$$

Assuming that $X(t;\beta)$ is expressed by a random phase model we have:

$$X(t;\beta)=\sum_n A_n\cos\left(\omega_n t+\Theta_n(\beta)\right) \tag{3.16}$$

Due to the linearity of (3.9) , if $Y_n(t;\beta)$ is the solution of

$$m\ddot{Y}_n(t;\beta)+b\dot{Y}_n(t;\beta)+cY_n(t;\beta)=\cos\left(\omega_n t+\Theta_n(\beta)\right) \tag{3.17}$$

Then the solution of (3.9) is given by:

$$Y(t;\beta)=\sum_n A_n Y_n(t;\beta) \tag{3.18}$$

The solution of (3.11) is known is equal to:

$$Y_n=R\left(\omega_n\right)\cos\left(\omega_n t+e_n+\Theta_n\left(\beta\right)\right) \tag{3.19}$$

where $R\left(\omega_n\right)=\dfrac{1}{\sqrt{\left(m{\omega_n}^2-c\right)^2+\left(b\omega_n\right)^2}}$ and $e_n=\arctan\left(\dfrac{b\omega_n}{m{\omega_n}^2-c}\right)$

Therefore according to the above the (3.12) becomes:

$$Y(t;\beta)=\sum_n A_n R\left(\omega_n\right)\cos\left(\omega_n t+e_n+\Theta_n\left(\beta\right)\right) \tag{3.20}$$

By the Wiener-Khinchin theorem we have that the spectrum of the response $Y\left(t;\beta\right)$ of the oscillator is:

$$S_{YY}(\omega)=\frac{2}{\pi}\int_0^\infty C_{\mathrm{YY}}(\tau)\cos\left(\omega\tau\right)d\tau \tag{3.21}$$

However it is easy to derive by simple algebra that:

$$C_{YY}(\tau) = \mathrm{E}^{\beta}\left[\cos\left(\omega_n t_1 + e_n + \Theta_n(\beta)\right)\cos\left(\omega_n t_2 + e_n + \Theta_n(\beta)\right)\right] =$$

$$= \frac{1}{2}\sum_n A_n R(\omega_n)\cos(\omega_n \tau) \tag{3.22}$$

and from the above it follows finally that:

$$S_{YY}(\omega) = R^2(\omega)\cdot S_{\mathrm{XX}}(\omega) \tag{3.23}$$

Therefore, if the sea spectrum is given, the spectrums of the ship's modes of freedom are known by (3.23) and then the mean added resistance can be calculated.

The above method, in conjunction with strip theory for treating the ship hydrodynamic problem, is used in the present thesis as the tool for calculating the wave added resistance of specific ships in a seaway, as discussed in detail in Sec.5.2 for an AFRAMAX tanker, which is then examined in optimizing weather ship routing in the Mediterranean Sea region.

Based on the above, the response scpectra concerning ship motions are derived using the RAOs defined by Eqs. (2.59) as follows

$$S_{\xi_k \xi_k}(\omega) = RAO_k{}^2(\omega)\cdot S_{\zeta_x \zeta_x}(\omega) \tag{3.24}$$

and similarly for the other physical quantities of interest.

Chapter 4

SHIP ROUTING OPTIMIZATION

In this chapter the foundation for the solution of the problem of interest, which is minimum-fuel navigation is posed and discussed. Section 4.1 describes the coordinate system and gives various useful definitions. In 4.2 the cost function is defined and in 4.3 the description of the method used to solve the optimal ship routing.

4.1 Coordinate system and map projections

The mathematical model is chosen to refer to a 2D Cartesian coordinate system. In such a coordinate system the minimum distance between two points is the straight line that connects them. However, the surface of the earth is not planar. In order for the optimization scheme to be meaningful, the curvilinear coordinate system of longitude λ and latitude φ used to identify true position on the spherical globe needs to be mapped to a plane through appropriate transformation. A number of such transformations exist, known as projections. A brief discussion about projections follows, but it is useful to be preceded by two basic navigational definitions:

Loxodrome

It is the projection of a curve intersecting the meridians at a constant angle. It is also called a rhumb line and is essentially the path of constant heading navigation. The loxodrome is the most common route followed by the ships because it is plotted on Mercator maps as a straight line. Therefore, the ships need only maintain a steady course along this route.The differential distance between positions (ϕ, λ) and $(\phi + d\phi, \lambda + d\lambda)$ in spherical coordinates, if measured along the rhumb line (loxodrome) connecting the two locations, is given by:

$$dS = U(t) \cdot dt = \bar{R}_{earth} \cdot \sqrt{d\phi(t)^2 + \cos^2(\phi(t)) \cdot d\lambda(t)^2} \tag{4.1}$$

where the spherical coordinates in the above equations are the latitude $\phi \in \left(-\frac{\pi}{2}, \frac{\pi}{2}\right)$, measured from the equator (positive north), and the longitude $\lambda \in (0, 2\pi]$ measured from the Greenwich meridian (increasing eastbound). $\bar{R}_{earth}$ is the mean radius of the earth.

Orthodrome

It is the projection of the shortest curve between two points on a sphere. The shortest connection between two points is part of a great circle. The orthodrome is the projection of a great circle segment into the plane. Although it represents the shortest distance curve it is not a straight line in spherical coordinates. Since navigational routes are commonly plotted on Mercator maps, a ship would have to constantly change course to follow the great circle path. This is a serious practical shortfall which has rendered the use of great circle navigation very limited. The great circle distance between points (ϕ_2, λ_2) and (ϕ_2, λ_2) is:

$$S = \bar{R}_{earth} \cdot \cos^{-1}\left(\sin(\phi_1)\sin(\phi_2) + \cos(\phi_1)\cos(\phi_2)\cos(\lambda_2 - \lambda_1)\right) \tag{4.2}$$

In the present work, the Mercator projection is adopted as it is compatible with Maltab mapshow commands and the output of the swan data (more on that below). The transformation equations are as follows:

$$X = \bar{R}_{earth} \ln\left[\tan\left(\frac{\pi}{4} + \frac{\varphi}{2}\right)\right] \tag{4.3}$$

$$\mathrm{Y} = \bar{R}_{earth}\lambda \tag{4.4}$$

4.2 Calculation of fuel consumption in waves

The thrust required for a ship to move with constant speed derived by the propulsion system is equal to the total resistance corrected using the appropriate efficiencies.

$$T(\mathbf{x}, \dot{\mathbf{x}}; t) = \frac{R_{calm} + R_{AW} + R_{wind}}{1 - t_d} \tag{4.5}$$

where t_d is the thrust deduction factor. Also, $\mathbf{x}$ is the vector showing the position of the ship in longitude and latitude and $\dot{\mathbf{x}} = d\mathbf{x}/dt$ is the time derivative of $\mathbf{x}$. Due to the presence of waves and wind, the thrust becomes also a function of the coordinates of the ship, as well as the direction the ship, actually the difference between the heading of the ship and the incidence angle of the waves. Substituting (2.7), (2.8) and (2.9) into (4.5) we obtain the load curve

$$K_T = \frac{R_{calm} + R_{AW} + R_{wind}}{\rho(1-t_d)(1-w)^2 U^2} J^2 \tag{4.6}$$

where K_T, J are the trust and advance coefficients of the propeller, respectively. The load curve together with the $K_T(J)$ curve of the corresponding propeller series define a nonlinear 2x2 system with unknowns the values of K_T, J. This system is solved numerically and the operating point of the propeller is yielded. Using the estimated J in conjunction with the torque coefficient $K_Q(J)$ of the propeller, the torque is calculated. The open water efficiency at that particular operating point is then obtained by

$$\eta_0 = \frac{K_T J}{2\pi K_Q} \tag{4.7}$$

Subsequently, the rate of fuel mass flow in the engine is given by :

$$q = sfc \cdot P_B \tag{4.8}$$

where sfc is the specific fuel consumption and P_B the engine Shaft Horse Power (SHP). From equations (2.14)-(2.20) the latter is expressed as follows:

$$P_B = \frac{R_{total} U}{\eta_D \eta_{TRM}} \tag{4.9}$$

where

$$R_{total} = R_{calm} + R_{AW} + R_{wind} \tag{4.10}$$

$$\eta_D = \eta_R \eta_O \eta_H \tag{4.11}$$

$$\eta_{TRM} = \eta_S \eta_{GB} \tag{4.12}$$

Fuel rate is finally expressed by the following formula:

$$q(\mathbf{x}, \dot{\mathbf{x}}; t) = sfc \frac{R_{total}(\mathbf{x}, \dot{\mathbf{x}}; t)}{\eta_R \eta_o(\mathbf{x}, \dot{\mathbf{x}}; t) \eta_H \eta_S \eta_{GB}} \tag{4.13}$$

Now, if $\mathbf{y} = \left(\phi(t), \lambda(t)\right)$ is a curve in parametric form in the earth coordinates, then the total fuel consumption is the line integral along (any) path $\mathbf{y}$ is calculated by:

$$J[\mathbf{y}] = \int_{t_0}^{t_f \; y} sfc \frac{UR_{tot}(t;\mathbf{y})}{n_R n_H n_S n_{GB} n_o(t;\mathbf{y}) n_W} dt \tag{4.14}$$

where t_0 is the departure time and t_f the arrival time. The latter t_f is of course unknown and is dependent on $\mathbf{y}$. As we can see the total fuel consumption is dependent on the path (ship route) $\mathbf{y}$ and so it defines a real functional $J[\mathbf{y}]: \mathrm{C}^1(\mathbb{R}^2) \to \mathbb{R}$.

4.3 Description of method

The purpose of this section is to find the shiproute $\mathbf{y}$ such as the total fuel consumption (4.14) is minimum. Therefore, we seek a minimum of the functional $J[\mathbf{y}]$. This problem is well formulated within the context of calculus of variations (see, e.g., Gelfand & Fomin 2000) leading to Euler-Lagrange equation. An extensive description of the framework is presented in Appendix A. However, it is stressed here that the formulation based on Euler-Lagrange equations, fails to provide accurate results due to various reasons (see Bijlsma (1975)). In this work we are going to apply a direct method based on the reformulation of the problem in a standard optimization setting.

Let $A = (\varphi_1, \lambda_1)$ and $B = (\varphi_2, \lambda_2)$ the coordinates of the departure and arrival point. Consider the loxodrome AB and an auxiliary orthogonal curvilinear coordinate system with x-axis along the loxodrome and y-axis in the normal direction, parametrized with respect to the physical distance. Using this coordinate system we consider the following representation of paths (simple non self intersecting curves ending at points *A* and *B*)

$$y(x) = \sum_{n=1}^{n=N} a_n \sin\left(\frac{n\pi x}{\ell}\right) \qquad x \in [0, AB] \;, \tag{4.15}$$

where $\ell = AB$ is the length of the loxodrome path joining the points *A* and *B* on the surface of the earth.

The pair $\left(0, y(0)\right)$ on the auxiliary coordinate system corresponds to the departure point and $\left(AB, y(AB)\right)$ on the arrival one.

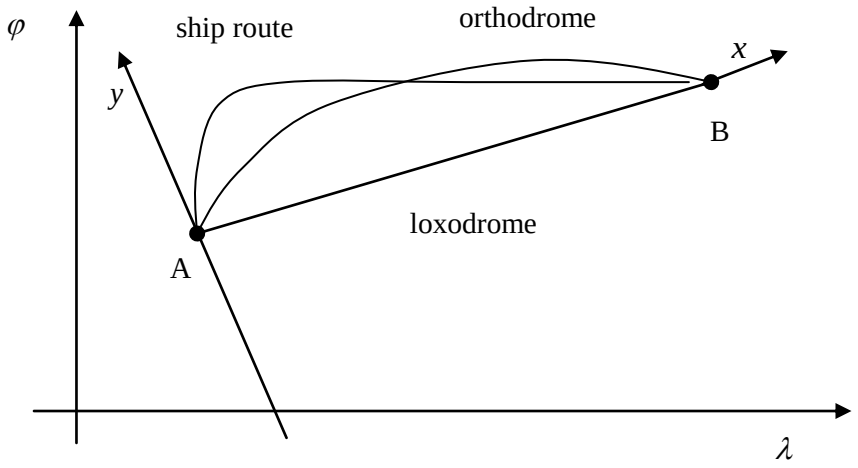

Figure 4.2 Coordinate systems on Mercator projection

What we gain with a function representation as in (4.15) is that the dimension of the optimization problem is reduced by half. This comes at the cost of the loss of the ability to express self intercecting solutions or backtracking ones. Such cases howerer, are extreme situations (storms, tornados) where the ship is probably not permitted to travel through.

Also, the choice of test functions $\sin(\frac{n\pi x}{\ell})$ $n=1,2,...,\infty$ and $x \in 0, AB$ is a most appropriate one, since it is well know that it constructs a basis on $L_2(0, AB)$ (square integrable) function space.

By inserting (4.15) into (4.14) the total fuel consumption is now only depended on the coeffiecients a_n of the sine-series representation:

$$J[y] = \int_{t_0}^{t_f(a_n)} sfc \frac{UR_{tot}(t;a_n)}{n_R n_H n_S n_{GB} n_o(t;a_n) n_W} dt = J[a_n] \tag{4.16}$$

Therefore, the infinite dimensional optimisation problem is reduced from finding the minimum of the functional $J[y]$, into finding the N dimensional minimum of the function $J[a_1,...,a_N]$. The method developed in the present thesis in order to solve the optimization problem is based on Downhill simplex (see Appendix A for more). The general algorithm used is described below:

- Step 1: The starting time, as well as departure and arrival points are defined. Then, the geographical data and the weather data are loaded.

- Step 2: Every possible path is approximated on the auxiliary orthogonal curvilinear system as a Fourier sine series of N terms as in Eq.(1). The fuel energy functional is now dependent on *N* variables a_n. With the use of downhill simplex method, the a_n $n=1,2,3,..,N$ terms that minimize (2) are found.

- Step 3: Printing of results/plotting route in real time.

Such a method however does not perform well for large N as stated before, both with regards to time and robustness. Therefore, for cases that high accuracy is needed, we implement the following alternative algorithm.

- Step 2a: Let $N_1 < N$ be a small initial truncation of (1) (in this work $N_1 = 4$).With the use of downhill simplex find a_i $i=1,...,N_1$ that minimize (2).

- Step 2b: Further minimise error by *K* iterations of $L<N_1$ terms of sine series.

What is gained from the above altrnative is computational time since high dimensional optimisation is extremely unrobust and slow (complexity of the algorithm is exponential with regards to the dimension). On the other hand, breaking the optimization in smaller dimensions allows one to achieve as much required accuracy of the solution, as needed, very quickly.

Chapter 5

MATLAB-GUI IMPLEMENTATION & NUMERICAL RESULTS

For the purpose of this thesis, the algorithms that were developed are combined into a Graphical User Interface (GUI) in Matlab® that integrates all of them into one software tool and could, with a little more elaboration, become a real product that could compete with the state of the art programs that nowadays ship companies use. The GUI itself supports a database of ships and weather forecast data and it has an island avoidance and multiple waypoints travel features. In this chapter we will describe the ship used in the numerical examples and its resistance calculation. Finally, we are going to discuss the island avoidance feature and the multiple waypoint travel.

5.1 AFRAMAX tanker

As an example we are going to use an AFRAMAX tanker 105000 tn DWT whose specs are as follows:

Length between Perpendiculars : $L_{BP} = 234m$

Total Length : $L = 238.5m$

Breadth : $B = 42m$

Draft : $T = 14.9m$

Displacement : $\Delta = 122770tn$

Deadweight : DWT=105000tn

Displacement Volume : $V = 119775m^3$

Hull Coefficient : $C_b = 0.818$

Vertical Buoyancy Center : $KB = 7.76m$

Longitudinal Buoyancy Center : $LCB = 6.8m$ (fore of middle section)

On full load condition the ship has:

Vertical Center of Gravity : $KG = 12m$

Longitudinal Center of Gravity : $LCG = 6.8m$

Metacentric Height : $GM = 5.6m$

Inertia moment with respect to longitudinal axis : $R_{xx} = 12m$

Inertia moment with respect to longitudinal axis : $R_{yy} = 63m$

<u>On ballast condition the ship has:</u>

Draft : $T_{balast} = 7.2m$

Displacement : $\Delta = 55000tn$

Displacement Volume : $V = 54000m^3$

Vertical Buoyancy Center : $KB = 3.8m$

Longitudinal Buoyancy Center : $LCB = 8.9m$ (fore of middle section)

According to the above and details taken from the general arrangement plan (see Fig. 5.1) a 3D model was constructed in RHINO to do the hydrostatic analysis and stability calculations of the ship. The ship is equipped with a Diesel engine (6S60MC type, MCR 15400 BHP @ 97RPM) joined directly with the propeller. The engine is able to move the ship, in clean hull condition, with a max speed of 14kn in calm water and full load condition ($T = 14.9$ m) and power margin of 15% for increase due to real sea state conditions. For this ship the clean hull resistance in calm water that corresponds to drafts $T = 7.2m$ and $T = 14.9m$ is displayed in Figure 5.2. Also the drawing of the ship's propeller , with pitch ratio $\frac{P}{D} = 0.695$, is displayed in Figure 4.3. The characteristic coefficients of the propeller in open water is shown in Figure 5.4(a) . The distribution of axial component wake is displayed on Figure 5.4(b) and its mean value is $1-w = 0.645$. Furthermore, the values of the hull-propeller hydrodynamic interaction coefficients are:

Thrust deduction factor: $1-t_d = 0.77$

Relative rotative efficiency: $\eta_R = 1.037$.

From the above it follows that the hull efficiency coefficient is:

$$\eta_H = \frac{1-t_d}{1-w} = 1.19$$

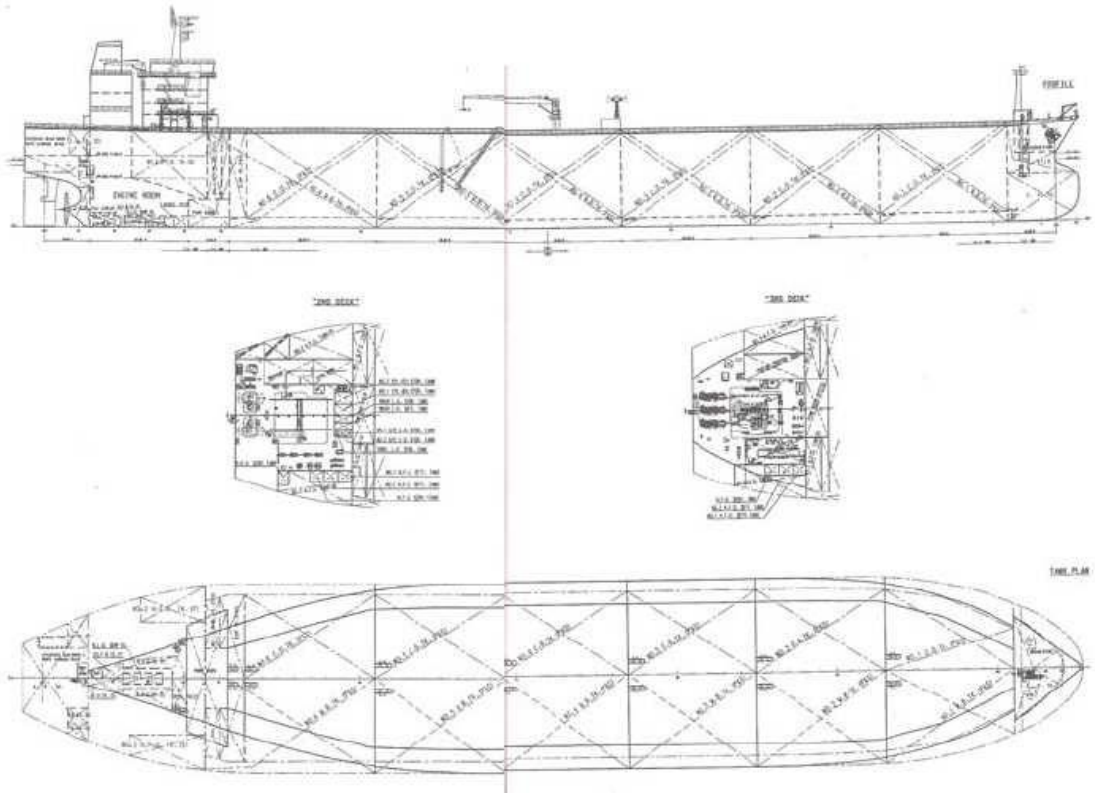

Figure 5.1 The general arrangement plan

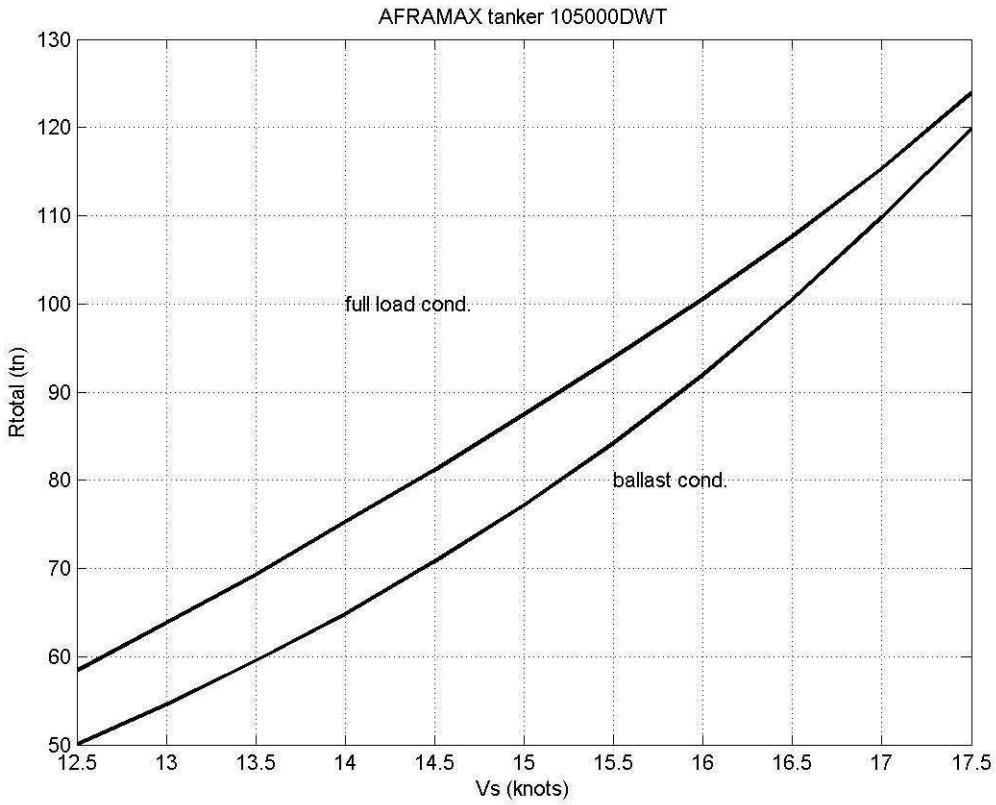

Figure 5.2 The calm water resistance for full load condition ($T = 14.9m$) and ballast condition ($T = 7.2m$); from Belibassakis et al (2013).

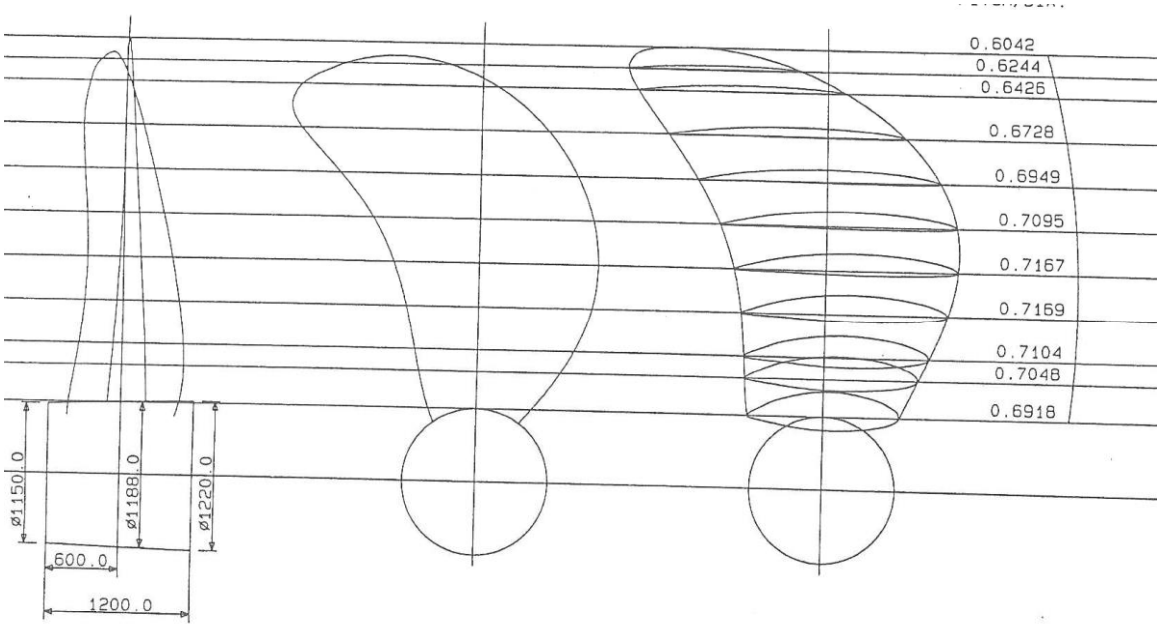

Figure 5.3 Drawing if the 4- propeller : z=4, $A_E = 0.5$, $r/R = 0.7$, $D = 7.2m$, tip skew=18.75^o , no rake

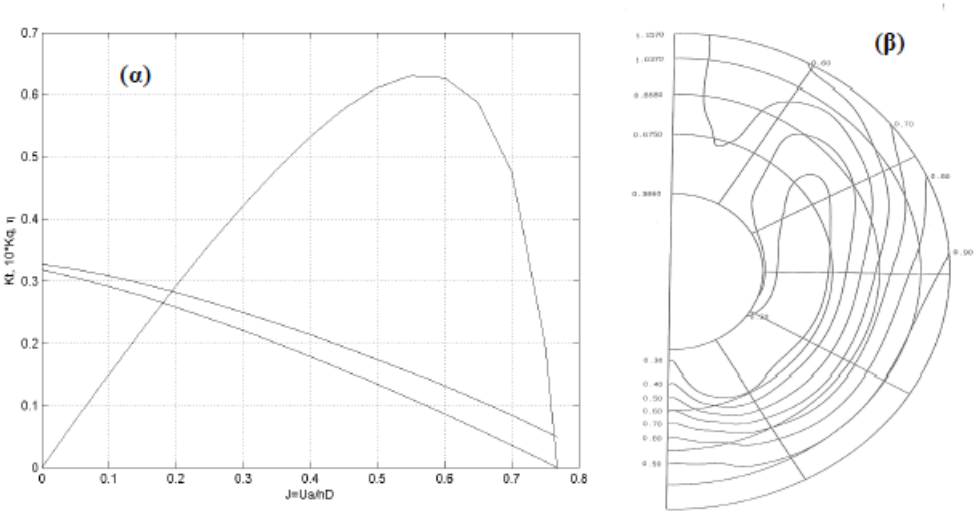

Figure 5.4 (a)Hydrodynamic characteristics of propeller. (b) Axial wake distribution; from Belibassakis et al (2013).

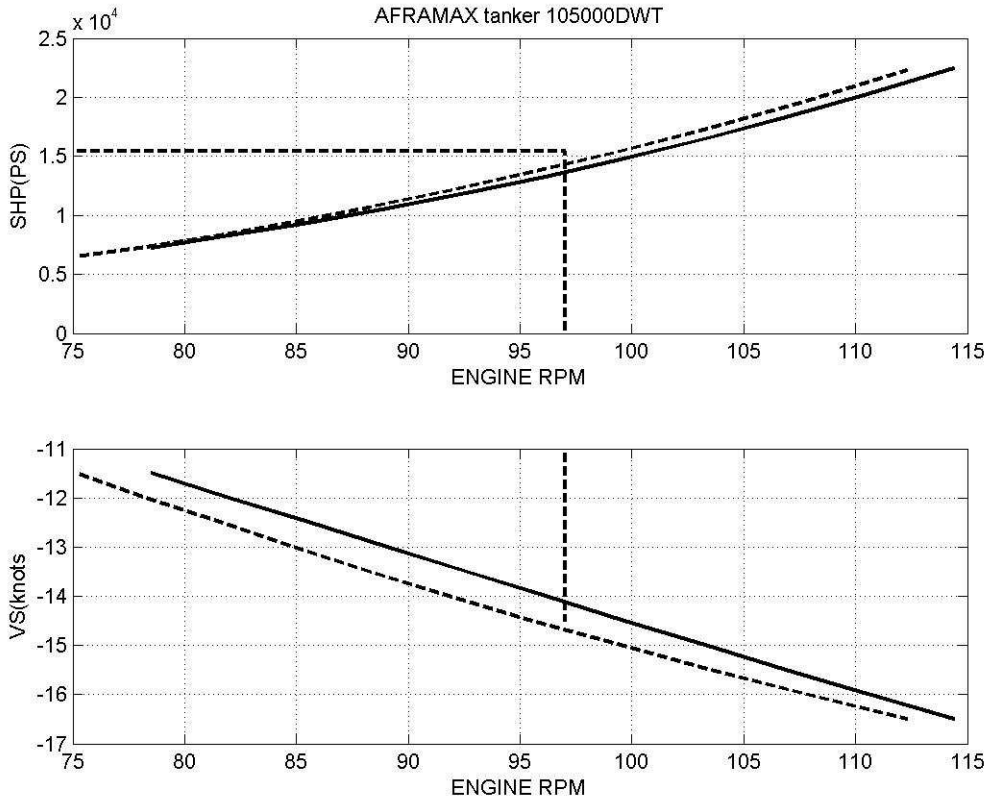

Figure 5.5 Performance of propulsion system on ballast (dashes) and full load condition (continuous line); see also Belibassakis et al (2013). .

5.2 Added Resistance Calculation

On the present work in order to derive the added resistance due to waves we used the energy method described in 2.4 (Loukakis & Sklavounos 1978) for side incident waves, for the calculation of the added resistance and the vertical motion of the ship at the area above the propeller; for more details see Belibassakis et al (2013). For the calculation of the of the added mass and dumping tensors, Froude-Krylov and diffraction forces strip theory (Salvensen et al 1970, Lewis 1988) was used. This method is based on the thinness of the shape of the hull, which generally are satisfied for normal ships (that satisfy $5.5<\frac{L}{B}<9,2<\frac{B}{T}<4$) .

Some special types of ships are of course excluded (example?). According to strip theory the surface integrals over the hull that define the hydrodynamic coefficients and excitation forces can be approximated by multiple integrals over the length of the hull and the wetter circumference of every section (see Figure 5.6) and are calculated from equivalent quantities that are defined by a hydrodynamic problem on every transverse section.

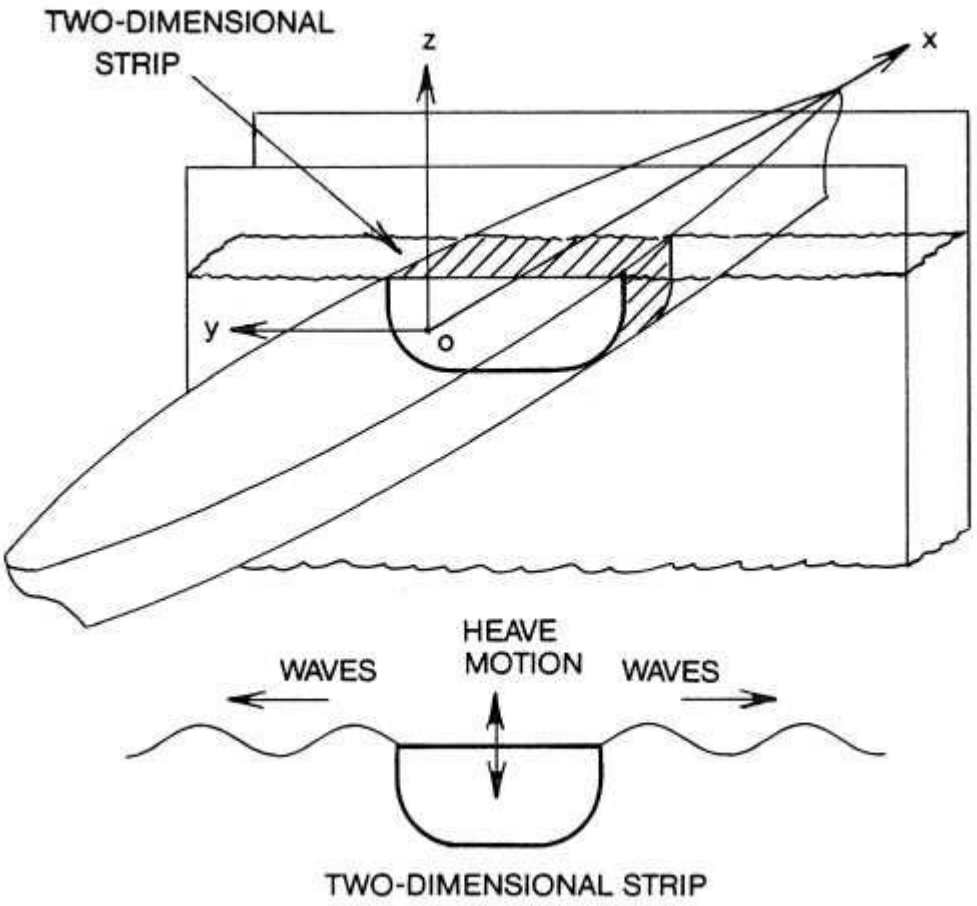

Figure 5.6 Strip Theory. The transverse sections are oscillating due to incident waves, while moving with constant speed U .

The numerical results for the added resistance of this AFRAMAX tanker are presented in Table 5.1, for different ship speeds on the interval $V_s = U = 11.5 \div 15.5 kn$. Sea state can be described through Beaufort scale , which is commonly used to define sea state in conjunction to wind speed. The relation between BF scale, wind speed (U_w) and the wave significant height and modal periods is given on the four first rows of Table 5.1.

For calculation purposes the spectral model JONSWAP was used. The latter biparametric model is given as

$$S_j(\omega, H_s, \mathrm{T}_p) = \frac{ag^2}{\omega^5} \exp\left(-\frac{5}{4}\left(\frac{\omega}{\omega_p} \right)^{-4} \gamma^{\delta} \right)$$

			Vs(kn)	11.5	12.5	13.5	14.5	15.5
BF	U_w(m/s)	H_s(m)	T_p(s)					
2	2.0	0.2	2.24	1.31	1.10	0.94	0.57	0.50
3	4.4	0.6	3.87	3.93	3.31	2.46	1.71	1.49
4	6.7	1.0	5.00	6.54	5.51	3.78	2.85	2.49
5	9.3	2.0	7.07	12.80	9.53	7.08	5.70	4.97
6	11.8	3.0	8.66	17.38	13.39	10.38	8.55	6.99
7	15.3	4.0	10.00	40.87	32.99	26.76	21.90	18.03
8	19.0	5.5	11.73	129.30	109.37	92.12	78.39	67.38

Table 5.1 Added resistance of the example ship in heading incident waves for different sea states (% of the calm water resistance at the same speed).

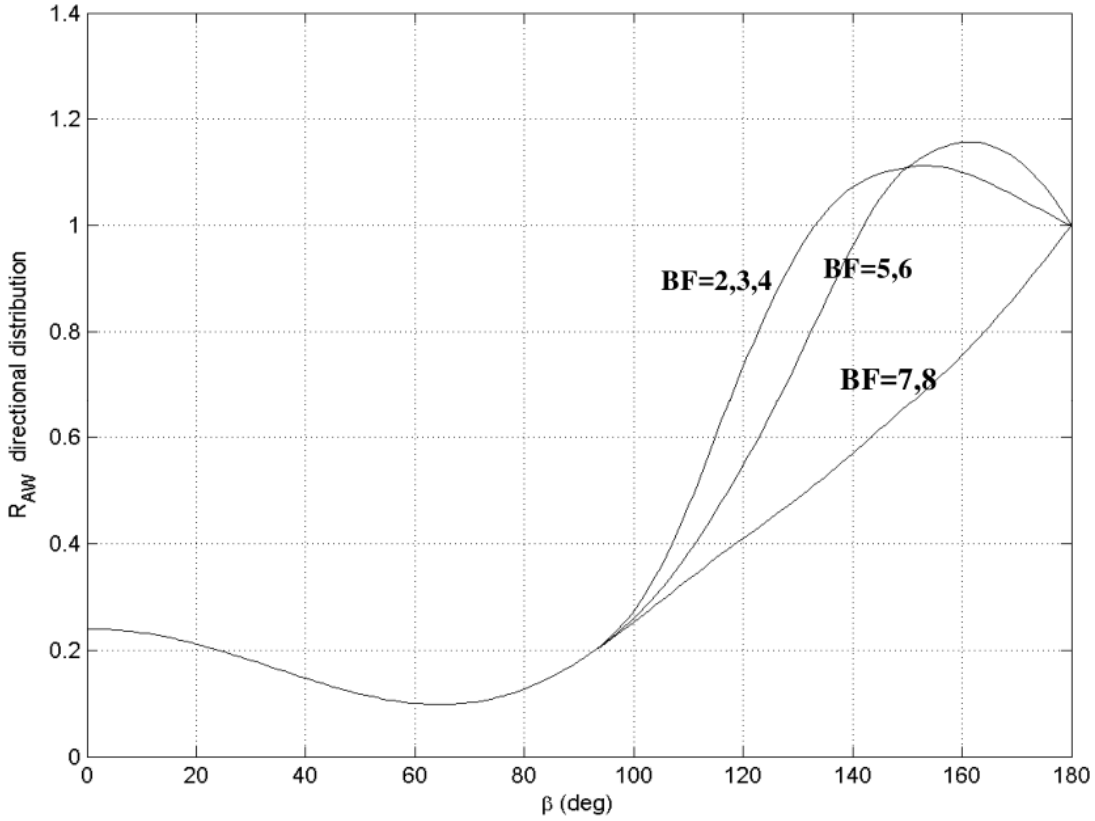

Figure 5.7 Effect of direction of the incident waves on the added wave resistance (b=180^0 is heading waves, b= 0^o for following – stern waves); from Belibassakis et al (2013).

where ω_p is the modal frequency, a is the Phillips constant, $\delta = \exp\left(-\frac{\left(\omega-\omega_p\right)^2}{\left(\sqrt{2}\sigma_0\omega_p\right)^2}\right)$, and $\gamma = 3.3$ (see Massel 1996). By using the analysis done in sections 3.2 and 4.4 the mean added resistance for different sea states can be calculated.

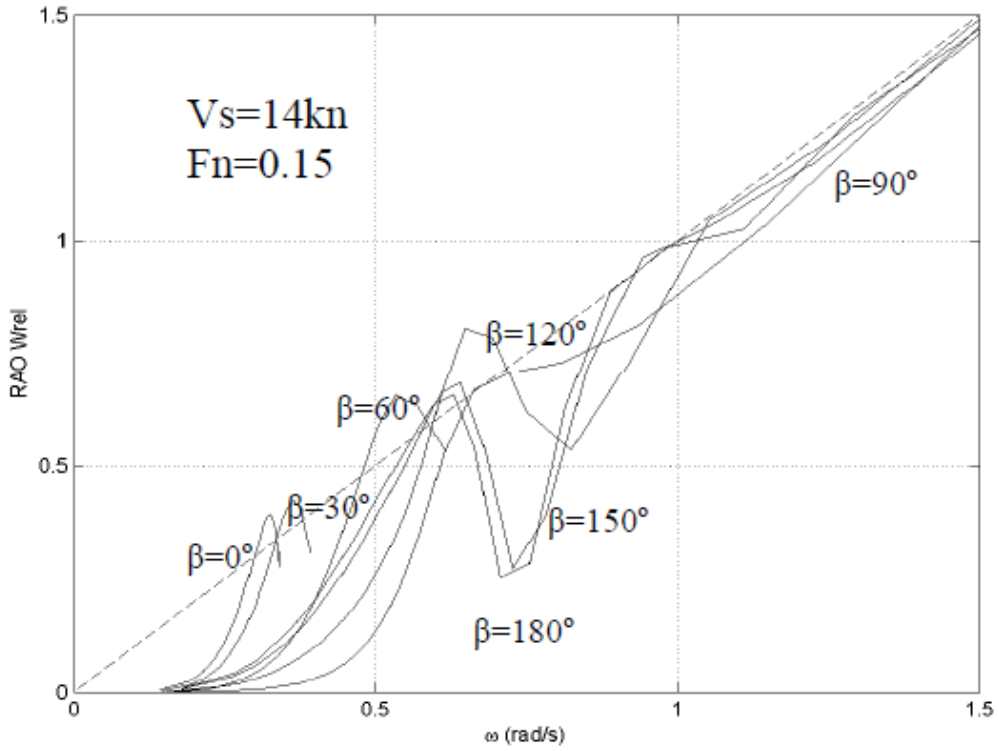

Figure 5.8 Response Amplitude Operator (RAO) for the relative vertical speed on the aft area of the ship; from Belibassakis et al (2013)..

It is evident now that the added resistance in this formulation is a function of H_s, T_p and the direction of the waves relevant to the ship.

5.3 Travel path control points and land avoidance features

The following algorithm can handle more complex routes in the form of user given way-points. If n points are given, the algorithm is run $n-1$ times for each subsequent pair. The optimal route and the time until arrival (t_f) is calculated and then t_f is added to the depar-ture date. Although this sounds trivial it is far from not, because all dates in the program are in ISO format (ex. 20160101.030000) while t_f is just a real number. Both quantities have to be converted into a ISO date-number, added, revert the result into ISO date format and then floor to the nearest SWAN data available . This gives at worst a rounding error of 1.5*hs* for every pair of waypoints, since SWAN data output come with a time resolution of 3 hours.

The following algorithm is also guaranteed to not give solutions that crash on land and islands. This is done by setting the added resistance to infinite in case it passes over land. If bathymetry in any point is less than 10 then it is considered land. This could not be done without the use of the downhill simplex algorithm, since only simplex (and possibly Genetic Algorithms) can handle discontinuities in the cost function. Validation of the said feature is given in Appendix A, section A.5.

5.4 Geographical and Weather Data

With regards to the geographical data, the database General Bathymetric Chart of the Oceans (GEBCO, www.gebco.net) is used for coastline data. The database GEBCO is a high quality bathymetry database that covers the whole planet with resolution 30''. The offshore wave simulations utilize a 3-level SWAN (Booij et al., 1999) based scheme, which was developed in the framework of Thales project CCSEAWAVS which aimed to estimate the effects of climate change on sea level and wave climate of the Greek seas, the coastal vulnerability and the safety of coastal and marine structures (see Makris et al 2016). This simulation scheme uses past and future projections climatic wind fields (also produced in the context of CCSEAWAVS) for the estimation of wave characteristics with resolution 0.2 degrees in the Mediterranean basin (Level 1). These data provide bound- ary information for repeating the simulation using a finer mesh 0.05 degrees inside an Eastern Mediterranean subsection (Level 2). Details of the methodology are also described in Athanassoulis et al (2015).

The initial scope of SWAN was to compute random, short-crested wind-generated waves in coastal regions and inland water. The model was later extended to allow simulation of waves in deep waters as well. As for the wind data, those were taken using the ICTP RegCM3 model. The dataset extends over the entire Mediterranean Sea, with spatial resolution of 25x25km and temporal resolution of 6 hours.

5.5 Numerical results

In this section the numerical results concerning the aforementioned AFRAMAX are presented and discussed. A first example is presented in Fig.5.9 for a trip from Port-Said Egypt to Sardenia. A second trip shown in Fig.5.10 is a more complex route beginning at Israel, then passing in sequence to Libya(tripolis), Sicily and Majorca (Spain) as seen in figure 5.11. The ship departs on 1^{st} of November 2016 , 12 am, which was an interesting test case since at

this time we see intense weather on the Mediterranean basin. The optimal routes had a 3% better fuel consumption with regards to the loxodrome which is the standart route in ship routing and 5% better than the orthodrome which is the route with smallest distance between waypoints. This is an appropriate result considering the small distances in Mediterranean and that intense weather conditions are rare and small compared to Atlantic or Pacific ocean.

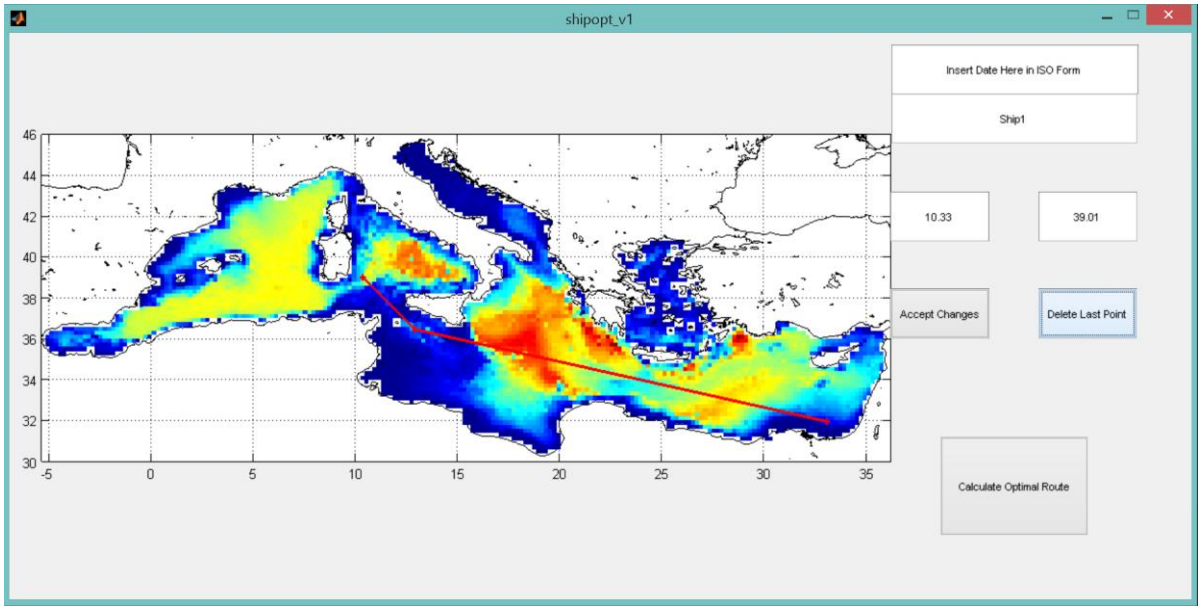

Figure 5.9 The multi point travel from Port Said to Sardenia as shown in the GUI.

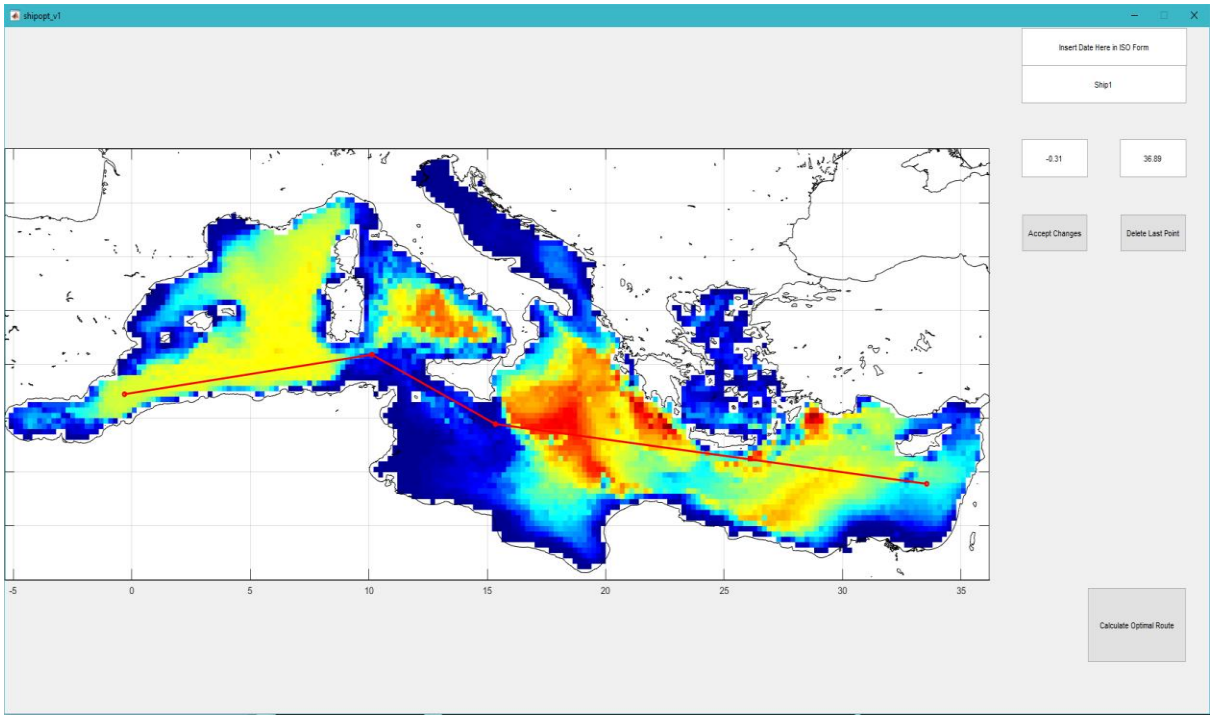

Figure 5.10 Example of a multiple waypoint route from Israel to Spain using the developed software tool. The bathymetry is indicated by using a colorplot.

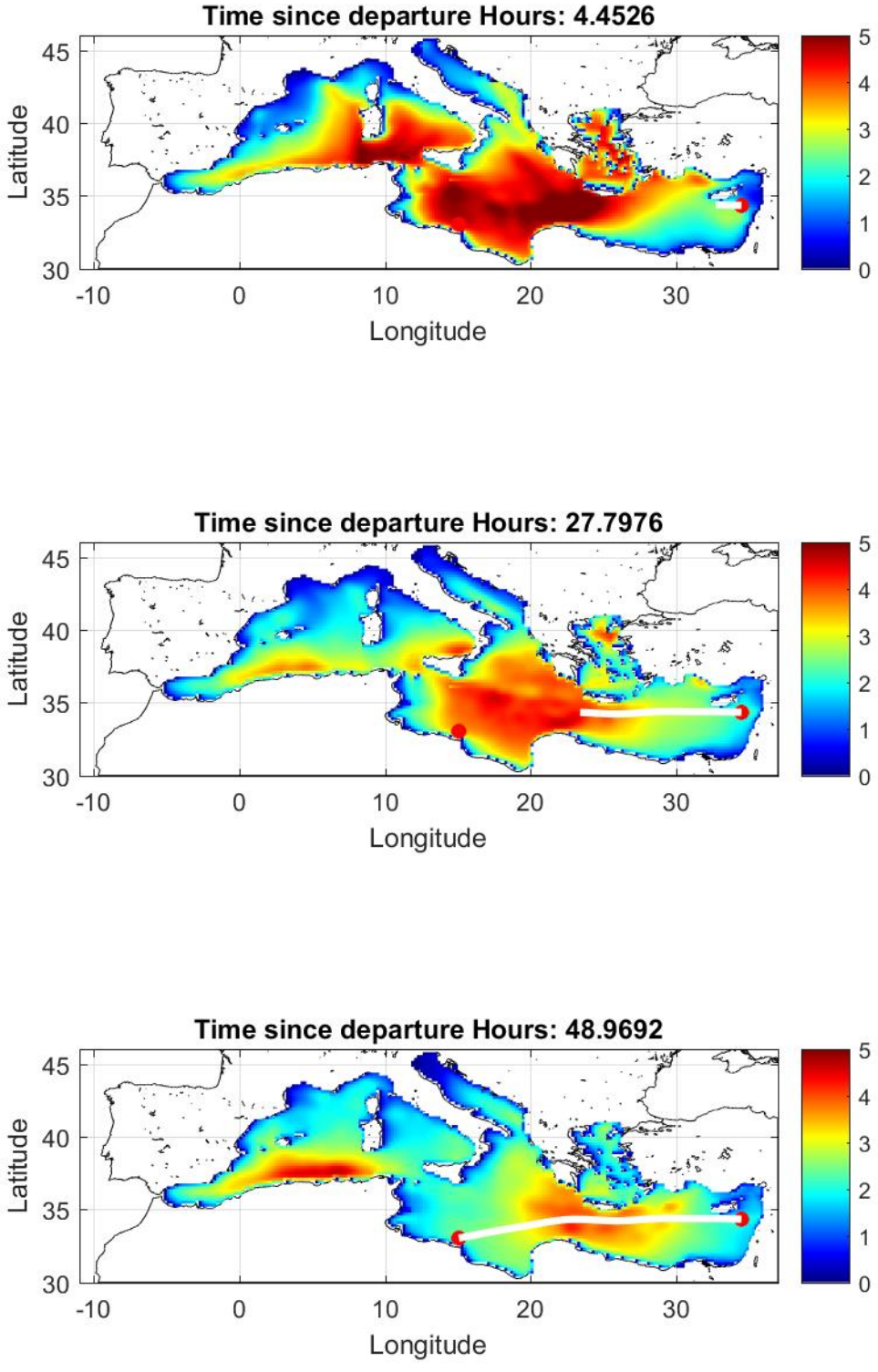

Figure 5.11 The optimal ship route between multiple points. First part of the route from Israel to Libya (Tripolis).

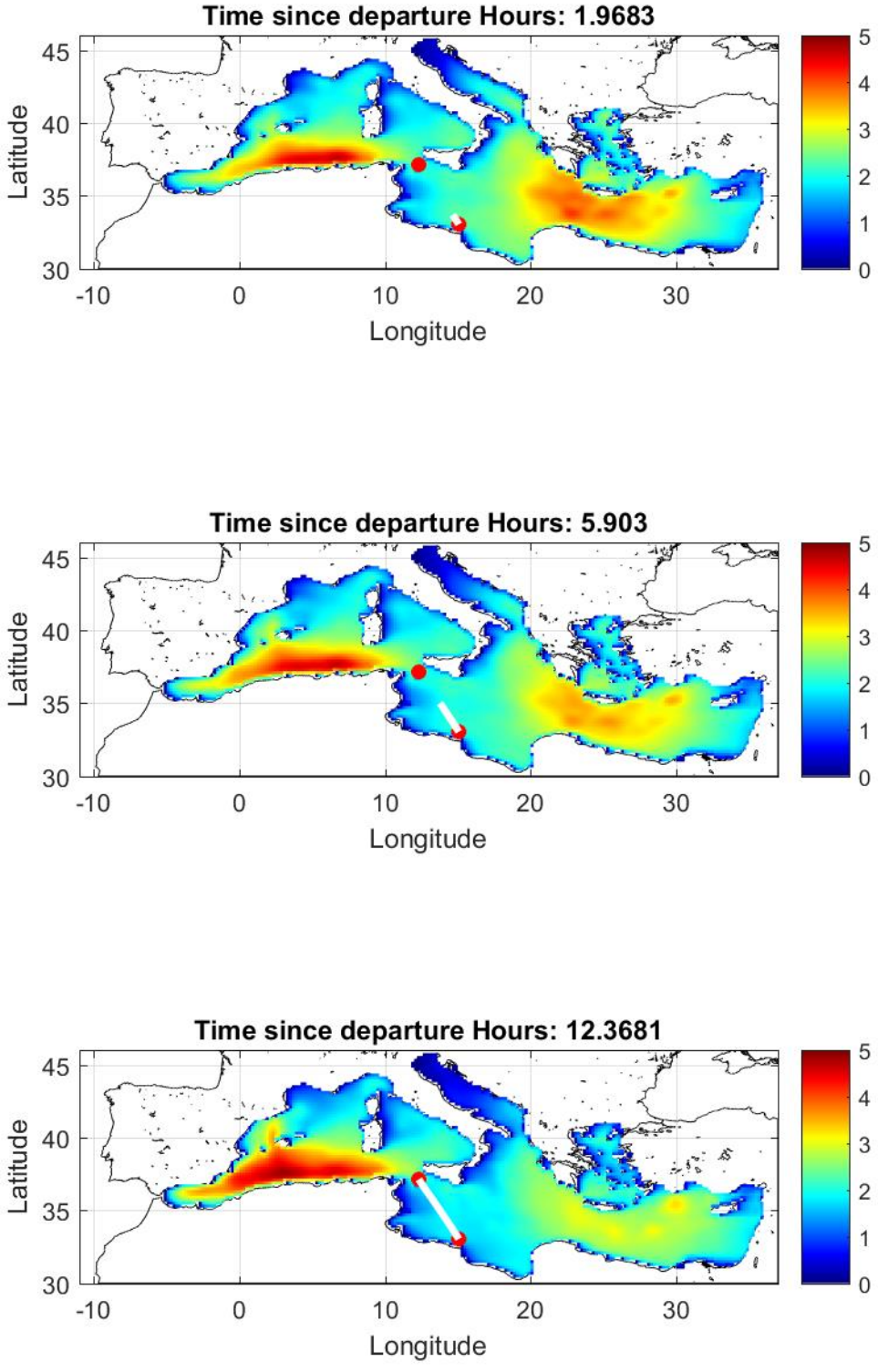

Figure 5.11 The optimal ship route between multiple points. First two subplots: part of the route from Israel to Libya (Tripolis) and last subplot from Libya (Tripolis) to Sicily

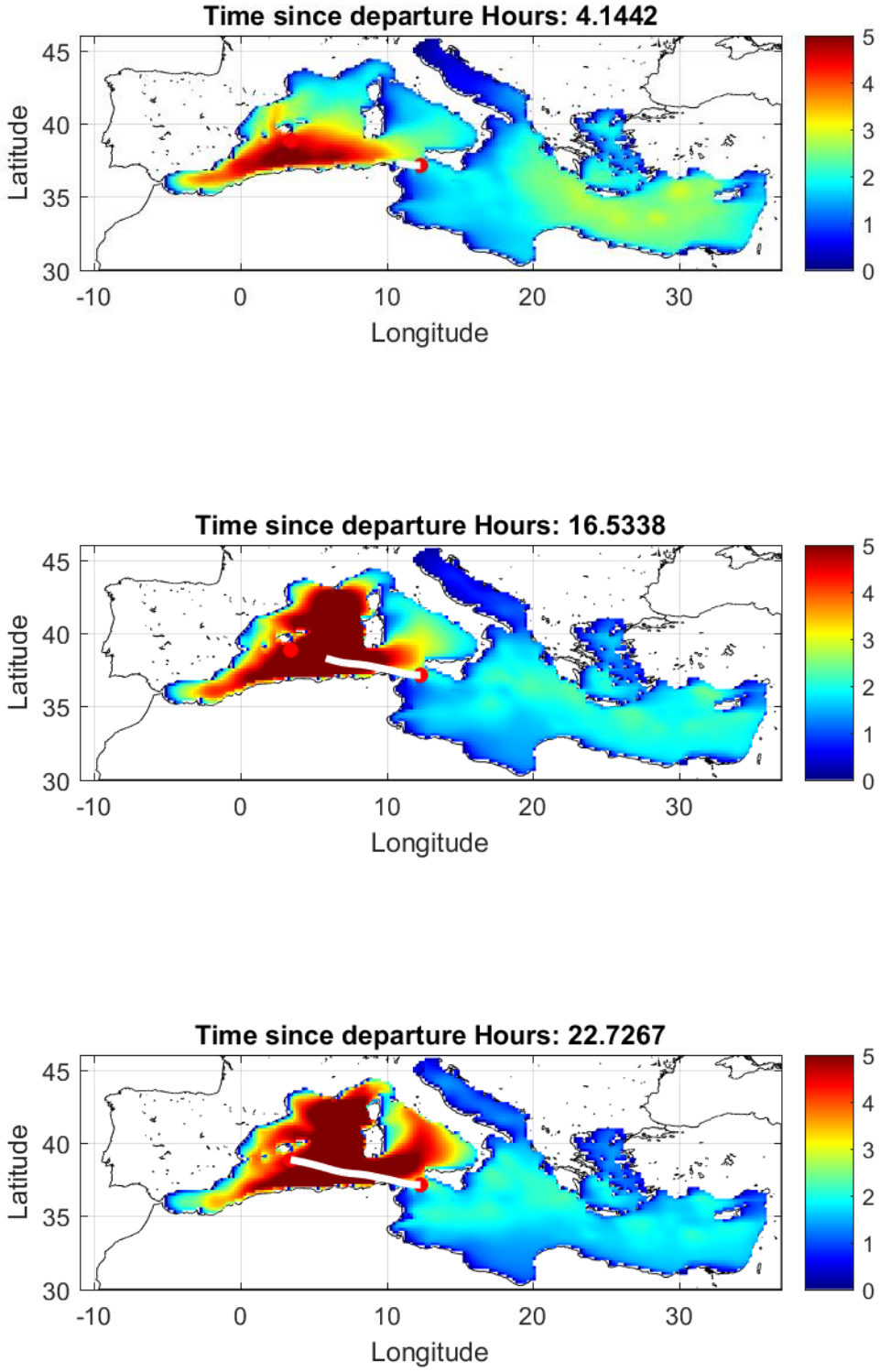

Figure 5.11 The optimal ship route between multiple points. Part of the route from Sicily to Spain

Conclusions and proposal for future work

In this work a method for the weather ship routing problem with regards to energy efficiency is presented. The accuracy of the optimization algorithm is validated against similar problems with analytical solutions as presented in detail in Appendices A & B.

The algorithm is implemented in conjunction with geographical and simulated weather data as a Matlab GUI showing good numerical performance concerning energy consumption reduction. Future extension will include the consideration of operability and other criteria as additional constraints of the optimization problem, and the extension of the tool worldwide. Another thing that has to be implemented is access to the GUI with a network of real weather data forcast instead of artificial ones.

One thing that most ship routing algorithms lack is a way to compare or validate their results. Although the optimization/dynamic algorithms are guaranteed to converge to a local minimum, the final ship routing results are rarely compared. This makes important to construct a setting, in which we can bechmark the solutions of the aforementioned programms on real conditions.

References

Andersson A., 2015 Multi-objective Optimisation of Ship Routes. Master's thesis Chalmers University of Technology, Göteborg.

Aneja Y.P., Aggarwal V., Nair K.P., 1983, Shortest Chain Subject to Side Constraints NETWORKS, 13, pp. 295-302

Athanassoulis, G., Belibassakis, K., 2012, Ship Dynamics, Lecture Notes, Scholl of NAME, Nat.Techn. Univ.Athens (in Greek).

Athanassoulis, G., Belibassakis, K., Gerostathis, T., Stefana kos, Ch., Spaan, G., 2003, WORLDWAVES: High quality coastal and offshore wave data within minutes for any global site, Proc. 22nd Int. Conference on Offshore Mechanics and Arctic Engineering, OMAE2003, Cancun, Mexico.

Athanassoulis, G.A., Belibassakis, K.A., Gerostathis, Th.P., Kapelonis, Z.G., 2014. Application of SWAN wave model for climatic simulation of sea condition at coastal areas of the Mediterranean. Proc. 6th Panhellenic Conf. Coastal Zones Manage. Athens, Greece.

Arribas, P.F. 2007, Some methods to obtain the added resistance of a ship advancing in waves, Ocean Engineering, 34, pp. 946–955.

Avgouleas, 2008 K. Avgouleas Optimal Ship Routing. Master thesis. Massachusetts Institute of Technology (2008)

Barstow, S., Mørk, G., Lønseth L, Schjølberg, P., Machado, U., Athanassoulis, G., Belibassakis, K., Gerostathis, T., Stefanakos, Ch., Spaan, G., 2003, WORLDWAVES: Fusion of data from many sources in a user-friendly software package for timely calculation of wave statistics in global coastal waters, 13th Intern. Offshore and Polar Conference and Exhibition, ISOPE2003, Honolulu, Hawaii, USA.

Barstow, S., Mørk, G., Lønseth L, Schjølberg, P., Machado, U., Athanassoulis, G., Belibassakis, K., Gerostathis, T., Stefana kos, Ch., Spaan, G., 2003, WORLDWAVES: High quality coastal and offshore wave data within minutes for any global site, Proc. 22nd Int. Conference on Offshore Mechanics and Arctic Engineering, OMAE2003, Cancun, Mexico.

Bekker JF, Schmid JP. 2006, Planning the safe transit of a ship through a mapped minefield. Journal of the Operations Research Society of South Africa, 22, pp.1–18.

Belibassakis, K.A., 2008, A boundary element method for the hydrodynamic analysis of floating bodies in general bathymetry regions, Engineering Analysis with Boundary Elements, 32, pp 796-810.

Belibassakis, K., 2009, Effects of wave-induced ship motion on propeller-hull interaction with application to fouling estimation and propulsion optimization. Proc. Int. Maritime Association Mediterranean Conference, IMAM 2009 Istanbul.

Belibassakis K.A., Politis, G.K., Gerostathis Th.P. 2013, Calculation of ship hydrodynamic propulsion in rough seas by non-linear BEM with application to reduction of energy losses in waves, 32th Int. Conference on Offshore Mechanics and Arctic Engineering (OMAE2013), June 9-14, 2013 - Nantes, France.

Bellman, 1952 R. Bellman. On the Theory of Dynamic Programming.Mathematics, 38 (1952), pp. 716-719

Bijlsma, 1975 S.J. Bijlsma. On Minimal-Time Ship Routing. Phd thesis. Delft University of Technology (1975)

Böttner, 2007 C.-U. Böttner. Weather routing for ships in degraded condition. International Symposium on Safetyb, Security and Environmental Protection, National Technical University Athens, Athens (2007)

Calvert S, Deakins E, Motte R. 1991, A dynamic system for fuel optimization Trans-Ocean. Journal of Navigation 44, pp.233–65.

Dewit C. 1988, Practical weather routeing of sail-assisted motor vessels. Journal of Navigation 41, p.134.

Dewit C. 1990, Proposal for low-cost ocean weather routeing. Journal of Navigation43, pp.428–39 .
Fang and Lin, 2015 M.-C. Fang, Y.-H. Lin. The optimization of ship weather-routing algorithm based on the composite influence of multi-dynamic elements (II): Optimized routings Applied Ocean Research, 50 (2015), pp. 130-140
Gelfand I. M., Fomin S. V., 2000, Calculus of Variations, Dover Publications, Inc
Gerritsma, J., Beukelman, W., 1972, Analysis of the resistance increase in waves of a fast cargo ship, International Shipbuilding Progress 19(217), pp. 285-293.
Hagiwara H, Spaans JA. 1987. Practical weather routing of sail-assisted motor vessels. Journal of Navigation vol.40, pp.96–119 .
Hagiwara H. 1989, Weather routing of (sail-assisted) motor vessels. Delft: Delft University of Technology.
Hamilton, 1961 H.D. Hamilton. Minimum-Time Ship Routing by Calculus of Variations Methods. Master's thesis. U.S. Naval Postgraduate School, Monterey (1961)
Hinnenthal J, Clauss G. 2010, Robust pareto-optimum routing of ships utilising de- terministic and ensemble weather forecasts. Ships and Offshore Structures;5, pp.105–14
IMO, 2007 IMO. (2007), MSC.1/Circ.1228 Revised guidance to the Master for avoiding dangerous situations in adverse weather and sea conditions. London.
ITTC 1998, Report of the Resistance Committee, 22nd Inter. Towing Tank Conf.
ITTC 2002, Report of the Resistance Committee, 23rd Inter. Towing Tank Conf.
ITTC 2005, Report of the Resistance Committee, 24th Inter. Towing Tank Conf.
James, 1957 R. James. Application of wave forecast to marine navigation. US Navy Hydrographic Office, Washington (1957)
Jones et al., 1993 D. Jones, C. Perttunen, B. Stuckman. Lipschitzian optimization without the lipschitz constant. Journal of Optimization Theory and Application, 79 (1) (1993), pp. 157-181
Jensen F., Kupperman W., Porter M., Schmidt H., 1994, Computational Ocean Acoustics. AIP Press.
Katsenelenbaum B.Z., Mercader del Rio L., Pereyaslavets M., Sorolla Ayza M., Thumm M., 1998, Theory of Nonuniform Waveguides, The Cross-Section Method. IEE London.
Klompstra MB, Olsde GJ, Van Brunschot PKGM, 1992, The isopone method in optimalcontrol. Dynamics and Control vol.2, pp.281–301 .
Kosmas OT, Vlachos DS. 2012, Simulated annealing for optimal ship routing. Computers & Operations Research vol.39, pp.576–81.
Krata and Szłapczynska, 2012 P. Krata, J. Szłapczynska. Weather Hazard Avoidance in Modeling Safety of Motor-Driven Ship for Multicriteria Weather Routing. International Journal on Marine Navigation and Safety of Sea Transportation, 1 (2012), pp. 71-78
Larsson and Simonsen, 2014 E. Larsson, M.H. Simonsen. DIRECT Weather Routing. Master's thesis. Chalmers University of Technology, Gothenburg (2014)
Lewis, E.V. (Ed), 1989, Principles of Naval Architecture, vol. 2 and 3, NJ: Society of Naval Architects & Marine Engin. (SNAME), New York.
Lin et al., 2013 Y.-H. Lin, M.-C. Fang, R. Yeung. The optimization of ship weather-routing algorithm based on the composite influence of multi-dynamic elements. Applied Ocean Research, 43 (2013), pp. 184-194
Loukakis, T.A., Sclavounos, P., 1978, Some extensions of the classical approach to strip theory of ship motion, including the calculation of mean added forces and moments" Journal of Ship Research, 22 (1), pp. 1–19.
Lunnon RW, Marklow AD. 1992, Optimization of time saving in navigation through an area of variable flow. Journal of Navigation vol.45, pp.384–99 .
Luus, 2000 R. Luus. Iterative Dynamic Programming. (1. ed.), CRC Press, Inc, Boca Raton, FL, USA (2000)
Maki A, Akimoto Y, Nagata Y, Kobayashi S, Kobayashi E, Shiotani S. 2011, A new weath-

er-routing system that accounts for ship stability based on a real-coded genetic algorithm. Journal Marine Science and Technology vol.16, pp. 311–22 .
Makris Ch., Galiatsatou P., et al, 2016, Climate change effects on the marine characteristics of the Aegean and Ionian Seas, *Ocean Dynamics*, vol.66 (12), 1603–1635.
Marie and Courtielle, 2009 S. Marie, E. Courtielle.Multi-Objective Optimization of Motor Vessel Route. International Journal on Marine Navigation and Safety of Sea Transportation, 3 (2) (2009), pp. 133-141
Muntean T., 2008, Ship propulsion train efficiency sensing, Wartsila Technical Journal, 02.
Nelder, J.A., Mead, R. 1965, Computer Journal, vol. 7, pp. 308–313.
Padhy CP, Sen D, Bhaskaran PK. 2008, Application of wave model for weather routing of ships in the North Indian Ocean. Natural Hazards vol.44, pp.373–85 .
Papadakis, N Perakis A., 1990, Deterministic Minimal Time Vessel Routing Operations Research, 426-438.
Petrov (1968) Variational Methods in Optimum Control Theory. Academic Press.
Press W Teukolsky S, Vetterling W Flannery B, 1997, Numerical Recipes, Cambridge University Press.
Salomons E.M., 2001, Computational Atmospheric Acoustics, Kluwer Academic Publ,
Salvesen, N., Tuck, E.O., Faltinsen, O., 1970, Ship motions and sea loads, Transactions SNAME 78, pp 250–87.
Sen and Padhy, 2015 D. Sen, C. Padhy. An Approach for Development of a Ship Routing Algorithm for Application in the North Indian Ocean Region. Applied Ocean Research, 50 (2015), pp. 173-191
Shao W, Zhou PL, Thong SK. 2012, Development of a novel forward dynamic programming method for weather routing. Journal of Marine Science and Techn. Vol.17, pp.239–51.
Spaans JA. 1995, New developments in ship weather routing. Navigation vol.169, pp.95–106 .
Suzuki K., Kai H., Hirai M., Tarafder Sh., 2009, Simulation of free surface flow of high speed ship in shallow or restricted water condition, Proc.10th Int. Conference on Fast Sea Transportation, FAST 2009, Athens, Greece.
Szlapczynska, 2015 J. Szlapczynska. Multi-objective Weather Routing with Customised Criteria and Constraints. Journal of Navigation, 68 (2015), pp. 338-354
Szlapczynska and Smierzchalski, 2007 J. Szlapczynska, R. Smierzchalski. Adopted Isochrone Method Improving Ship Safety in Weather Routing with Evolutionary Approach. International Journal of Reliability, Quality and Safety Engineering, 14 (6) (2007), pp. 635-645.
Szłapczynska and Smierzchalski, 2009 J. Szłapczynska, R. Smierzchalski. Multicriteria Optimisation in Weather Routing. International Journal on Marine Navigation and Safety of Sea Transportation, 3 (4) (2009), pp. 393-400
Tsuji Szlapczynska, 2015 J. Szlapczynska
Takashima K, Mezaoui B, Shoji R. 2009, On the fuel saving operation for coastal mer- chant ships using weather routing. International Journal on Marine Navigation and Safety of Sea Transportation vol.3, pp.401–6 .
Vettor, R.; Tadros, M.; Ventura, M., and Guedes Soares, C. Route planning of a fishing vessel in coastal waters with fuel consumption restraint. Guedes Soares, C. & Santos T. A., (Eds.). Maritime Technology and Engineering 3. London, UK: Taylor & Francis Group; 2016; pp. 167-173.
Weber, 1995 T. Weber. Optimale Planung und Steuerung von Schiffsreisen. Phd thesis, Berlin University of Technology (1995)
Zhang LH, Zhang L, Peng RC, Li GX, Zou W. 2011, Determination of the shortest time route based on the composite influence of multidynamic elements. Marine Geodesy vol. 34, pp.108–18.

Appendix A

Solution of certain problems of calculus of variations reformulated as multidimensional optimization problems

1. Introduction

The ship routing problem is to find the route of the ship which minimizes the integral of fuel consumption. Such problems can be generally tackled with the use of calculus of variations, which reduces the aforementioned problem to the solution of a system of differential equations. In this appendix, those equations will be derived and it will be shown why they are not suitable for solving real life problems. So, in order to solve this, an algorithm (of Rayleigh-Ritz type) is proposed. One key point of the proposed algorithm is the ability of solving constrained ship routing problems. In order to check its performance and accuracy, we need to compare it with problems that are similar to the ship routing problem and that have known exact solutions. Ray theory, provides the perfect test case. We will use the analytical and numerical solutions of ray theory as benchmark cases and validate our algorithms ability to solve obstacle problems with the use of calculus of variations.

2.1 General variation of a functional

In this chapter we shall first recall the basic results concerning the variation of functionals of specific integral form defined by the following form (see, e.g., Gelfand & Fomin,…….)

$$\mathscr{J}(y_1,..,y_n,y_1',..,y_n') = \int_{t_0}^{t_1} \mathscr{L}(y_1,..,y_n,y_1',..,y_n';t)dt \quad , \tag{1}$$

where $y_n(t)$, $n=1,2,....$, are continuously differentiable functions and $y_n'(t)=\frac{dy_n(t)}{dt}$, $n=1,2,....$, denote the corresponding derivatives. Moreover,

$\mathscr{L}(y_1,..,y_n,y_1',..,y_n';t)$ is the Lagrangian density. The form of the Lagrangian density is considered to be dependent on the functions $y_n(t)$, $n=1,2,....,$ and their derivatives $y_n'(t), n=1,2,....,$ as well as on the independent variable of integration (denoted here by *t*) . Clearly, if the density $\mathscr{L}(y_1,..,y_n,y_1',..,y_n')$ is real, the functional defined by Eq.(1) is a map of the function space $C^1[t_0,t_1]$ to real numbers $\mathbb{R}$.

In the most simple case *n*=1 the above Eq.(1) becomes

$$\mathscr{J}(y)=\int_{t_o}^{t_1}\mathscr{L}(y_1,y_1';t)dt \quad . \tag{2}$$

All curves corresponding to the admissible function $y(t)$, $t_0<t<t_1$ are considered to be of the class C^1 and we also assume that the end points of these curves can vary in an arbitrary way on the plane. Next, we define the distance between two curves $y(t)$ in the interval $t_0<t<t_1$, and $y^*(t)$, in the interval $t_0^*<t<t_1^*$, shown in Figure A.1, as follows

$$\rho(y,y^*)=\max\left|y-y^*\right|+\max\left|\frac{dy}{dt}-\frac{dy^*}{dt}\right|+P_0P_0^*+P_1P_1^* \tag{3}$$

where $P_0=(t_0,y(t_0))$, $P_0^*=(t_0,y^*(t_0))$ are the left-endpoints of the functions $y(t)$ and $y^*(t)$, $P_1=(t_1,y(t_1))$, $P_1^*=(t_1,y^*(t_1))$ are the right-endpoints, respectively.

Since $y(t)$ and $y^*(t)$, are defined on different intervals we have to extend the support of these functions into a common interval. This is done by using Taylor extrapolation and keeping terms up to first-order (see also Fig.A.1).

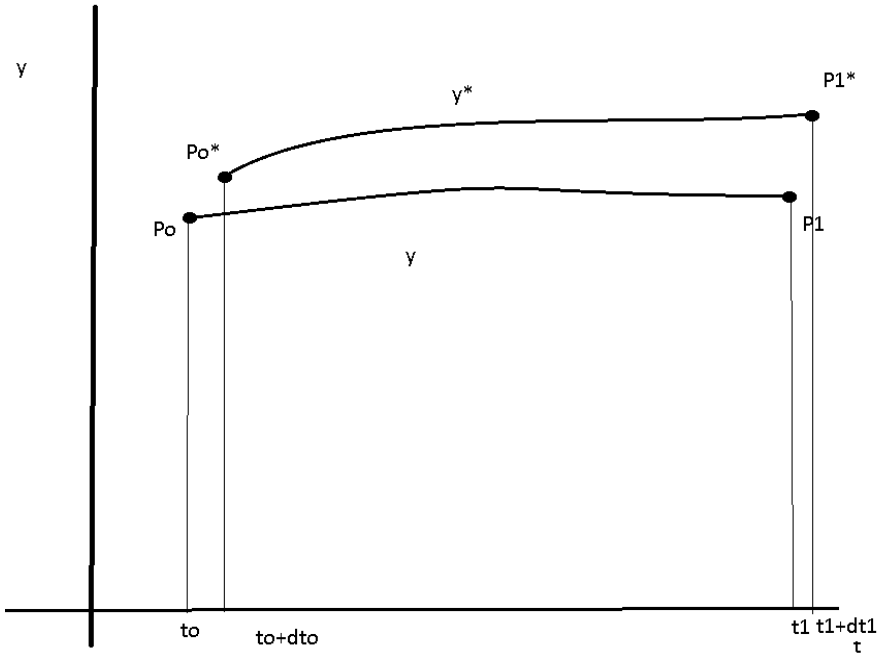

Figure A.1. Functions $y(t)$ in the interval $t_0 < t < t_1$, and $y^*(t)$, in the interval $t_0^* < t < t_1^*$.

To proceed let now $y(t)$ and $y^*(t)$, be two neighboring curves, in the sense of metric (3) in the common interval. We define the difference of the functions by

$h(t) = y^*(t) - y(t)$.

Let $P_o = (t_{0,} y_0)$, $P_1 = (t_1, y_1)$ and $P_o^* = (t_0 + \delta t_0, y_0 + \delta \mathrm{y}_0)$, $P_1^* = (t_1 + \delta t_1, y_1 + \delta \mathrm{y}_1)$,

The variation $\delta \mathscr{J}$ of the functional is defined as the expression which is linear in $h, h', \delta t_0, \delta t_1, \delta y_0$ and differs from $\mathscr{J}(y+h) - \mathscr{J}(y)$ by a higher order quantity, relative to $\rho(y, y^*)$. Thus,

$$\mathscr{J}(y+h) - \mathscr{J}(y) = \int_{t_0+\delta t_0}^{t_1+\delta t_1} \mathscr{L}(y+h, y'+h'; t)dt - \int_{t_0}^{t_1} \mathscr{L}(y, y'; t)dt =$$

$$= \int_{t_0}^{t_1} \mathscr{L}(y+h, y'+h'; t) - \mathscr{L}(y, y'; t)dt + \int_{t_1}^{t_1+\delta t_1} \mathscr{L}(y+h, y'+h'; t)dt - \int_{t_0}^{t_0+\delta t_0} \mathscr{L}(y+h, y'+h'; t)dt$$

(4)

The quantity $\mathscr{L}(t, y+h, y'+h')$ can be re-written by the use of Taylor's theorem around the point $(t, y(t), y'(t))$

$$\mathscr{L}(y+h, y'+h'; t) = \mathscr{L}(y, y'; t) + \frac{\partial \mathscr{L}}{\partial y}\delta y + \frac{\partial \mathscr{L}}{\partial y'}\delta y' + O(\|\delta y\|^2, \|\delta y'\|^2) \quad , \tag{5}$$

where $O(\|\delta y\|^2, \|\delta y'\|^2)$ denote terms of higher (second) order with respect to the remaining ones. Integrating Eq.(5) with regards to t, the only term that remains linear with regards to $h, h', \delta t_0, \delta t_1, \delta y_0$ is $\mathscr{L}(y, y'; t)|_{t=t_0}\ \delta t_0$. Thus, we have

$$\int_{t_1}^{t_1+\delta t_1} \mathscr{L}(y+h, y'+h'; t)dt = \int_{t_1}^{t_1+\delta t_1} \left(\mathscr{L}(y, y'; t)|_{t=t_1} + \frac{\partial \mathscr{L}}{\partial y}\delta y + \frac{\partial \mathscr{L}}{\partial y'}\delta y' + O(\|\delta y\|^2, \|\delta y'\|^2) \right) dt =$$

$$= \mathscr{L}(y, y'; t)|_{t=t_1}\ \delta t_1 + O(\|\delta y\|^2, \|\delta y'\|^2)\delta t_1, \tag{6}$$

and likewise ,

$$\int_{t_0}^{t_0+\delta t_0} \mathscr{L}(y+h, y'+h'; t)dt = \mathscr{L}(y, y'; t)|_{t=t_0}\ \delta t_0 + O(\|\delta y\|^2, \|\delta y'\|^2)\delta t_0 \ . \tag{7}$$

Again by expanding $\mathscr{L}$ using Taylor's theorem and keeping terms up to first-order we get ,

$$\int_{t_0}^{t_1} \mathscr{L}(y+h, y'+h'; t) - \mathscr{L}(\mathrm{y}, \mathrm{y}'; t)\,\mathrm{dt} = \int_{t_0}^{t_1} \left(\frac{\partial \mathscr{L}}{\partial y}\delta y + \frac{\partial \mathscr{L}}{\partial y'}\delta y' + O(\|\delta y\|^2, \|\delta y'\|^2) \right) dt \tag{8}$$

Then by integrating by parts, the term $\frac{\partial \mathscr{L}}{\partial y'}\delta y'$ becomes

$$\int_{t_0}^{t_1} \frac{\partial \mathscr{L}}{\partial y}\delta y + \frac{\partial \mathscr{L}}{\partial y'}\left(\frac{d}{dt}\delta y\right) + O(\|\delta y\|^2, \|\delta y'\|^2)\,\mathrm{dt} =$$

$$= \frac{\partial \mathscr{L}}{\partial y'}\delta y\Big|_{t=t_0}^{t=t_1} + \int_{t_0}^{t_1} \frac{\partial \mathscr{L}}{\partial y}\delta y - \left(\frac{d}{dt}\frac{\partial \mathscr{L}}{\partial y'}\right)\delta y + O(\|\delta y\|^2, \|\delta y'\|^2)\,\mathrm{dt} =$$

$$= \frac{\partial L}{\partial y'}h\Big|_{t=t_0}^{t=t_1} + \int_{t_0}^{t_1} \frac{\partial L}{\partial y}h - \left(\frac{d}{dt}\frac{\partial L}{\partial y'}\right)h + O(\|\delta y\|^2, \|\delta y'\|^2)\,\mathrm{dt}$$

So from (6), (7),(8) it finally follows that the general variation (4) can be written as (by definition the nonlinear terms are eliminated, since the variation is linear with regards to $\delta y, \delta y'$)

$$\delta \mathcal{J} \approx \frac{d\mathcal{L}}{\partial y'} h \Big|_{t=t_0}^{t=t_1} + \int_{t_0}^{t_1} \left[\frac{\partial \mathcal{L}}{\partial y} - (\frac{d}{dt} \frac{\partial \mathcal{L}}{\partial y'}) \right] h(t)dt - \mathcal{L}(y, y'; t)|_{t=t_0} \delta t_0 + \mathcal{L}(y, y'; t)|_{t=t_1} \delta t_1 \qquad (9)$$

We shall denote $\approx$ as equality except for terms of order higher than 1 relative to $\rho\left(y, y' + h'\right)$. Furthermore, it is clear that

$$h(t_o) \approx \delta y_o - y'(t_o)$$
$$h(t_1) \approx \delta y_1 - y'(t_1)$$

$$\delta \mathcal{J} \approx \int_{t_0}^{t_1} \left[\frac{\partial \mathcal{L}}{\partial y} - \frac{d}{dt} \frac{\partial \mathcal{L}}{\partial y'} \right] h(t)dt + \frac{\partial \mathcal{L}}{\partial y'}|_{t=t_1} \delta y_1 + (\mathcal{L} - \frac{\partial \mathcal{L}}{\partial y'} y')|_{t=t_1} \delta t_1 -$$
$$- \frac{\partial \mathcal{L}}{\partial y'}|_{t=t_o} \delta y_0 - (\mathcal{L} - \frac{\partial \mathcal{L}}{\partial y'} y')|_{t=t_0} \delta t_0 \qquad (10)$$

2.2 Generalization for n functions and fixed end-points

Here is described the variation of a functional of the form

$$\mathscr{J}(y_1,..,y_n,y_1',..,y_n') = \int_{t_0}^{t_1} \mathscr{L}(y_1,..,y_n,y_1',..,y_n';t)dt$$

It follows from Eq.(10) that the stationarity of $\mathscr{J}$ for fixed endpoints $y_i(t_o)$, $y_i(t_1)$, $i = 1,2,...n,$ is equivalent to

$$\frac{\partial \mathscr{L}}{\partial y_i} - \frac{d}{dt}\frac{\partial \mathscr{L}}{\partial y_i'} = 0 \quad i = 1,2,...,n \tag{11}$$

Equations (11) are called the Euler-Lagrange equations with boundary conditions $y_i(t_0) = P_0$, $y_i(t_1) = P_1$, where P_0, P_1 are given points in $\mathbb{R}^n$.

The aforementioned problem is a two point boundary value problem , whose solution is a curve that starts from P_0 , ends at P_1 and $\mathscr{J}$ is stationary in the neighborhood of it. In boundary value problems , we often have the non uniqueness of the solution. Combined with the non linearity of the Euler-Lagrange equations and one has a very complex setting-problem , where analytical solutions are rarely possible.

2.3 Obstacle problem

2.3.1 Variation in the case where end points lie on given curves.

Here we shall describe some equations that will be needed for the analytical obstacle problem formulation.

If y is an extremum of $\mathscr{J}$ it must be a solution of the Euler's equation. Thus, the integral in (10) becomes 0 and then

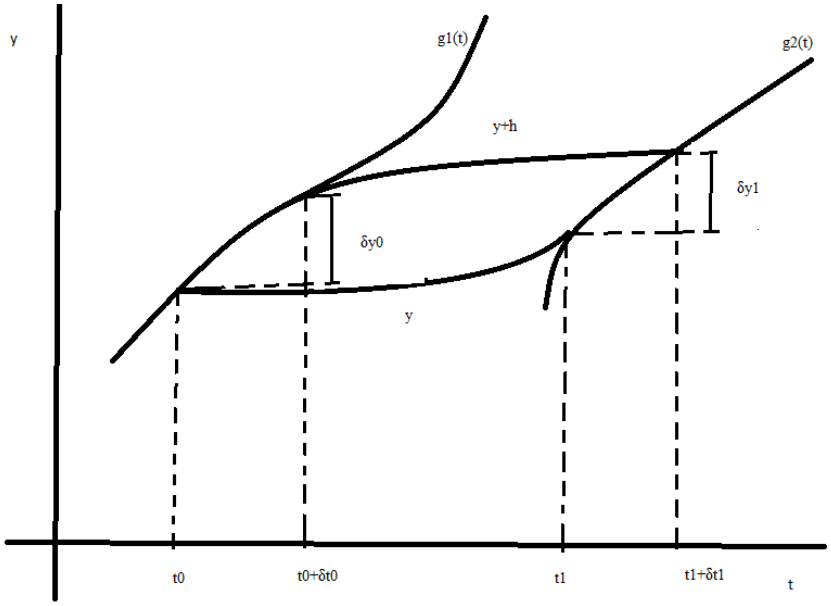

FigA2. The case where end points lie in curves.

$$\delta \mathcal{J} = \frac{\partial \mathscr{L}}{\partial y'}|_{t=t_1}\ \delta y_1 + (\mathscr{L} - \frac{\partial \mathscr{L}}{\partial y'}y')|_{t=t_1}\ \delta t_1 - \frac{\partial \mathscr{L}}{\partial y'}|_{t=t_o}\ \delta y_0 - (\mathscr{L} - \frac{\partial \mathscr{L}}{\partial y'}y')|_{t=t_0}\ \delta t_0\ , \qquad (11)$$

Which must also vanish in order for y to be an extremum.

If P_0 and P_1 lie on two given curves $g_0(t), g_1(t)$ respectively, then

$$\delta y_0 = (g_0'(t_0) + e_0)\delta t_0\ ,\ \delta y_1 = (g_1'(t) + e_1)\delta t_1$$

Where

$e_0, e_1 \to 0$ as $\delta t_0, \delta t_1 \to 0$ respectively as in fig A_2.

The condition (11) becomes

$$\delta \mathcal{J} = (\frac{\partial \mathscr{L}}{\partial y'}g_1' + \mathscr{L} - y'\frac{\partial \mathscr{L}}{\partial y'})\Big|_{t=t_1}\ \delta t_1 - (\frac{\partial \mathscr{L}}{\partial y'}g_0' + \mathscr{L} - y'\frac{\partial \mathscr{L}}{\partial y'})\Big|_{t=t_0}\ \delta t_0 = 0 \qquad (12)$$

Since δt_0 , δt_1 are independent (12), we can vary t_0 (so $\delta t_0 \neq 0$), while having t_1 fixed ($\delta t_1 = 0$) and then do the opposite , this implies the following boundary conditions

$$\left[\mathscr{L}+(g_o'-y)\frac{\partial\mathscr{L}}{\partial y'}\right]\Bigg|_{t=t_0}=0$$
$$\left[\mathscr{L}+(g_1'-y)\frac{\partial\mathscr{L}}{\partial y'}\right]\Bigg|_{t=t_1}=0 \qquad (13)$$

Equations (13) are called transversality conditions.

2.3.2 The Weierstrass-Erdmann Conditions

Let $y(t)$ be $C^1\left[t_0,t^*\right)\bigcup\left(t^*,t_1\right]$, thus there exists a derivative discontinuity on t^* .Also, let y satisfy the boundary conditions

$y(t_0)=y_0,\ y(t_1)=y_1$ as before.

In order for y to be a minimum of (2) it must satisfy the Euler's equation on each interval $\left[t_0,t^*\right]$ and $\left[t^*,t_1\right]$.

We write $\mathscr{J}(y)$ as follows

$$\mathscr{J}(y)=\int_{t_o}^{t_1}\mathscr{L}(y,\dot{y};t)\,dt=\int_{t_o}^{t^*}\mathscr{L}(y,y';t)\,dt+\int_{t^*}^{t_1}\mathscr{L}(y,y';t)\,dt \qquad (14)$$

We calculate the variation of each functional separately. The end points t_0 and t_1 are fixed. The point $t=t^*$ can move arbitrarily, but the two pieces of $y(t)$ most join continuously there. Using (10) , (14) becomes

$$\delta\mathscr{J}=\mathscr{L}y'\big|_{t=t^{*-}}\delta y_1+(\mathscr{L}-y'\frac{\partial\mathscr{L}}{\partial y'})\Big|_{t=t^{*-}}\delta t_1-\mathscr{L}y'\big|_{t=t^{*+}}\delta y_1-(\mathscr{L}-y'\frac{\partial\mathscr{L}}{\partial y'})\Big|_{t=t^{*+}}\delta t_1=$$
$$=\delta y_1(\mathscr{L}y'\big|_{t=t^{*-}}-\mathscr{L}y'\big|_{t=t^{*+}})+\delta t_1((\mathscr{L}-y'\frac{\partial\mathscr{L}}{\partial y'})\Big|_{t=t^{*-}}-(\mathscr{L}-y'\frac{\partial\mathscr{L}}{\partial y'})\Big|_{t=t^{*+}})=0$$

Where t^{*-},t^{*+} are the left and right limits around t^* respectively.

Since $\delta t_1,\delta y_1$ are arbitrary, by keeping one of two fixed while varying the other , it follows that,

$$\frac{\partial \mathscr{L}}{\partial y'}|_{t=t^{*-}} = \frac{\partial \mathscr{L}}{\partial y'}|_{t=t^{*+}}$$
$$(\mathscr{L} - \mathrm{y}'\frac{\partial \mathscr{L}}{\partial y'})|_{t=t^{*-}} = (\mathscr{L} - \mathrm{y}'\frac{\partial \mathscr{L}}{\partial y'})|_{t=t^{*+}} \quad (15)$$

Equations (15) are called the the Weierstrass-Erdmann Conditions and they hold at the point t^* where the extremal has a corner.

2.3.4 Minimization with inequality constraint

In this subchapter we study a very important problem for the ship optimal routing. It is quite common in ship routing problems, for the unbounded optimal solution to pass though land-mass / islands, which of course must be avoided. The mathematical formulation for ship routes that avoid obstacles-islands is as follows.

Minimize $\mathscr{J}[\mathrm{y}] = \int_{t_o}^{t_1} (y, \mathrm{y}'; \mathrm{t})\,\mathrm{dt}$, under the additional constraint $y(t) \geq g(t)$.

It is clear now that our boundary is now a closed one. That implicates our formulation since Euler –Lagrange is derived on open sets(i.e. $y(t)$ is an extremal $y+eh$ for h every in the admissible function space must also belong in the admissible function space, however that is not the case on the boundary of closed sets).In order to bypass this difficulty let us make the following change of variables.

$$z(t)^2 = y(t) - g(t) \geq 0 \quad (16)$$

No restriction has been imposed on z and z=0 corresponds to the boundary y=g.

Thus, the functional $\mathscr{J}(z) = \int_{t_1}^{t_2} \mathscr{L}(z^2 + g, 2zz' + g'; \mathrm{t})dt$

must satisfy Euler –Lagrange with regards to z .

$$\frac{\partial \mathscr{L}}{\partial z} - \frac{d}{dt}\frac{\partial \mathscr{L}}{\partial z'} = 0 \quad (17)$$

But,

$$\frac{\partial \mathscr{L}}{\partial z} = \frac{\partial \mathscr{L}}{\partial y}\frac{\partial y}{\partial z} + \frac{\partial \mathscr{L}}{\partial y'}\frac{\partial y'}{\partial z} = \frac{\partial \mathscr{L}}{\partial y}2z + \frac{\partial \mathscr{L}}{\partial y'}2z',$$

and,

$$\frac{\partial \mathscr{L}}{\partial y'} = \frac{\partial \mathscr{L}}{\partial y}\frac{\partial y}{\partial z'} + \frac{\partial \mathscr{L}}{\partial y'}\frac{\partial y'}{\partial z'} = 0 + \frac{\partial \mathscr{L}}{\partial y'}2z$$

$$\frac{d}{dt}\frac{\partial \mathscr{L}}{\partial z'} = 2z'\frac{\partial \mathscr{L}}{\partial y'} + 2z\frac{d}{dt}\frac{\partial \mathscr{L}}{\partial y'}.$$

Hence, (17) becomes $z(\frac{\partial \mathscr{L}}{\partial y} - \frac{d}{dt}\frac{\partial \mathscr{L}}{\partial y'}) = 0$ (18)

(18) implies that that the extremum of $\mathscr{J}$ may be achieved only on curves composed of the solutions of the Euler-Lagrange equation ($\frac{\partial \mathscr{L}}{\partial y_i} - \frac{d}{dt}\frac{\partial \mathscr{L}}{\partial y_i'} = 0 \quad i = 1, 2, ..., \mathrm{n}$) or pieces of the boundary $(z = 0)$.

Let the extremum be achieved on a composite curve, where the passage from the extremum to the boundary $y = g$ occurs at a point t^*.

$$\mathscr{J}(y) = \int_{t_o}^{t_1} \mathscr{L}(y, y'; \mathrm{t})\,\mathrm{dt} = \int_{t_o}^{t^*} \mathscr{L}(y, y'; t)\,\mathrm{dt} + \int_{t^*}^{t_1} \mathscr{L}(g, g'; t)\,\mathrm{dt} \quad (19)$$

The variation of (19) becomes

$$(\mathrm{y'} - \mathrm{g'})\frac{\partial^2 \mathscr{L}}{\partial y' \partial y'}(y, y'; t)\Big|_{t=t^*} = 0 \quad (20)$$

Thus, if $\frac{\partial \mathscr{L}(y, y'; t)}{\partial y' \partial y'}\Big|_{t=t^*} \neq 0$

$y'(t^*) = g'(t^*)$

Equation (20) follows from the second Weierstrass-Erdmann Condition and the mean value theorem.

3.1 Ray theory applications

It is well known from Fermat's principle that rays of light travel in paths of stationary time and this statement remains valid also for waves in inhomogeneous media where the index of refraction is a variable quantity; see e.g., Brekhovskii & Lysanov, Frisk, Jensen et al. To illustrate the above principle let γ be an arbitrary curve-path between two points $M_0 = x_i(\sigma_0)$, $M_1 = x_i(\sigma_1)$, (possibly corresponding to a source and receiver point) inside the propagation medium; see Figure A.3. Furthermore let $c(x_i)$ be the propagation speed of the wave, which is assumed to be known everywhere.

Denoting here by $d\sigma$ the differential length of curve (ray) γ, with parametric equations $x_i = x_i(\sigma)$ and parameter σ the physical length (i.e. $\|dx_i / d\sigma\| = 1$), the corresponding time it takes the wave to travel $d\sigma$ is obviously $dt = d\sigma / c(x_i)$. Thus, the functional of total time the wave needs to travel from point M_0 to M_1 along ray γ is

$$\tau[\gamma] = \int_{\gamma} \frac{d\sigma}{c(x_i)} = \int_{\sigma_0}^{\sigma_1} \frac{d\sigma}{c(x_i(\sigma))}, \quad M_0 = x_i(\sigma_0), \;\; M_1 = x_i(\sigma_1) \;, \tag{21}$$

and Fermat's principle states that the curve γ ($x_i = x_i(\sigma)$) will be a stationary point of the functional $\tau[\gamma(\cdot)]$, i.e. $\delta\tau[\gamma] = 0$.

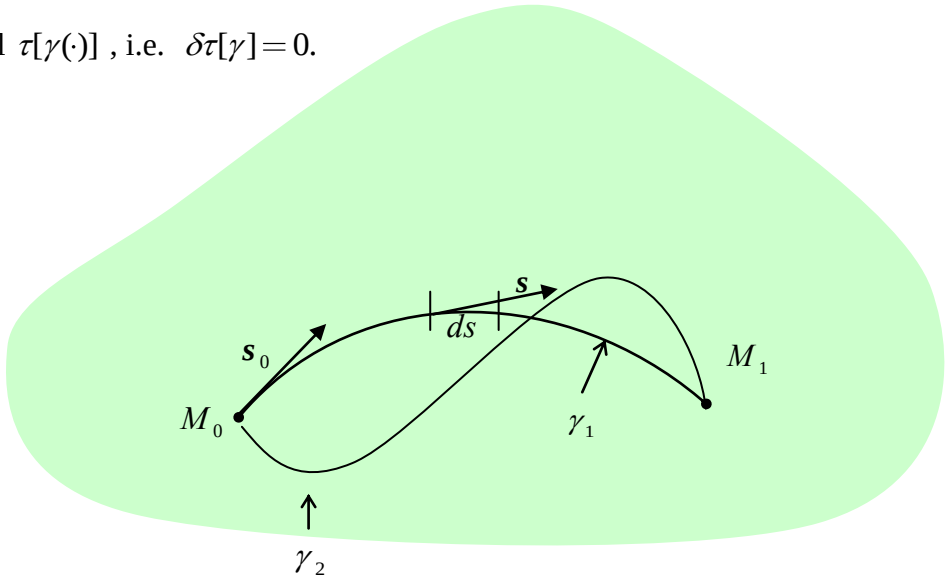

Figure A.3 Rays joining points M_0 and M_1.

The Euler-Lagrange equations for the ray function $\mathscr{L}\left(x_i, x_i'\right) = \frac{\| dx_i / d\sigma \|}{c(x_i)} = \frac{\| x_i' \quad \sigma \|}{c(x_i)}$ becomes the following nonlinear system of second-order equations

$$\frac{d}{d\sigma}\left(\frac{x_i'(\sigma)}{c(x_i(\sigma))}\right) - \frac{\partial}{\partial x_i}\left(\frac{1}{c(x_i)}\right) = 0, \quad i = 1,2,3. \tag{22}$$

The above system can be also equivalently written as a system of first-order equations by defining the generalized ray tangent vector (at each point σ along the ray)

$$\xi_i(\sigma) = \frac{1}{c}\frac{dx_i(\sigma)}{d\sigma} \quad . \tag{23}$$

Using the above equation, the system (22) is put in the form

$$\frac{dx_i(\sigma)}{d\sigma} = c(x_i)\,\xi_i(\sigma) \tag{23a}$$

$$\frac{d\xi_i(\sigma)}{d\sigma} = -c^{-2}\frac{\partial c}{\partial x_i} = -c^{-2}\cdot\nabla c \tag{23b}$$

from which the solution $x_i(\sigma)$ can be calculated. The most usual problem in ray applications is the initial value problem, where the coordinates of the source point $x_i(\sigma_0) = M_0$ are given and the system of rays emanating from the source are constructed as a solution to the system (23) corresponding to specific directions at the source (specifying the grazing angle) $x_i' \quad \sigma_0 \quad = given$. In this case, the solution $x_i(\sigma)$, for $\sigma_0 \le \sigma \le \sigma_1$ is calculated in straightforward way by integration of the system (23).

Let $\{s_i\}_N$ be a discritisation of $[\sigma_0, \sigma_1]$, with $\sigma_0 = s_0 < s_1 < s_2 < ... < s_N = \sigma_1$

For an arbitrary s_k we have

$$\left.\begin{aligned} x_i'(s_{k-1}) &\approx \frac{x_i(s_k)-x_i(s_{k-1})}{s_k-s_{k-1}} \\ \xi_i'(s_{k-1}) &\approx \frac{\xi_i(s_k)-\xi_i(s_{k-1})}{s_k-s_{k-1}} \end{aligned}\right\} \Rightarrow \left.\begin{aligned} x_i(s_k) &= x_i(s_{k-1})+(s_k-s_{k-1})x_i'(s_{k-1}) \\ \xi_i(s_k) &= \xi_i(s_{k-1})+(s_k-s_{k-1})\xi_i'(s_{k-1}) \end{aligned}\right\} \xrightarrow{(23)}$$

$$x_i(s_k) = x_i(s_{k-1})+(s_k-s_{k-1})c\left(x_i(s_{k-1})\right)\xi_i\left(s_{k-1}\right)$$
$$\xi_i(s_k) = \xi_i(s_{k-1})+(s_k-s_{k-1})-c\left(\mathrm{x}_i(s_{k-1})\right)^{-2}\cdot\nabla c\left(\mathrm{x}_i(s_{k-1})\right)$$

$x_i(s_0)=M_0$ given and it follows from (23) that

$\xi_i(s_0)=c\ \mathrm{x}_i(s_0)\ ^{-1}\cdot x_i'\ s_0$, where $x_i'\ \ s_0\ = given$.

Iterating this procedure for $i=1,2,...,N-1$ yield all the $x_i(\mathrm{s}_k),\xi_i(\mathrm{s}_k)$

As an example it is shown in FigA4 a source emitting rays at angles $(-30,30)$ on a medium with propagation speed $c(\mathbf{x})=c_1\cdot cosh(c_2\cdot(y+d))$, where $c_1=1510$, $c_2=6\cdot10^{(-4)}$ and $d=-300$

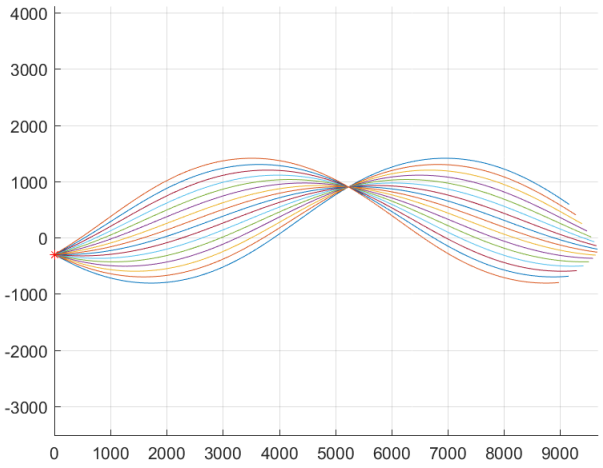

Figure A.4 Rays in the case of an environment with index of refraction .

3.2 BVP problem: Ray from source to receiver point

Now let us consider a similar problem of ray equations which is however more connected to the weather ship routing problem examined in the present work, and thus it helps us to illustrate the effectiveness and performance of the simplex minimization procedure developed for the solution. In this case, given the distribution of propagation speed $c(x_i)$, we seek the path of a transmitted ray from a source point $M_0 = x_i(\sigma_0)$ that reaches a given receiver point with coordinates $M_1 = x_i(\sigma_1)$. The system of Eqs (23) in conjunction with the above data constitutes a nonlinear boundary value problem.

One way to solve this problem is by the use of iterative methods like the shooting method. In numerical analysis, the shooting method is a method for solving a boundary value problem by reducing it to the solution of many initial value problems. Roughly speaking, we 'shoot' out ray trajectories emanating from the source point $M_0 = x_i(\sigma_0)$ in different directions specified by the initial tangent vector $x_i' \quad \sigma_0$, until we find two rays enclosing the desired boundary value $M_1 = x_i(\sigma_1)$. Then the above prediction is refined by appropriate successive iterations.

Let us illustrate the above procedure in the case of two-dimensional ray problem concerning the studied boundary value problem on the plane. More specifically, we consider the n-sequence of solutions $x_i\left(\sigma; a_i^n\right)$ of the initial value problem consisted of Eqs. (23) and the boundary data $x_i(\sigma_0) = M_0$ and $x_i' \quad \sigma_0 \; = a_i^n$,

$\alpha_n = \alpha_1 + \; n-1 \; \delta\alpha$, such that $\alpha_1 < \alpha_n < \alpha_1 + \; N-1 \; \delta\alpha$

where $\alpha = \tan^{-1}\left(a_2 / a_1\right)$ is the grazing angle. The above sequence covers a sector - opening angle $N-1 \; \delta a$ at the point of the source $M_0 = x_i(\sigma_0)$. Let now $x_i\left(\sigma = \sigma_1; \alpha_m\right) < M_1 \equiv x_i(\sigma_1) < x_i\left(\sigma = \sigma_1; \alpha_{m+1}\right)$, for some value *n*=*m* of the index *n*. The new values of initial directions (values of the tangent vector of the ray at the source) for solving the boundary value problem are estimated by

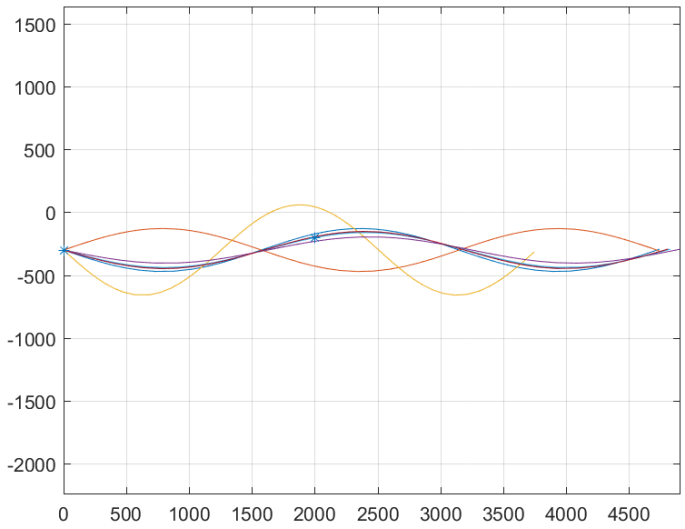

Fig.A5 The BVP solved with iterations of the IVP.

$\alpha_n = \alpha_m + \ n-1 \ \ \alpha_{m+1} - \alpha_m$.

This procedure is iterated until convergence, which results in the grazing angles focusing around the end boundary point.

Below, Fig.A5 we see an example of the said algorithm with source and receiver point and with the same

$c(\mathbf{x}) = c_1 \cdot cosh(c_2 \cdot (y + d))$, as in the IVP example.

3.3 Ray propagation with obstacle

In the preliminaries chapter we have derived the appropriate condition that holds on the point of interception of the boundary of the object and the path of the ray, which is the eq (20). We denote as $\mathbf{x}(t), \mathbf{g}(t)$ the parametric representations of the path of the ray and the object respectively.

Eq 20 means (in our formulation of ray propagation) that

$$\frac{dx_2}{dx_1} = \frac{dx_2 \ \ \sigma = \sigma^* \ / d\sigma}{dx_1 \ \ \sigma = \sigma^* \ / d\sigma} = \frac{dg_2 \ \ t = t^* \ / dt}{dg_1 \ \ t = t^* \ / dt}$$

A good example where this can been seen is in FigAxx.

Where σ^* and t^* are the parameter values for the curves $\boldsymbol{x}(\sigma)$ & $\boldsymbol{g}(t)$ at the interception point.

4.1 Treatment of the ray problem using downhill simplex algorithm

In real problems, like the ship routing, however, the mathematical rigorous approach does not perform very well. The sparseness of the data do not allow for accurate calculations of the derivatives of the ship fuel consumption which are needed and the time performance of the calculus of variations method would be the same or even worse than the direct method we are presenting below.

Considering again the familiar problem

$$\text{Minimize } \mathscr{J}[\mathrm{y}] = \int_{t_o}^{t_1} \mathscr{L}(y, \mathrm{y}'; \mathrm{t})\,\mathrm{dt} \quad \text{with boundary conditions } \begin{matrix} y(t_o) = 0 \\ y(t_1) = 0 \end{matrix}, \tag{22}$$

If we make the assumption, that $y \in L_2[t_o, t_1]$, then a basis of $L_2[t_o, t_1]$ satisfying the above boundary conditions is $\left\{ \sin\left(\frac{\mathrm{k}\,\pi(t - t_o)}{t_1 - t_o} \right) \right\}_{k \in \mathbb{N}}$ and then for a finite N , y admits the following truncation

$$y \approx \sum_{k=1}^{k=N} a_k \sin\left(\frac{k\pi(t - t_o)}{t_1 - t_o} \right) \tag{23}$$

By inserting (23) into (22) , $\mathscr{J}[y]$ becomes $\mathscr{J}(\alpha_1, a_2, ..., a_k)$, $i = 1, 2, ..., N$ reducing the minimization of (22) to an optimization of a function of N variables a_k . This is called the Rayleigh-Ritz method.

4.2 Optimization algorithms and downhill simplex

Downhill Simplex

The downhill simplex method is due to Nelder and Mead (1965); see e.g., Press et al (1997,Chap.10)..The method requires only function evaluations, not derivatives. It is not very efficient in terms of the number of function evaluations that it requires. However, the downhill simplex method may frequently be the best method to use if the figure of merit is "get something working quickly" for a problem whose computational burden is small. A simplex is the geometrical figure consisting, in N dimensions, of N + 1 points (or vertices) and all their interconnecting line segments, polygonal faces, etc. In two dimensions, a simplex is a triangle. In three it is a tetrahedron, not necessarily the regular tetrahedron. Given the simplex's starting points, the algorithm moves the points of the simplex where our function has smaller values, using reflections, expansions and contractions of our starting shape-simplex converging to the local minimum.

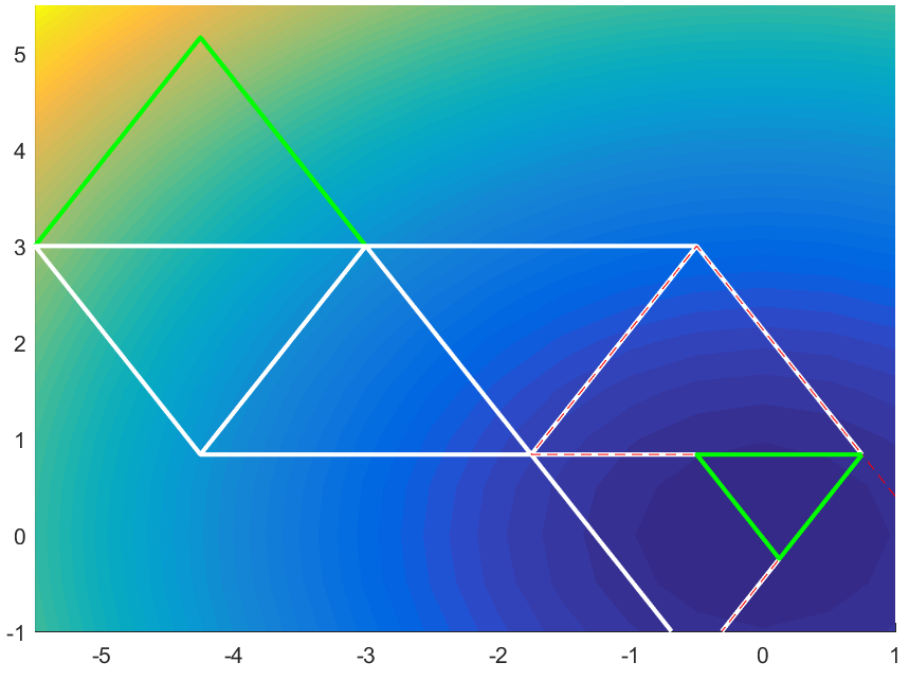

Figure A6. Application of downhill simplex algorithm to the minimization of function $f(x,y) = x^2 + y^2$. First 7 iterations, with first iteration being the left green triangle and the 7^{th} the right one.

Conjugate Directions

If we minimize a function along some direction u, then the gradient of the function must be perpendicular to u at the line minimum; if not, then there would still be a nonzero directional derivative along u. Take some particular point $\mathbf{P}$ in the coordinate system with coordinates **x**. Then any function f can be approximated by its Taylor series around $\mathbf{P}$.

$$f(\boldsymbol{x}) = f(\boldsymbol{P}) + \sum_i \frac{\partial f}{\partial x_i} x_i + \frac{1}{2} \sum_{i,j} \frac{\partial^2 f}{\partial x_i \partial x_j} x_i x_j + \ldots$$

$$\approx \boldsymbol{c} - \boldsymbol{b}\boldsymbol{x} + \boldsymbol{A}\boldsymbol{x}$$

Where $c \equiv f(\boldsymbol{P})$ $\quad \boldsymbol{b} = -\nabla f|_{\boldsymbol{P}}$ $\quad \boldsymbol{A}_{ij} = \left.\frac{\partial^2 f}{\partial x_i \partial x_j}\right|_{\boldsymbol{P}}$

Through the Taylor approximation, the gradient of f is easily calculated as

$$\nabla f = \boldsymbol{A} \cdot \boldsymbol{x} - \boldsymbol{b} \tag{24}$$

This implies that the gradient will vanish at a value of **x** obtained by solving $\boldsymbol{A} \cdot \boldsymbol{x} = \boldsymbol{b}$. We have that

$$\delta(\nabla f) = \boldsymbol{A} \cdot \delta\boldsymbol{x} \tag{25}$$

Suppose that we have moved along some direction u to a minimum and now purpose to move along some new direction v. The condition that motion along v not spoil our minimization along u is just that the gradient stay perpendicular to u, i.e., that the change in the gradient to be perpendicular to **u**. By equation (25) this is just

$$0 = \boldsymbol{u} \cdot \delta(\nabla f) = \boldsymbol{u} \cdot A \cdot \boldsymbol{v} \tag{26}$$

When (26) holds for two vectors **u** and **v**, they are said to be conjugate. When the relation holds pairwise for all members of a set of vectors, they are said to be a conjugate set. If you do successive line minimization of a function along a conjugate set of directions, then you don't need to redo any of those directions. A triumph for a direction set method is to come up with a set of N linearly independent, mutually conjugate directions. Then, one pass of N line minimizations will find the exact minimum of a quadratic form. For functions f that are not exactly quadratic forms, it won't be exactly at the minimum; but repeated cycles of N line minimizations will in due course converge quadratically to the minimum.

Powell's Quadratically Convergent Method

Powell first discovered a direction set method that does produce N mutually conjugate directions. In steps:

Initialize the set of directions u_i to the basis vectors,

$$u_i = e_i \qquad i = 1,...,N \quad (10.5.6)$$

Now repeat the following sequence of steps until the function stops decreasing:

• Save your starting position as $\boldsymbol{P}_0$.

• For i = 1,...,N, move $\boldsymbol{P}_{i-1}$ to the minimum along direction u_i and name this point $\boldsymbol{P}_i$.

• For i = 1,...,N − 1, set $u_i \leftarrow u_{i+1}$.

• Set $u_N \leftarrow \boldsymbol{P}_N - \boldsymbol{P}_0$.

• Move $\boldsymbol{P}_N$ to the minimum along direction u N and call this point $\boldsymbol{P}_0$.

Powell, in 1964, showed that, for a quadratic form like (10.5.1), k iterations of the above basic procedure produce a set of directions u_i whose last k members are mutually conjugate. Therefore, N iterations of the basic procedure, amounting to N(N + 1) line minimizations in all, will exactly minimize a quadratic form. Unfortunately, there is a problem with Powell's quadratically convergent algorithm. The procedure of throwing away, at each stage, u_1 in favor of $\boldsymbol{P}_N - \boldsymbol{P}_0$ tends to produce sets of directions that are linearly dependent. Once this happens, then the procedure finds the minimum of the function if only over a subspace of the full N-dimensional case. There are a number of ways to fix up the problem of linear dependence in Powell's algorithm, among them:

1. Reinitialization the set of directions u_i to the basis vectors e_i after every N or N + 1 iterations of the basic procedure.

2. The set of directions can equally well be reset to the columns of any orthogonal matrix. Rather than throw away the information on conjugate directions already built up, reset the direction set to calculated principal directions of the matrix A .

3. You can give up the property of quadratic convergence in favor of a more heuristic scheme (due to Powell), which tries to find a few good directions along narrow valleys instead of N necessarily conjugate directions.

Genetic algorithms

The genetic algorithm is a method for solving both constrained and unconstrained optimization problems that is based on natural selection, the process that drives biological evolution. The genetic algorithm repeatedly modifies a population of individual solutions. At each step, the genetic algorithm selects individuals at random from the current population to be parents and uses them to produce the children for the next generation. Over successive generations, the population "evolves" toward an optimal solution. You can apply the genetic algorithm to solve a variety of optimization problems that are not well suited for standard optimization algorithms, including problems in which the objective function is discontinuous, non-differentiable , stochastic, or highly nonlinear. The genetic algorithm can address problems of mixed integer programming, where some components are restricted to be integer-valued. The genetic algorithm uses three main types of rules at each step to create the next generation from the current population:

1.Selection rules select the individuals, called parents, that contribute to the population at the next generation.

2.Crossover rules combine two parents to form children for the next generation.

3.Mutation rules apply random changes to individual parents to form children.

Method Comparisons

The downhill simplex is the most robust out of all the aforementioned methods , can handle discontinuities which are important in our formulation, it is much faster than the genetic algorithm. The alternative simplex algorithm that we propose can handle very high dimensional optimization with very good computational performance.

5. Validation in the case of rays

We will now proceed with the comparisons between the simplex and the analytical /numerical solutions. We will use as examples one test case with variable index of refraction and one case with fixed (homogenous medium). For each of those cases we will also solve the obstacle problem with the simplex direct method, to verify its ability to by-pass islands and landmass when applied to the Mediterranean.

Example 1a. Unbounded setting

For the case of source and receiver point with $x_0 = (0, -700)$, $x_1 = (2000, -600)$,

$c(\mathbf{x}) = c_1 \cdot cosh(c_2 \cdot (y + d))$, where $c_1 = 1510$, $c_2 = 610^{-3.6}$ and $d = 700$

For the IVP with shooting angle θ we have the analytical solution

$$Z = -d + \frac{1}{c_2} \operatorname{asinh}\left(\tan(\theta)\sin(c_2(t))\right)$$

Both the analytical (green color) and the IVP numerical solution (blue color) is compared with the solution via simplex (red color) in Fig.A7.

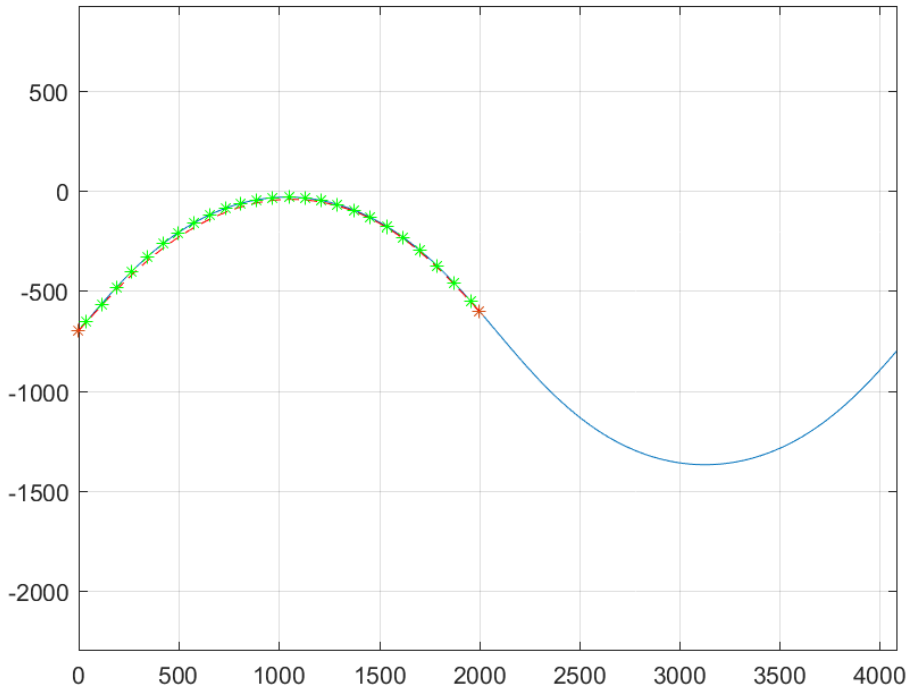

Figure.A7 Simplex vs IVP vs analytical.

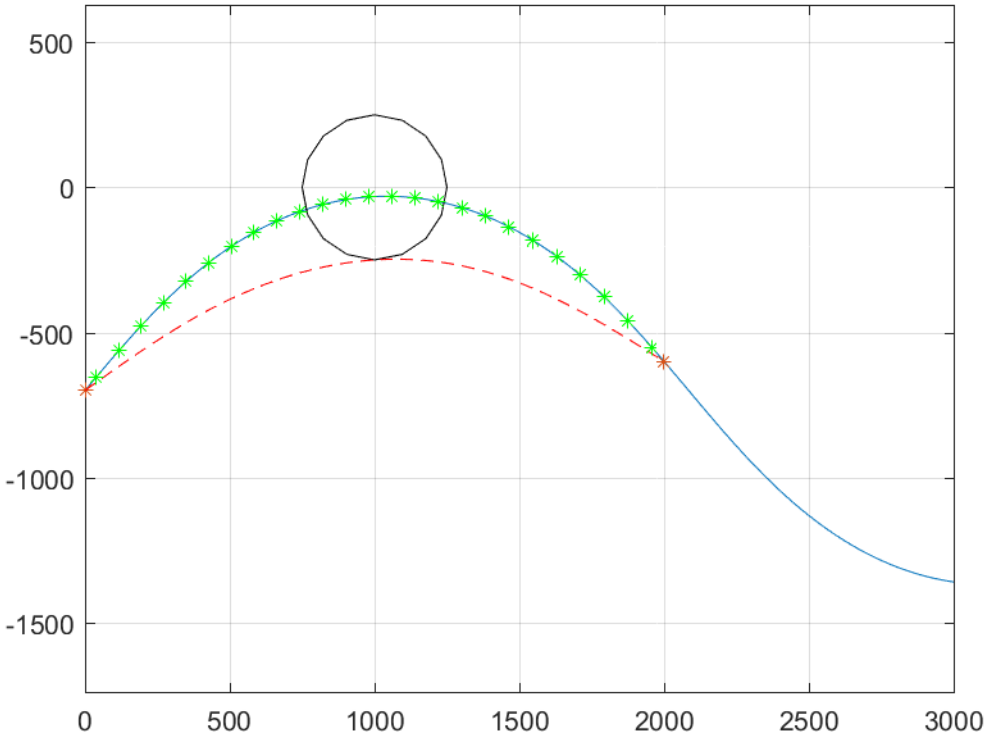

Fig.A8 The case with cosh profile, but with an obstacle on the path of the unbounded optimal solution(blue IVP/green analytical) vs the simplex (red).

Example 1b. The obstacle case.

In this case, we put an obstacle in the shape of a circle, with parametric equations $\left(250\cdot\cos(t)+1000,250\cdot\sin(t)-1000\right)$ $t\in(0,2\pi)$, in the path of the unbounded optimal solution and we observe that the simplex solution verifies the two analytical results we have derived from the previous subchapters. First, it is tangent to the obstacle at the point of the intersection and the end point. Second, at each interval before and after the intersection the solution satisfies the Euler Lagrange equation.

Example 2a. Unbounded homogeneous medium

In the case of the homogenous medium the analytical solution is obviously a straight line joining the boundary points. The simplex solution gives us exactly that.

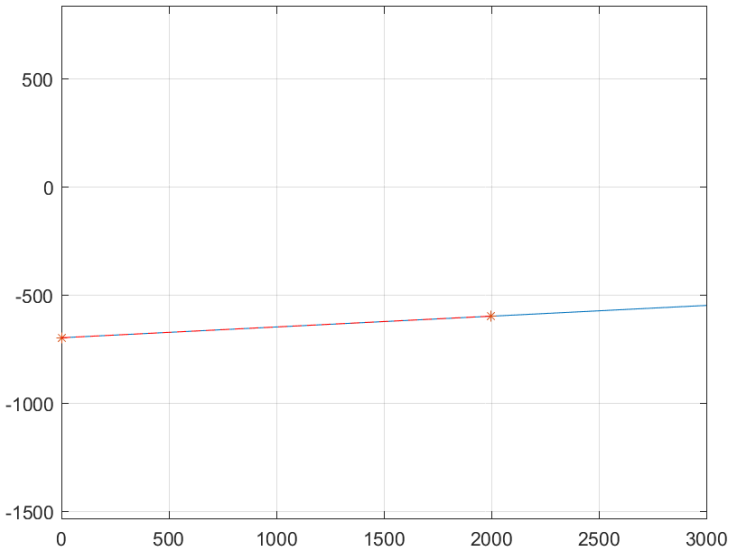

Figure.A9 Analytical solution for homogenous medium (blue) vs Simplex(red).

Example 2a. Homogenous medium with obstacle

This test case is more interesting than the last. We have put an obstacle in the shape of a circle with parametric equations $(1200\cdot\cos(t)+2000,1200\cdot\sin(t)-300)$ $t\in(0,2\pi)$ on the line that joins the boundary points. The solution satisfies the analytical results derived in previous subchapters equations (20& 23) and the analytical solution derived by Petrov (1968, p. 120).

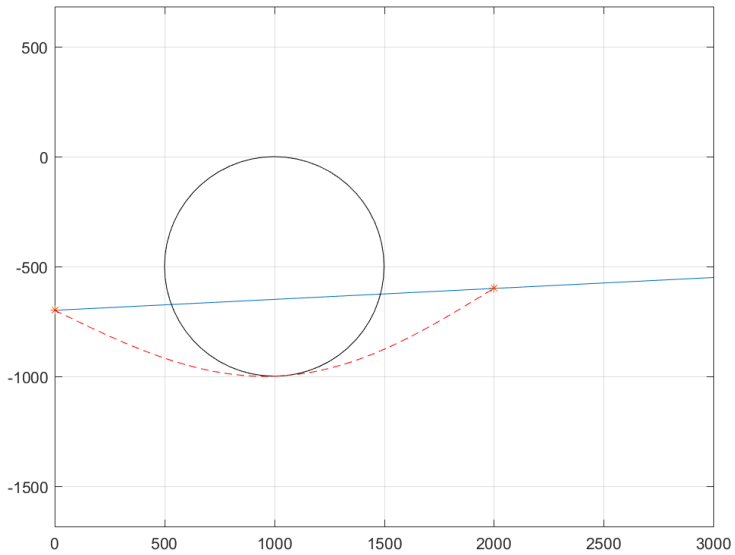

Figure.A10 Simplex solution to the obstacle problem on the homogenous case.

Appendix B
Validation of algorithm through the Sturm Liouville problem

Another very interesting test case for our algorithm is the Sturm-Liouville (or S-L) problem. We are going to describe the variational approach and derive the first eigenfunctions and eigenvalues using the Rayleigh–Ritz method and the downhill simplex as the optimization algorithm.

Sturm Liouville systems

The S-L theory, is the theory of the real second-order linear differential equation of the form

$$\frac{d}{dx}\left[p(x)\frac{du}{dx}\right] + q(x)u = -\lambda r(\mathrm{x})u \ , \ x \in [x_1, x_2] \tag{24}$$

It can also be seen as an eigenvalue problem with regards to u

$$\mathrm{Lu} = \lambda \mathrm{u}$$

Where $Lu = -\frac{1}{r(\mathrm{x})}\left(\frac{d}{dx}\left[p(x)\frac{du}{dx}\right] + q(x)u \right)$

$r(x), p(x), q(x)$ are given and the functions $p(x)$ and $r(x)$ are required to be everywhere positive and bounded away from zero.

The S-L problem can be reformulated as a variational problem as follows. We are considering the simple case where the boundary values are $u(x_1) = 0$, $u(x_2) = 0$.

It can be shown (see Gelfand and Fomin 1963) that the eq (24) is the Euler-Langrange equation of the following variational problem and both eq (24) and the boundary values can be obtained by solving:

Minimise the functional $\mathcal{J}[u]$ defined as follows:

$$\mathcal{J}[u] = \frac{\int_{x_1}^{x_2} \left[p(x)u'(x)^2 + q(x)u(x)^2 \right] dx}{\int_{x_1}^{x_2} r(x)u(x)^2 dx} \tag{25}$$

Where the eigenvalue λ is equal to

$$\lambda = \frac{\int_{x_1}^{x_2} \left[p(x)u'(x)^2 + q(x)u(x)^2 \right] dx}{\int_{x_1}^{x_2} r(x)u(x)^2 dx} \ . \tag{26}$$

By using the Rayleigh–Ritz method we calculate the eigenfunction and eigenvalue $u_1(x)$ and λ_1 (which is the lowest non–trivial eigenvalue for this equation and boundary conditions) respectively. The next eigenfunction/eigenvalue can be obtained by minimizing $Q[\mathrm{u}] = \int_{x_1}^{x_2} \left[p(x)u'(x)^2 + q(x)u(x)^2 \right] dx$ under the additional constaint $\int_{x_1}^{x_2} r(x)u_1(x)u(x)dx = 0$.

Thus, the $\mathrm{i_{th}}$ eigenfunction/eigenvalue can be found by minimizing $Q[\mathrm{u}]$ under the additional constraints $\int_{x_1}^{x_2} r(x)u_1(x)u(x)dx = 0$, $\int_{x_1}^{x_2} r(x)u_2(x)u(x)dx = 0, \ldots, \int_{x_1}^{x_2} r(x)u_{i-1}(x)u(x)dx = 0$.

The additional constraint's meaning, is that we seek a function that minimizes $Q[u]$, that is also orthogonal to the previous functions found, with respect to the inner product

$$\langle f, g \rangle_r = \int_{x_1}^{x_2} r(x) f(x) g(x) dx$$

The first Eigenfunction and eigenvalue of the S-L problem using Rayleigh–Ritz method and downhill simplex

Let us consider the hydro-acoustics waveguide confined between two horizontal soft boundaries (zero dirichlet boundary conditions) at positions $z = 0, z = -h$.

The Helmholtz equation in 2 dimensions for a line source in plane geometry, with sound speed and density depending only on depth z is,

$$\frac{\partial^2 p}{\partial x^2}+\rho(z)\frac{\partial}{\partial z}\left(\frac{1}{\rho(z)}\frac{\partial p}{\partial z}\right)+\frac{\omega^2}{c^2(z)}p=-\delta(x_s)\delta(z-z_0) \qquad (27)$$

Where ω is the angular frequency of the source, p is the pressure. The line source is parallel to the x axis and intercepts the z axis at z_0.

Using separation of variables, we seek a solution in the form $p(x,z)=\Psi(z)\Phi(x)$. After substituting and dividing by $\Psi(z)\Phi(x)$ we get,

$$\left[\frac{1}{\Phi}\frac{d^2\Phi}{dx^2}\right]+\left[\frac{1}{\Psi}\rho(z)\frac{d}{dz}\left(\frac{1}{\rho(z)}\frac{d\Psi}{dz}\right)+\frac{\omega^2}{c^2(z)}\right]=0$$

In each bracket the contents are functions of x,z respectively. Therefore, the only way the equation can be satisfied is if each component is equal to a constant, let us denote it k_{xm}. We obtain the following modal equation,

$$\rho(z)\frac{d}{dz}\left(\frac{1}{\rho(z)}\frac{d\Psi_m(z)}{dz}\right)+\left(\frac{\omega^2}{c^2(z)}-k_{xm}^2\right)\Psi_m(z)=0 \qquad (28)$$

With $\Psi_m(0)=0$, $\Psi_m(-h)=0$.

This is an S-L problem and below we solve it using the variational method, in order to validate our algorithm.

As an example we consider $c(z)=1500\frac{m}{s}, \rho(z)=\text{constant}, \omega=2\pi\cdot 100, \text{h}=500\,\text{m}$. This classical S-L system has the analytical solution $\text{a}\sin\left(\frac{k\pi z}{-h}\right)$, $k=1,2,\ldots$, $0\le z\le -h$. The corresponding eigenvalues are $\left(\frac{k\pi}{h}\right)^2$. The first eigenfucntion Ψ_1 is calculated using simplex using the variational principle described by eq. (25) and is plotted in the figure below with blue straight line. The analytical solution is also plotted using dots.

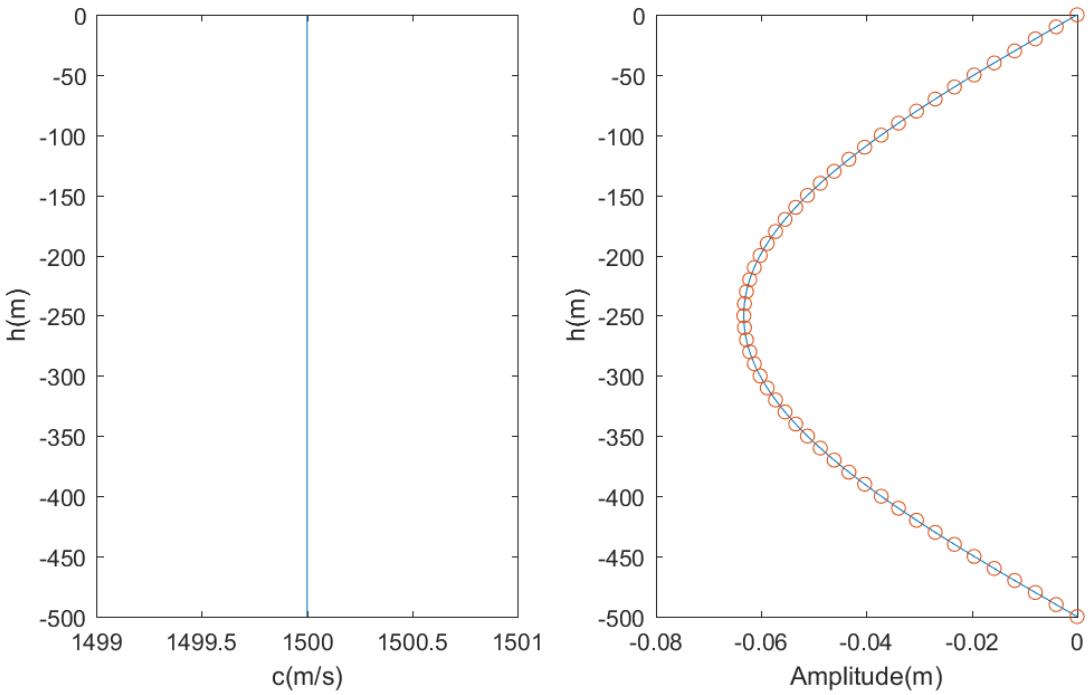

Figure B1. Left, graph of $c(z)$. Right, first eigenfunction derivation using simplex.

As a second example, we consider the case of an inhomogeneous vertical soundspeed profile $c(z)$ charadcterized by a minimum (summer profile) as plotted in Fig.B2. The first eigenfucntion Ψ_1 is calculated again by using simplex using the variational principle described by eq. (25). The analytical solution for this problem does not exist so in order to validate the solution we solve the corresponding differential equation (28) using finite differences; see e.g., Jensen et al (1994). The solution of the first eigenfunction obtained numerical by the finite difference method using N=500 points is plotted in Fig.B2 using cyan line.

Something that has to be remarked in this example is that the solution is an extreme case in the sense that it requires a lot of sine series terms to be approximated. The downhill simplex algorithm blows up for a merit function of more than 12 variables, therefore it is necessary to use the alternative algorithm developed in the present thesis, which is described in section 4.3. The solution using simplex for 11 sine terms is compared against the alternative algorithm using 50 terms and are plotted below.

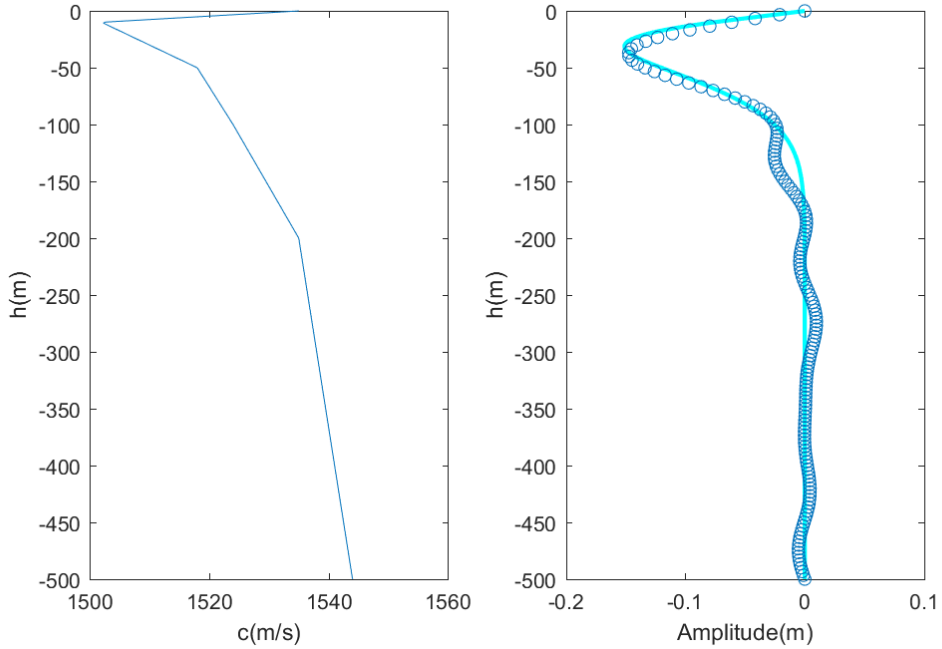

Figure B2. Left, graph of $c(z)$, which represents a typical summer sound speed profile. Right, first eigenfunction derivation using finite differences (cyan straight) vs solution with downhill simplex with 11 terms of sine series .

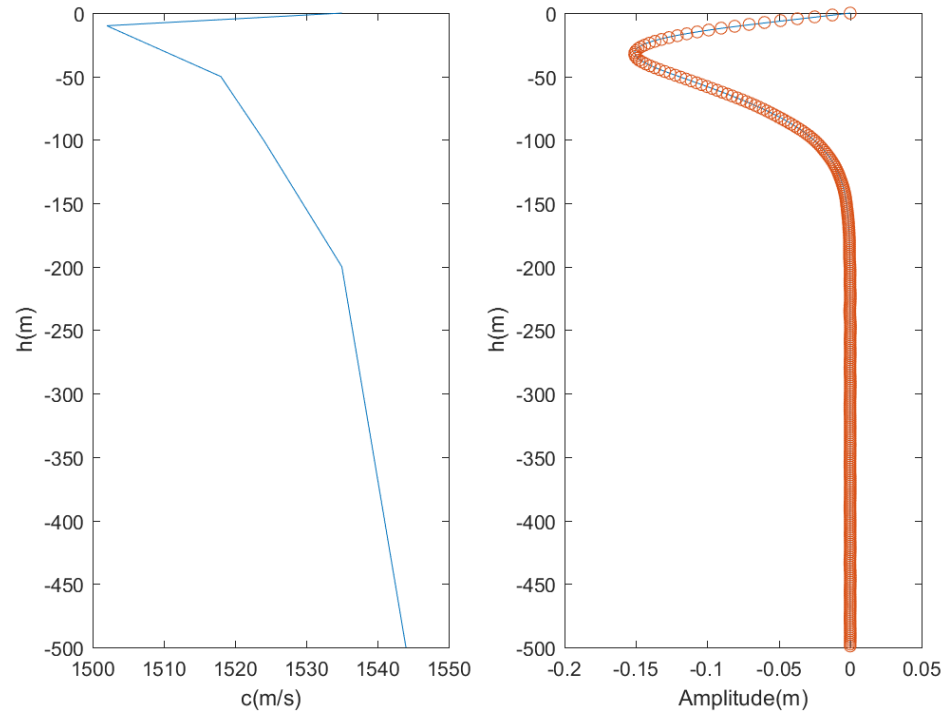

Figure B3. First eigenfunction derivation using the alternative algorithm with 50 terms of sine series.

Appendix C

Matlab® and GUI implementation

In this chapter we are going to describe in detail the Matlab® GUI created in the present thesis. The Graphical User Interfaces) provide point-and-click control of software applications, eliminating the need to learn a language or type commands in order to run the application. GUIDE (GUI development environment) provides tools to design user interfaces for custom apps. Using the GUIDE Layout Editor, one can graphically design their UI. GUIDE then automatically generates the MATLAB code for constructing the UI, which can be modified, to program the behavior of their application.

GUI Showcase

First, we are going to explain what everything on the GUI does and how to use it. When running the shipopt_v1.m, a window opens that contains the following:

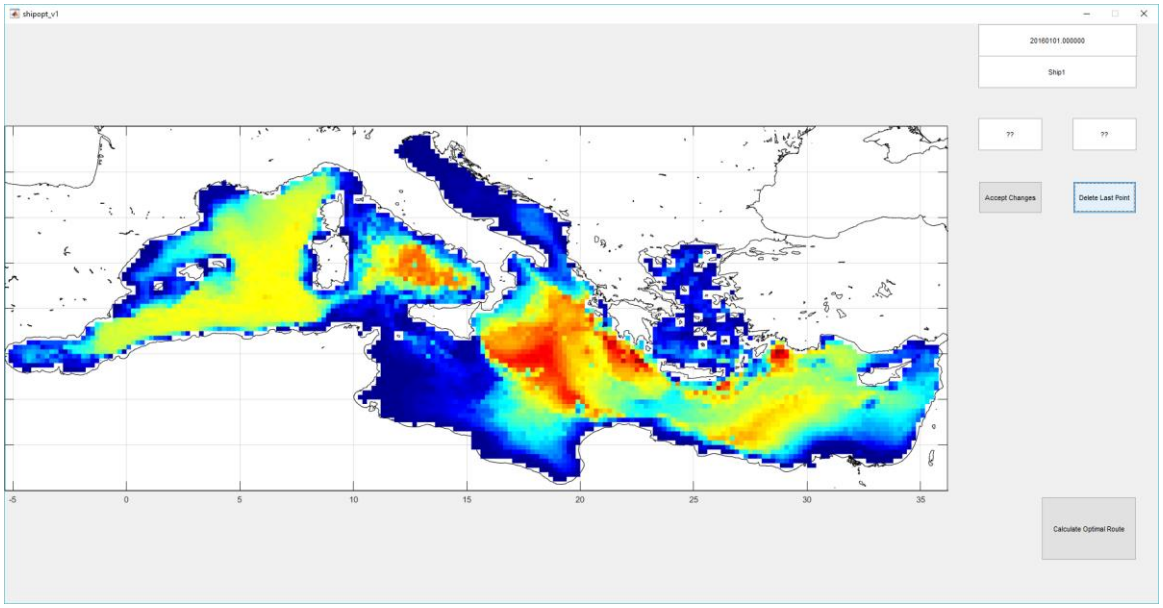

In the middle of the window, upon loading, the Mediterranean coast line and bathymetry are loaded and plotted in the figure. The user here can click on the map to insert waypoints. The first waypoint is the departure point, the last is the arrival point. If more than one points are given, let them be n number of points, then the ship optimal route is found $n-1$ times for

each of the waypoint pairs in the order they were given. For each pair the travel time is calculated and then added to the departure date, which becomes the departure date for the next pair.

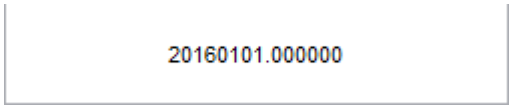

Here, the date of the departure is inserted in ISO format. For instance, 21 of January 2013 7:43 pm corresponds to 20130121.194300 .

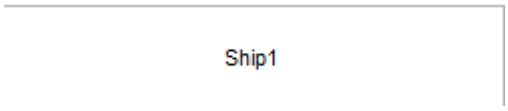

Here, the name of the ship is typed by the user. This is needed, because, we have created a database with different ships and it requires the name of the ship in order to load its data (engine load characteristics, resistance tables, etc).

This box displays the coordinates (longitude and latitude) of the last input point given by the user, so that they can edit it with exact precision.

Pressing Accept Changes button saves the changes made by the user in the longitude-latitude box, while Delete changes removes the last point given from the memory.

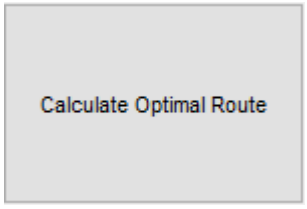

Pressing this button initializes the algorithm for finding the optimal route between the n waypoints given.

Geographical data

Coastline Data

The coastline data consists of two arrays 1x70715 , one for the longitude and one for the latitude. The order of the points of the coastline can be arbitrary, as long as every element of the arrays with the same index corresponds to the coordinates of the same point. This format is compatible with the Matlab command mapshow(lon,lat), which we use to plot the coastline in this work.

Bathymetry Data

The bathymetry data consists of a Matlab object, that contains 2 arrays: lon02(1x209), lat02(81x1), and one matrix: bath02 (81x209). At each point with coordinates lon02,lat02 corresponds a water depth of bath02. Any point that corresponds to land, has a bathymetry of NAN (not a number). This is of very big importance in our obstacle-land avoiding feature, since any path crossing that point, will make the fuel consumption integral infinite.

81x209 double

	1	2	3	4	5	6	7	8	9	10	11
18	NaN	NaN	NaN	NaN	NaN	NaN	NaN	NaN	NaN	NaN	NaN
19	NaN	NaN	NaN	NaN	NaN	NaN	NaN	NaN	NaN	NaN	NaN
20	NaN	NaN	NaN	NaN	NaN	NaN	NaN	NaN	NaN	NaN	NaN
21	NaN	NaN	NaN	NaN	NaN	NaN	NaN	NaN	NaN	NaN	NaN
22	NaN	NaN	NaN	NaN	NaN	NaN	NaN	NaN	NaN	NaN	NaN
23	NaN	NaN	NaN	NaN	NaN	NaN	NaN	NaN	NaN	NaN	NaN
24	NaN	NaN	NaN	NaN	NaN	NaN	NaN	NaN	NaN	NaN	NaN
25	NaN	NaN	NaN	NaN	NaN	NaN	NaN	NaN	NaN	NaN	NaN
26	NaN	NaN	NaN	NaN	NaN	NaN	NaN	NaN	NaN	NaN	NaN
27	NaN	NaN	NaN	NaN	71	100	24	NaN	NaN	NaN	29
28	NaN	NaN	457	284	408	105	152	130	431	295	269
29	NaN	61	324	512	1024	1461	1249	1118	962	665	1120
30	NaN	260	447	719	1269	1452	1437	861	1145	1385	823
31	935	647	828	989	1159	1312	1335	1265	1284	1176	1578
32	NaN	398	705	866	1008	1083	1208	1054	424	675	750
33	NaN	NaN	67	239	351	580	635	549	886	903	925
34	NaN	NaN	NaN	NaN	NaN	86	289	492	588	539	545
35	NaN	NaN	NaN	NaN	NaN	NaN	NaN	NaN	NaN	NaN	NaN
36	NaN	NaN	NaN	NaN	NaN	NaN	NaN	NaN	NaN	NaN	NaN
37	NaN	NaN	NaN	NaN	NaN	NaN	NaN	NaN	NaN	NaN	NaN
38	NaN	NaN	NaN	NaN	NaN	NaN	NaN	NaN	NaN	NaN	NaN
39	NaN	NaN	NaN	NaN	NaN	NaN	NaN	NaN	NaN	NaN	NaN

Table C1. Example of bathymetry data array bath02.

Weather Data Structure

The weather data is composed by the wind and the wave data. The wave data are taken using swan and the wind ones from RegCM3. The wave data consist of three objects Hsig, Dir, that contain the value of the important wave height and its direction respectively and Tp that contains the modal periods. The direction is measured in degrees with respect to the equator. Each, contains matrixes with name Hsig_<iso date>, (or Dir_<iso date>) and Tp-_<iso_date>, from January of 2015 up until December of 2016, with an interval of three hours between each data.

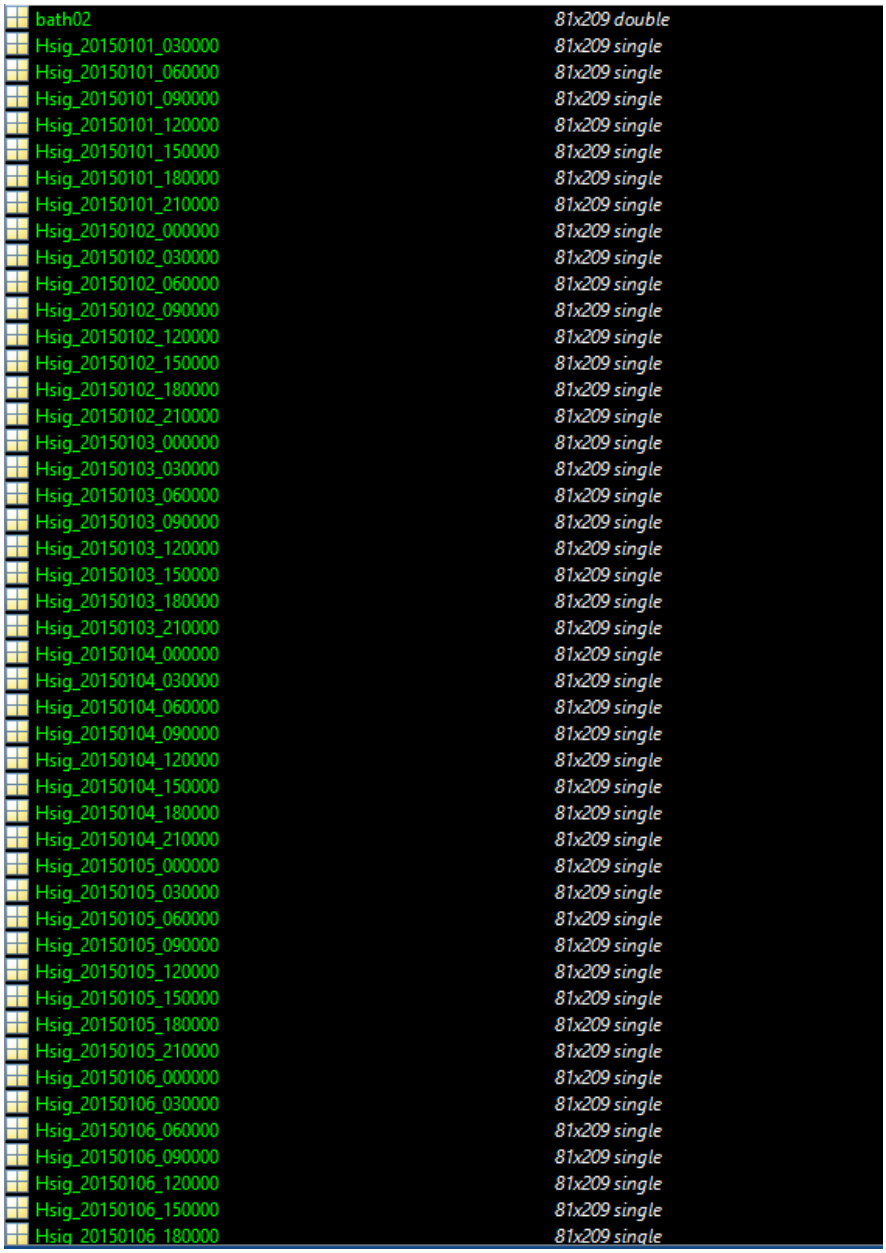

bath02	81x209 double
Hsig_20150101_030000	81x209 single
Hsig_20150101_060000	81x209 single
Hsig_20150101_090000	81x209 single
Hsig_20150101_120000	81x209 single
Hsig_20150101_150000	81x209 single
Hsig_20150101_180000	81x209 single
Hsig_20150101_210000	81x209 single
Hsig_20150102_000000	81x209 single
Hsig_20150102_030000	81x209 single
Hsig_20150102_060000	81x209 single
Hsig_20150102_090000	81x209 single
Hsig_20150102_120000	81x209 single
Hsig_20150102_150000	81x209 single
Hsig_20150102_180000	81x209 single
Hsig_20150102_210000	81x209 single
Hsig_20150103_000000	81x209 single
Hsig_20150103_030000	81x209 single
Hsig_20150103_060000	81x209 single
Hsig_20150103_090000	81x209 single
Hsig_20150103_120000	81x209 single
Hsig_20150103_150000	81x209 single
Hsig_20150103_180000	81x209 single
Hsig_20150103_210000	81x209 single
Hsig_20150104_000000	81x209 single
Hsig_20150104_030000	81x209 single
Hsig_20150104_060000	81x209 single
Hsig_20150104_090000	81x209 single
Hsig_20150104_120000	81x209 single
Hsig_20150104_150000	81x209 single
Hsig_20150104_180000	81x209 single
Hsig_20150104_210000	81x209 single
Hsig_20150105_000000	81x209 single
Hsig_20150105_030000	81x209 single
Hsig_20150105_060000	81x209 single
Hsig_20150105_090000	81x209 single
Hsig_20150105_120000	81x209 single
Hsig_20150105_150000	81x209 single
Hsig_20150105_180000	81x209 single
Hsig_20150105_210000	81x209 single
Hsig_20150106_000000	81x209 single
Hsig_20150106_030000	81x209 single
Hsig_20150106_060000	81x209 single
Hsig_20150106_090000	81x209 single
Hsig_20150106_120000	81x209 single
Hsig_20150106_150000	81x209 single
Hsig_20150106_180000	81x209 single

Table C2. Example of Hsig_ construct componenents.

Hsig_20150103_030000

81x209 single

	80	81	82	83	84	85	86	87	88	89	90
45	2.1007	2.0686	2.0269	1.9960	1.9679	1.9460	1.9264	1.9043	1.8799	1.8515	1.8253
46	1.9698	1.9837	1.9763	1.9662	1.9563	1.9411	1.9229	1.9003	1.8703	1.8394	1.8104
47	1.9097	1.9590	1.9815	1.9917	1.9874	1.9760	1.9505	1.9213	1.8889	1.8558	1.8228
48	1.9235	1.9906	2.0309	2.0525	2.0485	2.0316	2.0010	1.9687	1.9356	1.9012	1.8663
49	1.9925	2.0638	2.1061	2.1268	2.1229	2.1056	2.0738	2.0430	2.0120	1.9821	1.9457
50	2.0817	2.1486	2.1850	2.1998	2.1973	2.1831	2.1638	2.1406	2.1148	2.0836	2.0423
51	2.1581	2.2216	2.2554	2.2719	2.2759	2.2714	2.2619	2.2421	2.2181	2.1864	2.1324
52	2.1989	2.2653	2.3008	2.3192	2.3265	2.3255	2.3178	2.3036	2.2844	2.2506	2.1859
53	2.1690	2.2396	2.2764	2.2980	2.3093	2.3139	2.3116	2.3035	2.2898	2.2530	2.1851
54	2.0626	2.1373	2.1805	2.2077	2.2275	2.2395	2.2439	2.2472	2.2366	2.2033	2.1379
55	1.9247	2.0012	2.0515	2.0850	2.1079	2.1219	2.1287	2.1306	2.1268	2.1053	2.0373
56	1.7909	1.8676	1.9232	1.9616	1.9783	1.9870	1.9929	1.9892	1.9883	1.9783	1.9049
57	1.6763	1.7532	1.8116	1.8492	1.8574	1.8532	1.8418	1.8388	1.8325	1.8148	1.7150
58	1.5693	1.6610	1.7305	1.7723	1.7702	1.7565	1.7359	1.7111	1.6493	1.5840	1.4060
59	1.5240	1.6368	1.7242	1.7778	1.7677	1.7399	1.6881	1.6029	1.3817	1.2355	0.4536
60	1.5519	1.6821	1.7838	1.8469	1.8005	1.7335	1.6281	1.4121	0.4387	0.3573	NaN
61	1.6074	1.7393	1.8403	1.8964	1.7013	1.5828	1.4470	0.4554	NaN	NaN	NaN
62	1.6106	1.7151	1.7948	1.8147	0.5123	0.5055	0.4866	NaN	NaN	NaN	NaN
63	1.4263	1.4812	1.5220	1.4660	NaN	NaN	NaN	NaN	NaN	NaN	NaN
64	0.4902	0.4972	0.5007	0.4887	NaN	NaN	NaN	NaN	NaN	NaN	NaN
65	NaN	NaN	NaN	NaN	NaN	NaN	NaN	NaN	NaN	NaN	NaN
66	1.2539	NaN	NaN	NaN	NaN	NaN	NaN	NaN	NaN	NaN	NaN

Table C3. Example of Hsig_20150103_030000 matrix.

Same holds for the wind data, but instead of having measure and direction, the data consists of two objects called U and V, that are the horizontal and vertical component respectively of the wind vector on the earths curvilinear coordinates.

Ship Data Structure

The ship data is a structure with the name of the ship, containing the following attributes:

B : Width.

D : Depth.

CB: Cb coefficient.

L : Length.

Disp: Displacement

U : Service speed

Kk: Wind resistance coefficient

rwind: Wind density

tt: An array with the polynomial interpolation coefficients of K_T .

qq: An array with the polynomial interpolation coefficients of K_Q

wake: Wake fraction

thrd: Thrust reduction factor

relrot: Relative rotative coefficient

rho: Water density.

Vw: The different service speeds that correspond to the calculated added resistance.

Hs: The different important wave heights that correspond to the calculated added resistance.

Rw: The added resistane for different service speeds and sea states.

bspcons: The engine specific fuel consumption in g/kWh.

Finally the central GUI flowchart is shown in Fig.C1, where also the names of the basic m-files are listed.

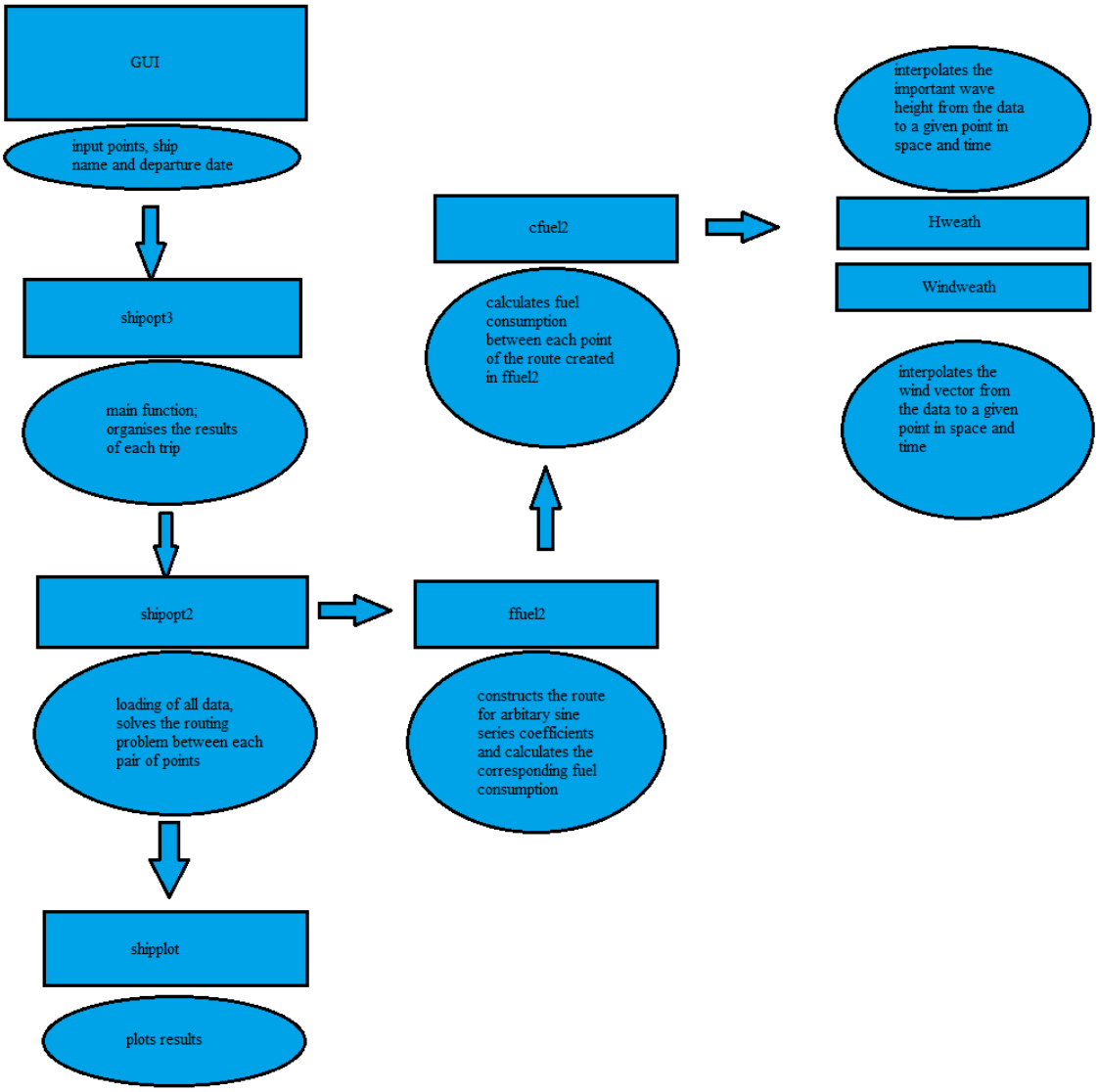

Figure C1 GUI flowchart.